

The Motion Generation of Stable Vertical  
Ladder Climbing Capable of Recognizing  
Rungs for a Four-limbed Robot

四肢ロボットの安定かつ棧の認識が可能な  
垂直はしご昇降の運動生成

December 2018

Xiao SUN

孫 瀟



The Motion Generation of Stable Vertical  
Ladder Climbing Capable of Recognizing  
Rungs for a Four-limbed Robot

四肢ロボットの安定かつ棧の認識が可能な  
垂直はしご昇降の運動生成

December 2018

Waseda University

Graduate School of Advanced Science and Engineering

Department of Integrative Bioscience  
and Biomedical Engineering

Research on Biorobotics

Xiao SUN

孫 瀟



Dissertation submitted for the degree of Ph. D. in Engineering

Supervisor: Atsuo Takanishi

Members of the Committee:

Atsuo Takanishi

Mitsuo Umezu

Tomoyuki Miyashita

Hiroyasu Iwata

Kenji Hashimoto



## **Abstract**

Robot technique arises to be playing essential roles in the prospective evolution of technology and its application has spread to various fields. Among them, disaster response (inspection of disaster sites, rescue, removal of obstacles in dangerous environment, etc.) performed by robots as the substitution of human beings has been a very promising trend for less risk of casualties, better accessibility, longer working time and so on.

Nowadays although various types of disaster response robots have been developed and some of them have been put into practical use, the mainstream of their locomotion style is rather horizontal, with wheels or caterpillars to move on uneven terrains. However, locomotion in the vertical direction for disaster response robots is much less studied. Flying is an attractive solution (like drone robots), but its use is unfortunately quite limited, such as in the case of indoor environment, and manipulation capability of flying robots is also a drawback in comparison with other types of disaster response robots. In this thesis, climbing of vertical ladders is focused as a common and popular solution for vertical locomotion that is expected to be indispensable in disaster environment, regardless of indoor and outdoor situation.

Vertical (for the simplicity, “vertical” will be omitted for the rest of this thesis) ladder climbing by robots has been studied for about 3 decades and high-level control systems has been applied so far. However, as for the actual application of the robot climber in complicated situations, such as disaster response and maintenance of infrastructures and plants where the robots are expected to be working individually, corresponding attention and consideration are much less and need to be increased.

In the comparison between horizontal locomotion and ladder climbing, although fall recovery may be possible for biped walking or quadruped walking depending on the hardware design and control methods to decrease the damage of falling and bring the robot back to stable states, in ladder climbing the robot may be at a much higher position from the ground, making it very difficult for the robot to recover and keep functioning correctly in case of falling. Therefore, this thesis

mainly deals with the stable ladder climbing, where “stable” in this thesis is defined as the stability in the following 3 states:

- 1) Contact state: When all end-effectors of robot are in contact with the ladder;
- 2) Swing state: When one or more end-effector(s) is(are) moving in the air to the target position;
- 3) Transition state: When one or more end-effector(s) is(are) about to contact the target ladder, which is a middle state between state 1) and 2).

Due to the unique characteristics of ladder climbing, its stability analysis also differs from conventional multi-legged locomotion styles, such as biped and quadruped walking and needs to be studied systematically. However, former studies focused partially on 3 states described above, which might be insufficient for guaranteeing complete stability in ladder climbing. Specifically, main contents about stability in this thesis consist of points presented below:

- 1) Motion generation of ladder climbing (for “contact state” and “swing state”). In ladder climbing, the constraints of start and end position as well as path of each step are stricter than multi-legged walking. With the consideration of this point, trajectory of end-effectors is mainly generated with the application of “event-based planning” that allows independent planning of path and time profile in trajectory planning of the robot so that planning of motion obeying the constraints would be easier. Combined with inverse kinematics based on Jacobian and climbing “gaits” (climbing pattern about the number and the order of limbs to move), appropriate ladder climbing motion can be planned and generated.
- 2) Sensor feedback (for “swing state” and “transition state”). Unfortunately, appropriate motion planning and generation alone cannot satisfy stable ladder climbing, since there are still multiple factors (both external and internal ones) that may lead to error. If not compensated, stability may be lost in “transition state” with inappropriate or even failed contact between the robot and ladder. According to different types of error that may appear, an error compensation system consists of hardware design, multiple proximity sensors, motion for



error sensing and corresponding error compensation motion is proposed and described in this thesis.

In addition, for some gaits (especially for 2-point contact ladder climbing that 2 limbs move at the same time for one step) the robot may rotate and fall from the ladder with inappropriate posture and reaction force at supporting limbs. Therefore, stability analysis to avoid rotation on the ladder is proposed and discussed and the corresponding control of reaction force with the feedback between the robot and ladder is proposed according to the stability analysis.

- 3) Integration of all components above for maintaining stability in ladder climbing. To obtain maximal effect in keeping stability and get rid of mutual interference, integration with switching of each components in different states of ladder climbing and appropriate motion planning are proposed.

The contents above will be introduced respectively in related chapters and results of simulation or experiments as well as data and statistics will be presented to evaluate the effectiveness and capability of our proposed system.



## **Acknowledgments**

In retrospect to my study in Takanishi Laboratory for 4 years, all that I feel is that I have been so lucky and blessed to be supported and encouraged by surrounding people. Never could I persist in my study and obtain achievements without their patient guidance and kind help.

To begin with, I would like to thank Professor Atsuo Takanishi for kindly inviting me to Takanishi Laboratory, a place where human-sized robots were originated and developed and amazing latest updates of research have been keeping produced. In addition, I am so honored to be a part of ImPACT, a large-scale project held by the government of a country, which is an extremely precious experience that few robot researchers could have. His advice also made a big difference to my study. When my study was getting close to a dead-end, it was his suggestion that led me to a right way to the destination. His erudition always makes me feel so relieved and assured to ask him questions. Moreover, I benefited so much from his philosophy about engineering as well. “The answer is always in the field where real robots work” remains to be the most impressive sentence that he told us and influenced me. Professors in the Committee (Prof. Umezu, Miyashita, Iwata and Hashimoto) also gave me inspiring ideas and suggestions from different perspectives and I really appreciate that.

Associate Professor Kenji Hashimoto is an indispensable and irreplaceable key person in my study as the chief manager of the project group that I have been working in. His flawless management, wide horizon, astonishing will and enthusiasm for research have always been exemplary to us and what we students longed for. Hardly could I remember how many times that I was saved by him. Although we did not have many chances to talk to each other, I want to thank Associate Professor Hiroyuki Ishii for his encouragement and his advice to my Ph.D. course as well.

Recalling the period when I just entered Takanishi Laboratory, I was confused by the new environment and so much new knowledge and rules to learn. Besides the help and advice from Professor Takanishi and Hashimoto, the students around me also helped a lot in that hard period. My special thanks go to Dr. Tatsuhiro

Kishi first, who shared the same working desk with me for nearly 3 years throughout my Ph.D. study and was also definitely the person that gave me biggest help in research among students. In the same period, the cooperation and assistance of other Ph.D. students in Takanishi Laboratory were significant to me as well. Dr. Takuya Otani always gives me meaningful suggestions from the perspective of being a Ph.D. student. Dr. Katsuaki Tanaka helped me a lot as a Japanese Ph.D. student. His help in managing symposium with me was especially crucial and I could not imagine what the symposium would be like without him. Dr. Weisheng Kong often invites me to their underground laboratory and answers me questions about Ph.D. graduation process. Mr. Yukitoshi Minami taught me a lot about WABIAN-2 and knowledge related to biped walking robots. As the member in the same research team, Mr. Takashi Matsuzawa worked so hard and helped me so much in managing the whole team. Without him, this thesis would not be written in such a short period.

I want to thank all members who were or have been in our research group for their hard work and cooperation in research, experiments, management assist, daily chores and so on. Especially, I would like to thank second-year graduate students for each year: Mr. Kazuhiro Uryu, Shinya Hamamoto, Tomotaka Teramachi, Shota Hayashi (Haoxiang Qiu in Chinese) and Masahiro Okawara. The cooperation with you was so great and I have been so enlightened by our cooperative works.

Last but not least, I would like to thank my parents for their warm love. I am sorry to make them worried for these years and did not returned home for nearly 2 years. It is my father who made me decide to be a scholar and it is my mother who raised me from my birth and made me a healthy and strong man both physically and mentally.

## Nomenclature

### Abbreviations

JIS	- Japan Industrial Standards
MIL	- Military Standard
UGV	- Unmanned Ground Vehicle
UAV	- Unmanned Aerial Vehicle
DoF	- Degree of Freedom
CoM	- Center of Mass
FK	- Forward Kinematics
IK	- Inverse Kinematics
IMU	- Inertia Measurement Unit
AoY	- Axis of Yawing
MCP	- Multi-Contact Planner
BFGS	- Broyden-Fletcher-Goldfarb-Shanno
ROS	- Robot Operating System
ToF	- Time of Flight
LBS	- Laser Beam Section
FoV	- Field of View
LRF	- Laser Range Finder



## Table of contents

Chapter 1.	Introduction.....	1
1.1	Background.....	1
1.2	Categories of disaster response robot .....	3
1.3	Main topics of this thesis .....	6
1.4	Related researches.....	8
1.4.1	LCR-1.....	8
1.4.2	Gorilla-III.....	8
1.4.3	HRP-2.....	11
1.4.4	Robots of Honda R&D.....	11
1.5	Objectives of this thesis .....	11
1.6	Outline .....	12
Chapter 2.	Robots used in this thesis .....	15
2.1	Overview.....	15
2.2	Introduction of The Prototype.....	16
2.3	Introduction of WAREC-1.....	18
2.4	Summary .....	20
Chapter 3.	Motion generation system.....	23
3.1	Introduction.....	23
3.2	Gaits of ladder climbing .....	25
3.3	End-effector trajectory planning.....	27
3.3.1	Prerequisite math knowledge .....	28
3.3.2	Path planning.....	30
3.3.2.1	Selection of mid-points in path planning.....	33
3.3.2.2	Path length minimization (optional).....	33
3.3.3	Separation of path and time: Arc-length parameterization .....	34
3.3.4	Time profile planning.....	36
3.4	Body trajectory planning .....	39
3.4.1	Background: Stability analysis.....	39

3.4.2	Body trajectory in different climbing gaits .....	42
3.5	Whole-body motion planning .....	44
3.6	Kinematics .....	44
3.6.1	Forward kinematics .....	45
3.6.2	Inverse kinematics.....	48
3.7	Experiments in simulation .....	52
3.7.1	Conditions .....	52
3.7.2	Results .....	52
3.7.3	Discussions.....	54
3.8	Summary .....	54
Chapter 4.	Sensor feedback systems.....	57
4.1	Background and introduction.....	57
4.2	Force sensor feedback control .....	58
4.2.1	Overview .....	58
4.2.2	Sufficient stability conditions for reaction force norm .....	59
4.2.3	Conditions and distribution of reaction force at contact points .....	63
4.2.4	Experiment: Comparison .....	67
4.2.4.1	Conditions.....	67
4.2.4.2	Results .....	68
4.2.4.3	Discussions .....	68
4.3	Proximity sensor feedback system.....	71
4.3.1	Error sensing and compensation motion .....	74
4.3.2	Measures for robustness .....	76
4.3.3	Integration of trajectory planning and proximity sensor feedback .....	77
4.3.4	Experiment 1: Reliability and accuracy test.....	79
4.3.4.1	Conditions.....	79
4.3.4.2	Results .....	79
4.3.4.3	Discussions .....	80
4.3.5	Experiment 2: Climbing a ladder with a higher rung.....	82
4.3.5.1	Conditions.....	83



4.3.5.2	Results .....	85
4.3.5.3	Discussions .....	85
4.3.6	Experiment 3: Climbing a ladder with an inclined and higher rung .....	85
4.3.6.1	Conditions.....	85
4.3.6.2	Results .....	88
4.3.6.3	Discussions .....	88
4.3.7	Experiment 4: Comparison in simulation.....	88
4.3.7.1	Conditions.....	88
4.3.7.2	Results .....	88
4.4	Total integration experiment.....	89
4.4.1	Total flow of ladder climbing motion .....	89
4.4.2	Conditions .....	91
4.4.3	Results .....	91
4.4.4	Discussions.....	94
4.5	Summary .....	94
Chapter 5.	Conclusions .....	95
5.1	Contributions.....	95
5.2	Limitations .....	96
5.2.1	Developed but incomplete capability of environment recognition .....	96
5.2.2	No solution to time-variant ladder in different standards .....	96
5.2.3	No manipulation capability in ladder climbing.....	96
5.3	Future works .....	97
References.....		99
Appendix.....		105
A.	Pseudo-inverse matrix.....	105
B.	Inverse kinematics.....	107
C.	Riemannian manifold .....	113
D.	Application of proximity sensor system .....	117
D.1	Introduction: Continuous motion from the ground to a ladder .....	117
D.2	Posture adjustment after transition.....	124

D.3 Experiment.....	125
E. Specification of the ladder in JIS used in this thesis .....	129
Publications.....	131

## List of figures

Fig. 1.1 Three indexes to measure the extremity of environment [9].	3
Fig. 1.2 Quince [11].	5
Fig. 1.3 MHI-MEISTeR [12].	5
Fig. 1.4 Ladders in Asian countries.	6
Fig. 1.5 Off-shore wind turbine and the ladder inside ([13], [14]).	7
Fig. 1.6 High-rise chimney and ladders on it [15].	7
Fig. 1.7 LCR-1 [16].	9
Fig. 1.8 Gorilla-III [17].	9
Fig. 1.9 HRP-2 climbing a ladder [20].	10
Fig. 1.10 Ladder climbing by the robot developed by Honda R&D [21].	10
Fig. 1.11 E2-DR climbing a ladder [22].	10
Fig. 1.12 Outline of this thesis.	14
Fig. 2.1 The Prototype [23].	15
Fig. 2.2 Mechatronic system configuration of The Prototype [24].	15
Fig. 2.3 Design and scale of the end-effector [25].	17
Fig. 2.4 Different usages of the end-effector.	17
Fig. 2.5 End-effectors of other ladder climbing robots for foot.	17
Fig. 2.6 Overview and DoF configuration of WAREC-1 [26].	19
Fig. 2.7 System configuration of WAREC-1.	19
Fig. 2.8 WAREC-1 crawling on uneven terrain.	21
Fig. 2.9 WAREC-1 climbing a vertical ladder with safety cage.	21
Fig. 3.1 Trouble cases that may happen between the end-effector and rung.	23
Fig. 3.2 Whole-body motion planning scheme.	24
Fig. 3.3 Climbing “gaits” with high difficulty.	25
Fig. 3.4 3-point contact climbing (in 4 steps, with body keep moving).	26
Fig. 3.5 2-point contact climbing (not used in this thesis).	26
Fig. 3.6 2-point contact climbing.	26
Fig. 3.7 Critical points with risk.	32
Fig. 3.8 Generated end-effector path of climbing up motion in XoZ space.	32
Fig. 3.9 Comparison of path length of climbing up motion.	34
Fig. 3.10 The curve of time profile designed for the robot.	37
Fig. 3.11 Trajectory of end-effector for climbing up motion in 3D space.	38
Fig. 3.12 Illustration of WAREC-1 on a ladder.	40
Fig. 3.13 Phases of whole-body motion planning for pace gaits [36].	44

Fig. 3.14 Coordination system of WAREC-1.....	45
Fig. 3.15 Orientation presentation by Axis-angle ([35], [36]).....	46
Fig. 3.16 Generated 3-point contact ladder climbing motion in simulator.....	53
Fig. 3.17 Generated 2-point contact ladder climbing motion in simulator.....	53
Fig. 4.1 Flowchart of reaction force feedback to maintain stability.....	66
Fig. 4.2 2-point contact ladder climbing by WAREC-1: Successful.....	69
Fig. 4.3 2-point contact ladder climbing by WAREC-1: Failed.....	69
Fig. 4.4 Reaction force in Z-axis measured in 2-point contact ladder climbing.....	70
Fig. 4.5 Reaction force in Z-axis measured in 2-point contact ladder climbing.....	70
Fig. 4.6 Width of hook and groove on the end-effector.....	72
Fig. 4.7 Typical cases of failed grab of rungs.....	72
Fig. 4.8 Proximity sensor VL6180X [42].....	72
Fig. 4.9 System configuration of proximity sensors.....	72
Fig. 4.10 The position and orientation of proximity sensors at the end-effectors...	73
Fig. 4.11 The process of proximity sensors passing the target rung.....	74
Fig. 4.12 Flowchart of hanging an end-effector on the target rung.....	78
Fig. 4.13 Flowchart of hanging an end-effector on the target rung.....	79
Fig. 4.14 Trial 1 for hanging end-effector to rung: Failed.....	81
Fig. 4.15 Trial 2 for hanging end-effector to rung: Failed.....	81
Fig. 4.16 Trial 3 for hanging end-effector to rung: Failed.....	81
Fig. 4.17 Trial 4 for hanging end-effector to rung: Succeeded.....	81
Fig. 4.18 An example of handmade temporary ladder.....	82
Fig. 4.19 Ladder attachment 1 on the ladder.....	83
Fig. 4.20 Snapshots of climbing a ladder with Ladder Attachment 1.....	84
Fig. 4.21 Ladder attachment 2 on the ladder.....	85
Fig. 4.22 Snapshots of climbing a ladder with Ladder Attachment 2.....	86
Fig. 4.23 Proximity sensor data of right hand in the Case 2.....	87
Fig. 4.24 Proximity sensor data of left hand in the Case 2.....	87
Fig. 4.25 WAREC-1 climbing a ladder with error.....	89
Fig. 4.26 WAREC-1 climbing a ladder with error.....	89
Fig. 4.27 Flowchart of motion generation for WAREC-1.....	90
Fig. 4.28 Snapshots of the total integration experiment.....	92
Fig. 4.29 Reaction force in Z-axis in 2-point contact ladder climbing.....	93
Fig. 4.30 Proximity sensor data of right hand in the total integration.....	93
Fig. D.1 Motion planning for 2 stages in approaching the target ladder.....	118
Fig. D.2 Approaching motion, stages 1.....	119

Fig. D.3 Approaching motion, stage 2.....	120
Fig. D.4 Ladder attaching of The Prototype. ....	121
Fig. D.5 Gorilla stance.....	123
Fig. D.6 Initial position and orientation with error before transition. ....	123
Fig. D.7 Posture adjustment after transition.....	124
Fig. D.8 Snapshots of the sequence of “approaching”. ....	126
Fig. D.9 Snapshots of the sequence of “transition” .....	127



## List of Tables

Table 1-1 Main disasters occurred in Japan and other countries.....	1
Table 2-1 Specifications of The Prototype. ....	16
Table 2-2 Specifications of WAREC-1.....	18
Table 2-3 Features of WAREC-1 in comparison with The Prototype. ....	20
Table 3-1 Comparison of 3-point contact and 2-point contact climbing.....	26
Table 3-2 Comparison of path length. ....	34
Table 3-3 Value of parameters in path length comparison. ....	34
Table 3-4 Mass distribution and length data of WAREC-1. ....	40
Table 3-5 Explanation of variables. ....	42
Table 3-6 Explanation of variables related to quaternion.....	48
Table 3-7 Conditions of simulation.....	53
Table 4-1 Definition of variables. ....	67
Table 4-2 Conditions in Experiment 1. ....	67
Table 4-3 Comparison of sensor options. ....	71
Table 4-4 Explanation of variables related to sensor.....	76
Table 4-5 Statistics of error compensation results. ....	80
Table 4-6 Change of specification after equipping Ladder Attachment 1.....	84
Table 4-7 Time data in the experiment of Fig. 4.20.....	85
Table 4-8 Change of specification after equipping Ladder Attachment 2.....	87
Table 4-9 Time data in the experiment of Fig. 4.22.....	88
Table 4-10 Conditions of the total integration experiment.....	91
Table D-1 Time spent in each sequence. ....	125
Table E-1 Specifications about vertical ladders in JIS (JIS B 9713-4) .....	129





# Chapter 1. Introduction

## 1.1 Background

Having been a huge threat to human beings since their appearance on the earth, natural disaster has occurred all over the world. It is extremely difficult to predict and avoid in advance due to its characteristics: sudden occurrence without a sign and enormous unstoppable power. Sometimes disaster with large scale might even be the trigger of other types of disaster, and the Great East Japan Earthquake in 2011 and the destructive Tsunami accompanied as well as Fukushima Daiichi Nuclear Power Plant accident is a representative instance. Table 1-1 presents some examples of natural disaster occurred in Japan and other countries for the recent years with statistics data.

Table 1-1 Main disasters occurred in Japan and other countries.

Time	Country	Name of disaster	Remark
2008.5	China	Sichuan Earthquake (M8.0)	Deaths: over 69,000; Injuries: 374,643 [1]
2011.3	Japan	Great East Japan Earthquake (M9.0)	Deaths: 15,893; Injuries: 6,152; Accompanied by Tsunami and the accident of nuclear power plant [2]
2014.9	Japan	The eruption of Mountain Ontake	Biggest eruption in Japan since World War II [3]
2016.4	Japan	Kumamoto Earthquake (M6.5)	Followed by the eruption of Mountain Aso [4]
2017.9	Mexico	Mexico Earthquake (M7.1)	Deaths: 370; Injuries: over 4,500 [5]
2018.7	Japan	2018 Japan floods	Deaths: 225; Injuries: 421 [6]

Considering the capability human has at present, the most effective solution still remains to be prompt response to the disaster after it occurs. However, it is true that disaster response by a human is not without the risk of secondary disaster, such as the aftershock and fire after big earthquakes. For some disaster areas, they are even impossible for humans to enter. One of the most typical examples is the Fukushima Daiichi Nuclear Power Plant filled with strong lethal radiation. Thanks to the rapid evolution of robot technology, disaster response robots emerge into our sight as an option of the substitute of human to perform rescue tasks in disaster areas. This possibility has drawn wide and public attention in the world, especially for countries with high-level robot techniques.

For worldwide events, “DARPA Robotics Challenge Finals” [7] held in June 2015 was a big stage for robots from countries all over the world to get together and compete with each other about their rescue capability in man-made situations that could be found in disaster situations. However, frequent fall and errors in both hardware and software (the difficulty of tasks to be completed was not very high and some were even very easy for human) in the competition reminded us that disaster response robots at present are still far from completion and their range of application is still highly limited.

As for the situation in Japan, several robot-related projects were launched for disaster response, and this study is a part of the “Tough Robotics Challenge” in the project ImPACT (Imposing Paradigm Change through Disruptive Technologies Program) launched and managed by Cabinet Office, Government of Japan [8]. In “Tough Robotics Challenge”, the aim of the project is to develop “tough” robots capable of performing disaster response tasks in extreme environment and this thesis is also a part of this project.

To realize the objective of developing robots working in extreme environment, the first thing we must do is to define “extreme environment”. In our perspective, we proposed the following 3 indexes: narrowness, unevenness and inclination so that the extremity of environment in disaster areas can be measured by these 3 indexes illustrated in Fig. 1.1.

The next question that has to be cleared is: what should a robot be like and

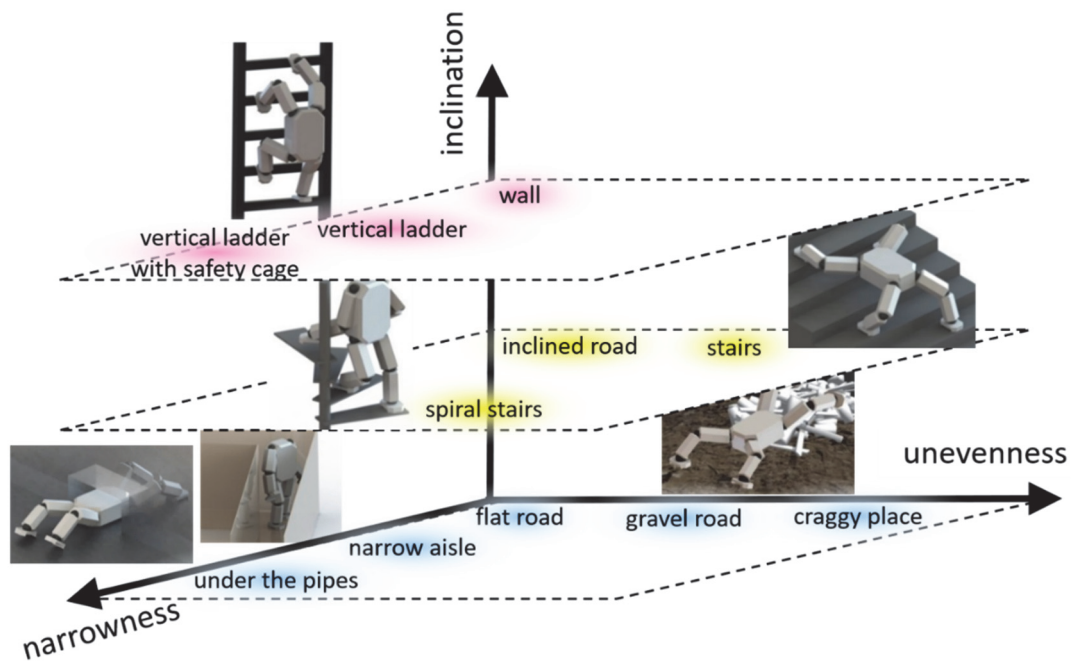


Fig. 1.1 Three indexes to measure the extremity of environment [9].

capable of in extreme environment? After the Great East Japan Earthquake in 2011, committees of the Council on Competitiveness-Nippon (COCN) in Japan consisting of about 100 members from Japanese government ministries, companies, and universities proposed an establishment plan for a disaster response robot center and published a report in 2013. The 2013 report of COCN [10] lists and examines the required specifications and functions for disaster response robots. It claims that the capability of locomotion and manipulation is the essential function for disaster response robots. Moreover, robots must have the capability of sensing and recognition to gather information in extreme environment. In this thesis, locomotion capability with preliminary environment recognition is mainly discussed, since the capability of manipulation and other rescue tasks are based on the fact that the robot must be able to reach the destination and perform the target task.

## 1.2 Categories of disaster response robot

There are various types of natural disaster, thus the forms of robots expected to be applicable to deal with them also vary. The followings are some major types

of robots applied or to be applied in disaster response [10]:

(1) UGV (Unmanned Ground Vehicle):

UGV with wheels is applied mainly to the ground that normal vehicles usually run on. However, there is technical issue about remote control and communication. As for UGV with caterpillars, they are developed with the purpose of locomotion on steps, rubble, uneven terrain, etc. The achievements of this type of UGV are mainly for military use. Nevertheless, in disaster sites their locomotion capability and reliability are limited, with the requirement of tougher, lighter, and better locomotion capability for the body and caterpillars.

(2) Legged robots:

Legged robots are developed for the application of manipulation on inclined terrain, transportation on uneven terrain and so on. Although the stability of multi-legged walking has been an issue to solve, recently it becomes much easier to stabilize the walking. At present, robots with performance close to practical use, such as BigDog and TITAN IV have been developed. Few researches and developments were made for the application of the legged robots to disaster response, but now in the United States project like PETMAN aiming at locomotion capability on uneven terrain was launched and competition of DARPA Robotics Challenge was also held to appeal legged disaster response robots.

(3) Exoskeleton robots:

With the target of assistance in moving heavy objects for human, exoskeleton robots such as XOS Exoskeleton and HAL were developed and are also close to the application.

(4) UAV (Unmanned Aerial Vehicle):

Helicopters with the length of meters have been applied, with the instance of Yamaha RMAX in the disaster of volcanic eruption and many others. Unfortunately, issues of communication and safety still remain. Besides, small-sized drones within 1 meter are close to the practical use and their indoor flying has been studied. For them, there are issues about stability and safety of strong/sudden wind, flying in narrow spaces, payloads, flying time and so on.

(5) Wall climbing robots:

For this category, it becomes technically feasible for climbing on a plain metal surface, but it is not the case for uneven walls or walls with obstacles. For those concrete walls with no magnetic attraction, although suckers have been

utilized for wall climbing robots, but it is difficult to guarantee sufficient attraction force for walls with uneven surface as well.

(6) Robots in narrow spaces:

A representative example of this type of robot is snake-shaped robots, being capable of digging in rubble and other narrow places like gaps. However, issues of overturn, turning performance and location estimation are there to be improved.

For locomotion, there is no doubt that a robot with high locomotion capability should be able to go over various different situations that may exist in disaster areas. Among current rescue robots that have been engaged into disaster areas, such as Quince (Fig. 1.2), MHI-MEISTeR (Fig. 1.3) and so on sent into nuclear power plants in Fukushima, wheeled robots and crawler robots represent the mainstream. Looking Fig. 1.1 back, we could find that they can overcome situations with “narrowness” or “unevenness” easily, but it is not the case for



Fig. 1.2 Quince [11].

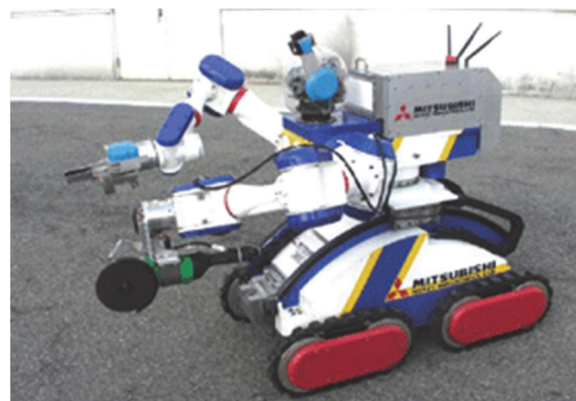


Fig. 1.3 MHI-MEISTeR [12].



(a) Tokyo, Japan

(b) Beijing, China

(c) Daejeon, Korea  
(with safety cages)

Fig. 1.4 Ladders in Asian countries.

situations with “inclination”. Flying robots like drones seem to be a good option, but it is true that they are not omnipotent in vertical locomotion, especially for indoor tasks or narrow places with little light. As for snake-shaped robots, their versatility in locomotion styles is impressive, but their manipulation capability is still limited due to the feature of their structure. Therefore, we choose legged robots that cover all locomotion situations in Fig. 1.1 as well as the manipulation capability.

### 1.3 Main topics of this thesis

As the alternative solution of flying for vertical locomotion in disaster areas, vertical ladder climbing is more likely to be practical, which is also the major topic of this thesis. In the following texts, if not explicitly indicated, “ladder” all stands for “vertical ladder” and the word “vertical” will be omitted because inclined ladders are not within the scope of this thesis. Moreover, we choose four-limbed robots as the platform for disaster response because in locomotion aspect legged robots can deal with the extreme environment with any index (indexes) mentioned in Fig. 1.1, and four-limbed robots can maintain high output in manipulation tasks, which may be difficult for other types of robot.



Fig. 1.5 Off-shore wind turbine and the ladder inside ([13], [14]).



Fig. 1.6 High-rise chimney and ladders on it [15].

Why do we choose ladder climbing performed by legged robots as the major concern of our study? The answers are summarized as follows:

- 1) Ladder climbing is required in disaster response as well as routine maintenance of infrastructures and plants, but few attempts have been put into the application. In fact, ladders are much closer to us than we can imagine. Fig. 1.4 shows examples of ladders that the author saw in some Asian countries. Ladders are popular because of the following features: (i) Low cost; (ii) Easy to be attached to walls; (iii) Less space required than stairs or other types of

vertical locomotion structures; (iv) No power source required. These features make ladder climbing a popular option in vertical locomotion. As for the specific examples of routine maintenance of infrastructures and plants, high-rise chimney (long ladders attached outside) shown in Fig. 1.5 and off-shore wind turbine (ladders hid inside) shown in Fig. 1.6 can be given.

- 2) Ladder climbing is with risk and danger for human climbers. Ladder climbing is a type of high energy consuming locomotion because the climber has to sustain his, her or its self-weight for all the time during climbing and even climbing a short range would cause sore of muscle. It is not hard to imagine that climbing a long ladder is not without the risk of falling and even injury or death of the climber. And robot climbers would eliminate this risk.
- 3) Even if the climber is fully equipped with safety tools, such as ropes to fix the climber to ladders or safety cages attached on the ladder, they would be meaningless if the ladder itself gets aged and breaks. Thus, a robot ladder climber is always safer than a human ladder climber.

In summary, with the ladder climbing capability and other locomotion styles to be performed by our robots, a four-limbed robot first becomes available for locomotion in most of the situations expected in disaster areas.

## **1.4 Related researches**

### **1.4.1 LCR-1**

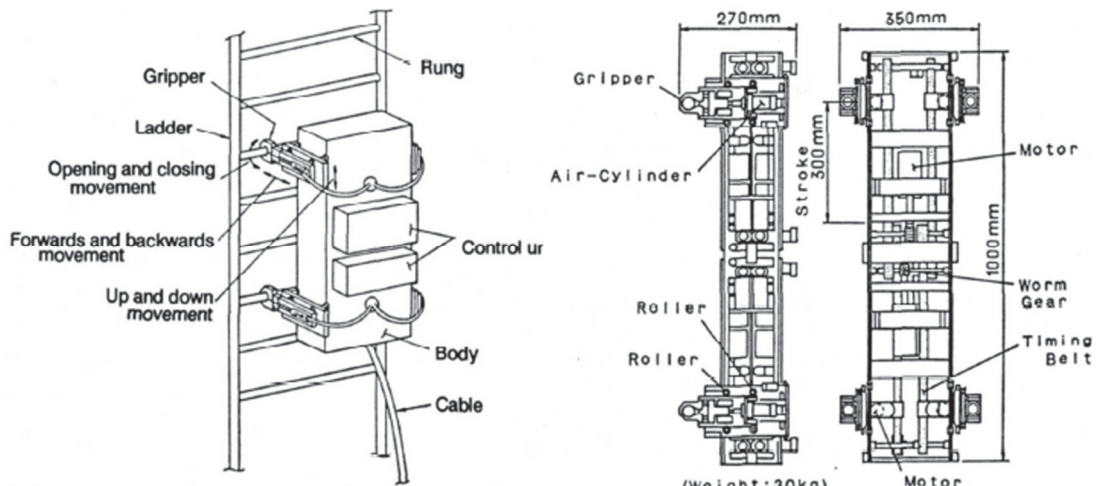
As a matter of fact, the history of robot ladder climbing is not long, and it is particularly true for human-sized robots. Dated back to 1989, H. Iida et al. developed "LCR-1", a four-limbed robot that could climb up and down the ladder with 4 gripper actuators equipped at the end of each limb to hold the rungs of the ladder (Fig. 1.7). It is one of the pioneers in robot ladder climber. Unfortunately, not many details of LCR-1 were given, neither were the algorithms about ladder climbing.

### **1.4.2 Gorilla-III**

In 2008, Fukuda et al. developed "Gorilla-III", a four-limbed robot with height of 1.0m and weight of 22kg (based on the size of real gorillas) that can climb a ladder as well as brachiation (Fig. 1.8). This is the first influential robot (although it is a little bit small and light for human) capable of ladder climbing in a manner that is close to human. It climbed the ladder with the maximum speed of 0.05m/s



and grip recognition of rung by output voltage of joints is applied to judge whether rung grip of end-effectors is successful or not. Besides, optimal allocation of load was also proposed [18], which is also the source of inspiration of reaction force control in this thesis (the second half of Chap. 4). In stability analysis of ladder climbing for Gorilla-III, single-mass model and equilibrium of moment around AoY (Axis of Yawing), an axis connecting the contact points between the robot and rungs of ladder were utilized [19], which is also one of the origin of ideas in this thesis about stability analysis. A half-circle path was used in trajectory generation of ladder climbing.



(a) Overview and explanations of parts (b) model structure and sizes  
 Fig. 1.7 LCR-1 [16].

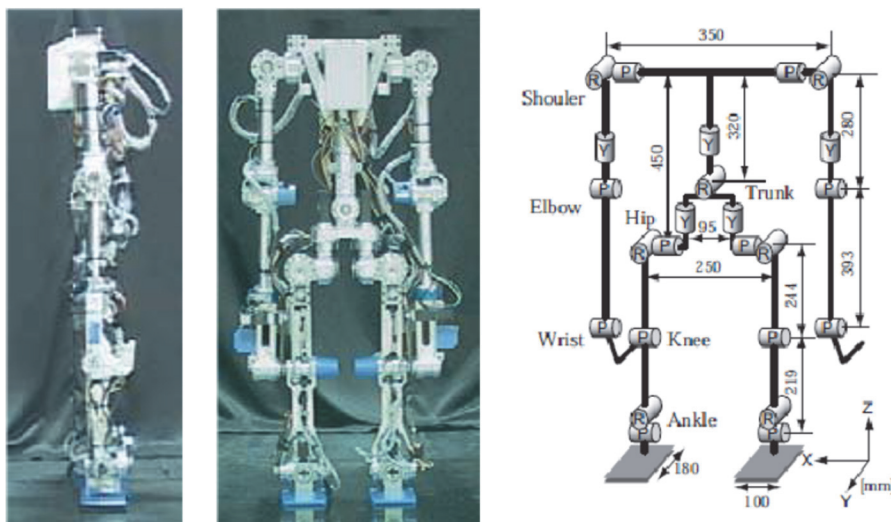


Fig. 1.8 Gorilla-III [17].

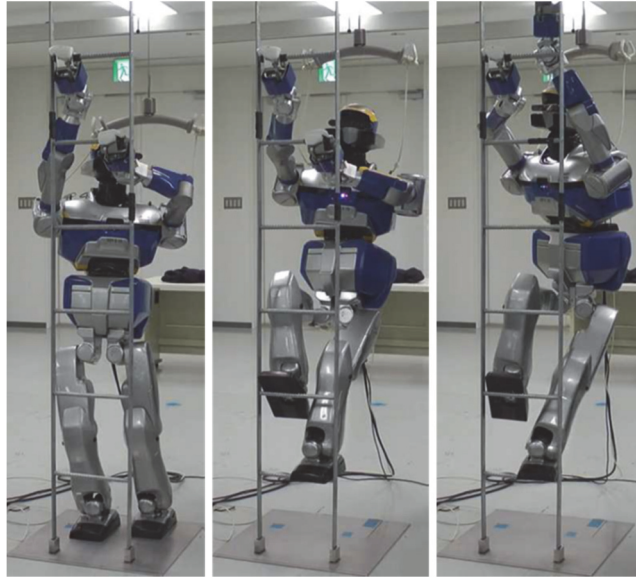


Fig. 1.9 HRP-2 climbing a ladder [20].

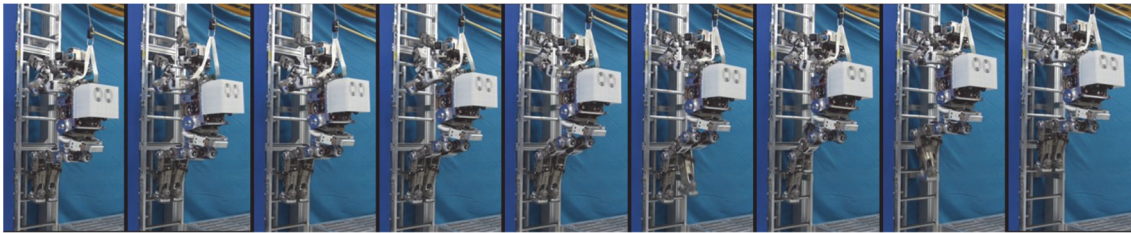


Fig. 1.10 Ladder climbing by the robot developed by Honda R&D [21].



Fig. 1.11 E2-DR climbing a ladder [22].

### **1.4.3 HRP-2**

Known as a universal humanoid platform for biped walking, HRP-2 was also applied to ladder climbing. Vaillant et al. proposed MCP (Multi-contact Planner) for planning and control of ladder climbing for HRP-2 and utilized FSM (Finite State Machine) to generate ladder climbing motion in 3-point contact that can avoid contact with obstacles in simulation. Static equilibrium was considered in this study. Fig. 1.9 presents HRP-2 climbing a ladder.

### **1.4.4 Robots of Honda R&D**

Nozawa et al. applied CoM feasible region to ladder climbing of a robot developed by Honda R&D in 2016. Whole-body motion planning with dynamic stability of the robot was considered and discussed. The robot succeeded in climbing a ladder with the speed of 10s/rung (Fig. 1.10). After that, E2-DR (the newest model) released by Honda R&D also succeeded in ladder climbing as Fig. 1.11 shows. However, few details were open to the public about the algorithms related to ladder climbing of E2-DR.

## **1.5 Objectives of this thesis**

As the title of this thesis, the objective of this thesis is to develop systems consisting of the following approaches to generate and guarantee stable ladder climbing of a four-limbed robot:

- 1) Appropriate and easy-to-use motion generation. According to the unique features of ladder climbing, a suitable motion generation system should be established so that unique constraints of ladder climbing could be satisfied. Besides the existing whole-body motion planning applied for humanoid robots, motion planning and generation that deals with spatial and time (mainly related to hardware limits of the robot) constraints independently in ladder climbing would simplify this issue greatly.
- 2) Stability in “swing” state of ladder climbing. When end-effector(s) is(are) moving in the air, the ladder climbing may fail if the equilibrium of force and moment cannot be maintained. Therefore, solutions of both motion generation and force feedback control in consideration with stability are introduced and applied in this thesis. This point is especially significant when the robot is climbing a ladder in 2-point contact (to be introduced in Chapter 3), which is

a climbing gait that 2 limbs of the robot move simultaneously and is rarely realized for human-sized robots.

- 3) System to guarantee successful and appropriate contacts between the robot and ladder. Unlike other types of locomotion, ladder climbing has strict constraints on contact points between the robot and the ladder rungs and even slight error of position may cause failure in contact and ladder climbing itself. Taking this issue into consideration, this thesis proposes a sensor system to obtain position and orientation data of rungs of a ladder as well as corresponding motion planning to make sure that each contact with the ladder is correct and accurate. Moreover, recognition of ladder rung with varied or even unknown specifications would also be enabled with this system, which has not been claimed to be realized by any robot before.

With 3 points above realized and integrated, the robot literally becomes capable of “stable” ladder climbing in the expected real application.

Note that this thesis deals with the ladders that:

- 1) Obey the specification in JIS (Japanese Industrial Standards). This is because the research in this thesis is studied and developed in Japan. Ladders in other standards like MIL (Military Standard) is not within the scope of this thesis but would be discussed for the future work.
- 2) Are time-invariant. In another word, this thesis only considers ladders that will not change, including deformation, destruction and any other factor accompanied with change of shape during the ladder climbing. Similar to the point above, solution to time-variant ladders would be a major concern for the future work.

## 1.6 Outline

The structure of this thesis is illustrated in Fig. 1.12. It is organized as follows:

In Chapter 1 “Introduction”, the background and motivation of this research are introduced, combined with previous and related works for reference and objectives of this research.

In Chapter 2 “Robots used in this thesis”, 2 robots developed by us, “The Prototype” and “WAREC-1” are introduced as the hardware platforms of ladder climbing. Their specifications, mechatronic systems and main features related to ladder climbing and other types of locomotion styles as well as manipulation are described, which are also the base of the contents of following chapters.

In Chapter 3 “Motion generation system”, the whole-body motion planning of ladder climbing for the four-limbed robots developed by the authors are introduced. Whole-body motion planning in this thesis is divided into 3 components: (i) Climbing gaits; (ii) End-effector trajectory planning and (iii) Body trajectory planning. Main gaits of ladder climbing and their features are introduced, and respective strategies are given. With climbing gait determined, end-effector trajectory planning is described. In this thesis planning of path and time profile in end-effector trajectory can be done individually after mathematical conversion so that spatial and hardware constraints of the robot can be dealt with separately, making trajectory planning flexible and easier. Besides, minimization of path length with given mid-points of the path are proposed in this thesis to shorten the total path that end-effector must travel, contributing to the reduction of total time required in ladder climbing. Finally, body trajectory planning is given according to different climbing gait with consideration of stability, and these 3 components form whole-body motion planning in this thesis. Besides, inverse kinematics used for the robots are also explained, which are mainly based on pseudo-inverse of Jacobian.

In Chapter 4 “Sensor feedback systems”, 2 main sensor systems are described: (i) Proximity sensor feedback system to compensate error existing between the robot and ladder; (ii) Force sensor feedback system with PID reaction force controller manages to reduce the bias of reaction force at hand and foot in 2-point contact climbing gait, which is one of the main reasons of failure in ladder climbing. For (i), specification and framework of proximity sensor system are introduced and algorithm of calculating error as well as the corresponding motion planning of error compensation are proposed. Experiments show that besides the error compensation, proximity sensor feedback system is also capable of recognizing a ladder with unknown varying specification, such as rung interval and inclination of the rung. For (ii), the details about the PID controller as well as the calculation of reaction force required for stable 2-point contact ladder climbing are also presented. Finally, the total integration of all systems in Chapter 3 and Chapter 4 are made and experiments verified the effectiveness of integrated systems, with discussion of results.

Finally, in Chapter 5 “Conclusion”, contribution of this thesis is summarized in major points. Meanwhile, limits of this thesis and prospective works based on limits analyzed are given as well.

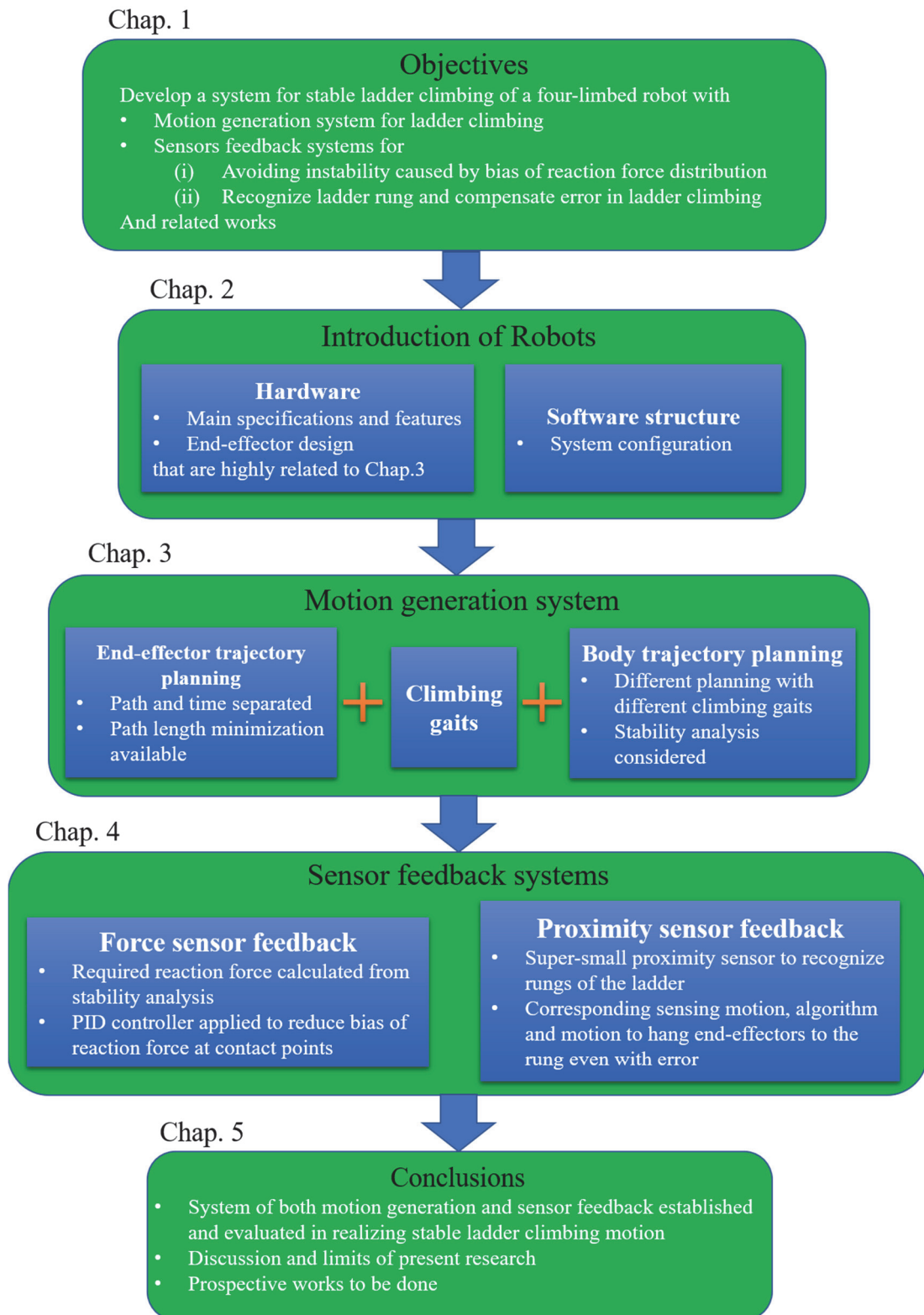
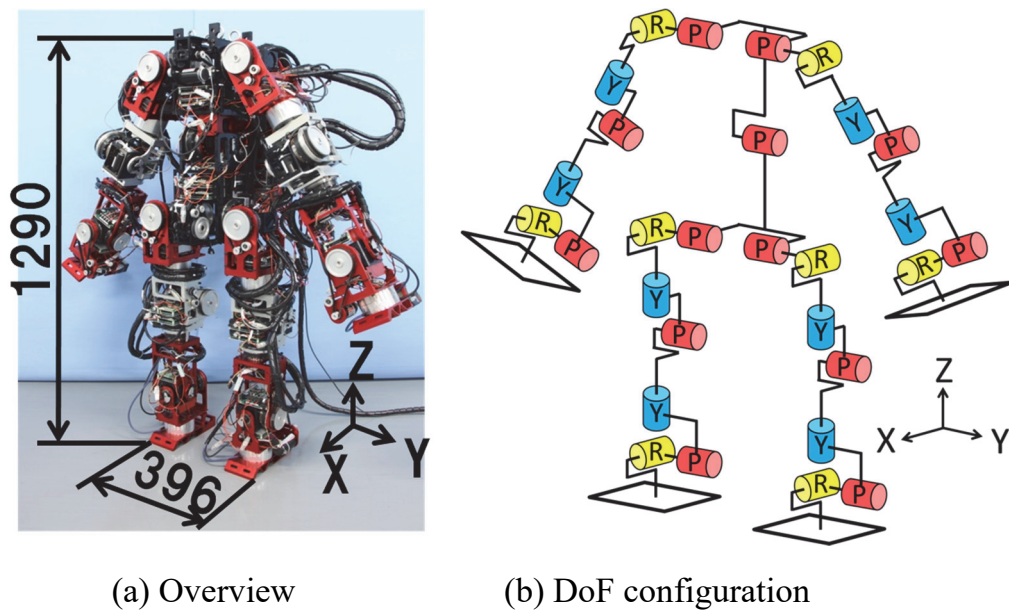


Fig. 1.12 Outline of this thesis.

## Chapter 2. Robots used in this thesis

### 2.1 Overview

Prior to the description and explanation about the main parts of this thesis, in this chapter the features of robot platforms used this thesis, including those highly concerned with this thesis, will be introduced as the prerequisite knowledge. Especially, the end-effector trajectory generation in ladder climbing motion to be



(a) Overview

(b) DoF configuration

Fig. 2.1 The Prototype [23].

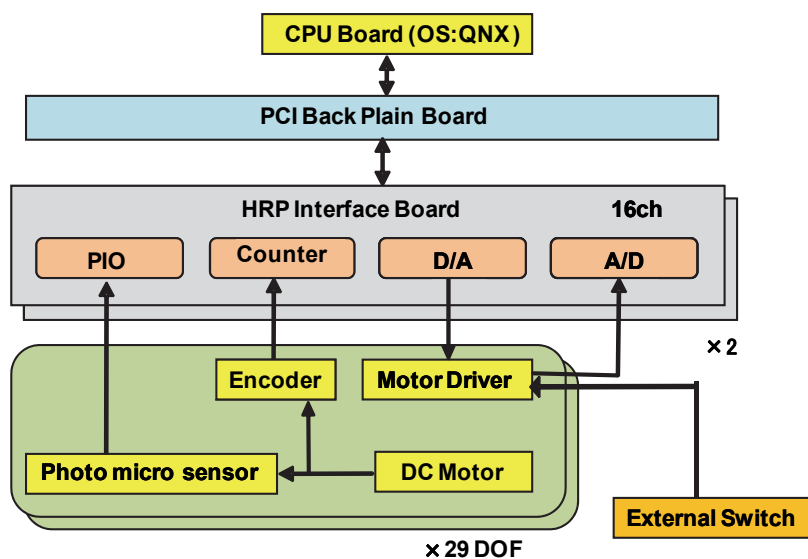


Fig. 2.2 Mechatronic system configuration of The Prototype [24].

introduced in Chap. 3 and sensor feedback for error compensation to be introduced in Chap. 4 are highly dependent on the hardware design of end-effector, and so are the size and weight of the robots for whole-body motion generation to be introduced in Chap. 3. These details about the robots will be included in the brief introduction about the overall specification of robots as well as system configuration in this chapter to offer complete fundamental information of the robot platforms in this thesis.

The study in this thesis began at nearly at the same time point as the initiation of project “ImPACT” and to meet the requirement of developing robot platforms to validate our proposed concepts and ideas for disaster response robot, the following 2 robots were developed: The Prototype and WAREC-1.

## 2.2 Introduction of The Prototype

The first robot to be introduced was designed and assembled in 2014. It has no official name and for the convenience it is called “The Prototype” in this thesis. Its overview and DoF (Degree of Freedom) configuration can be seen in Fig. 2.1. Its mechatronic system configuration is illustrated in Fig. 2.2.

As is explained in Chapter 1, our disaster response robot should be capable of performing various locomotion styles to deal with complicated and diverse types of environment in disaster areas. Taking this point into consideration, we chose four-limbed robot (legged robot) instead of popular robots that have been engaged into disaster area, such as wheeled robots and crawler robots. This choice is especially important because the concentration of locomotion style for this robot in this study is on the vertical ladder climbing, which is highly required in both indoor and outdoor and both disaster response and routine maintenance of infrastructures, but few robots were created to meet these needs.

Table 2-1 Specifications of The Prototype.

Term	Value
Height mm	1290
Width mm	396
Weight kg	110
Number of DoF	One limb: 7 Body: 1 (Pitch) Total: 29
Sensors equipped	One force/torque sensor for each limb (4 in total)



The main specifications of The Prototype are listed in Table 2-1. One of the biggest feature of this robot is that all its 4 limbs share the same structure, which is different from humanoid robots. This design eliminates the difference of all limbs to guarantee that all limbs are functionally identical. In this way, all limbs can be used for both arm and leg, and thus the robot can continue working with rest of the limbs in case that one limb is broken or out of control. Besides, symmetric design and configuration of limbs also make it possible for the robot to perform locomotion (like biped walking) or manipulation even if it is upside down. There are also 4 force/torque sensors equipped beside end-effectors for the force

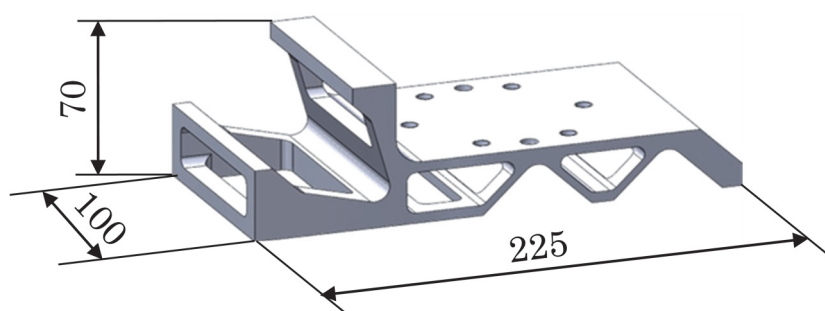
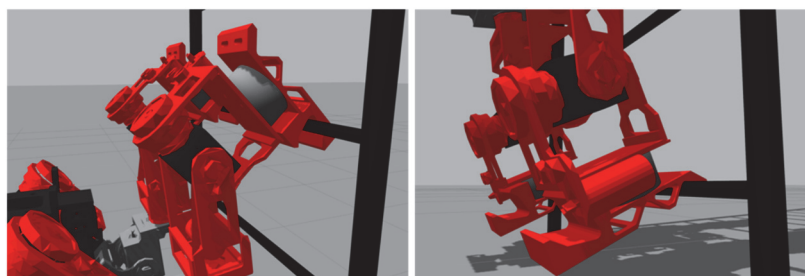
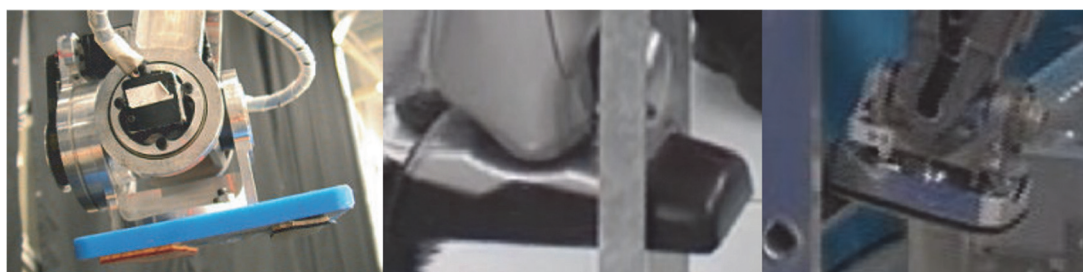


Fig. 2.3 Design and scale of the end-effector [25].



(a) Working as a hook (b) Working as a foot

Fig. 2.4 Different usages of the end-effector.



(a) Gorilla-III [17]

(b) HRP-2[20]

(c) Robot of Honda  
H&D [21]

Fig. 2.5 End-effectors of other ladder climbing robots for foot.

control.

The end-effector equipped at the end of each limb of The Prototype is also identically designed for ladder climbing. It can be used for both hand and foot while climbing the ladder. Its overview and its 2 usages in ladder climbing are presented in Fig. 2.3 and Fig. 2.4, respectively. Its overall scale and design concept are for the climbing of ladder in JIS (Japanese Industrial Standard) [25].

To avoid the complication of mechatronic system, we did not choose robot hand with multiple actuators as the end-effector, since ladder climbing requires high output actuators to sustain the self-weight of the robot, and robot hand that makes this possible would be unnecessarily big for ladder climbing.

As is shown in Fig. 2.3, there are one hook-shaped part and two groove-shaped parts on the end-effector so that end-effectors would not slip out from rungs of the ladder. In comparison with other ladder climbing robots, our end-effector not only unifies the design for hands and feet, but also avoids slippery of feet while other robot climbers tended to use flat plate-shaped end-effectors for foot (Fig. 2.5) with the risk of slippery remained if there is no sufficient friction force.

### 2.3 Introduction of WAREC-1

The second robot as well as the newest robot developed is called WAREC-1 (WAseda REsCuer-No.1). Its overview and DoF configuration are depicted in Fig. 2.6 and its specification is presented in Table 2-2.

WAREC-1 is the improved version of The Prototype. Both the features inherited from The Prototype and features improved are concluded in Table 2-3. Its mechatronic system configuration is depicted in Fig. 2.7.

Table 2-2 Specifications of WAREC-1.

Height mm	1690
Width mm	497
Weight kg	155
Number of DoF	One limb: 7 Total: 28
Sensors equipped	One force/torque sensor for each limb (4 in total) Two proximity sensors for each end-effector (8 in total) One IMU in the body Ten depth cameras around the body (optional)

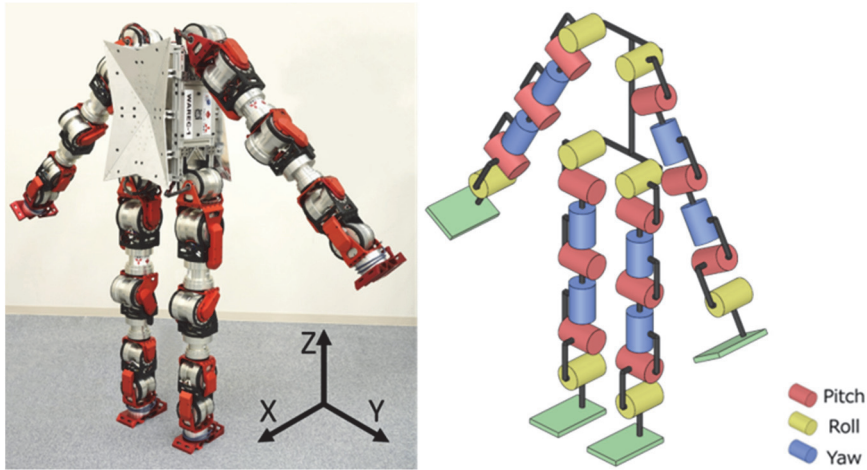


Fig. 2.6 Overview and DoF configuration of WAREC-1 [26].

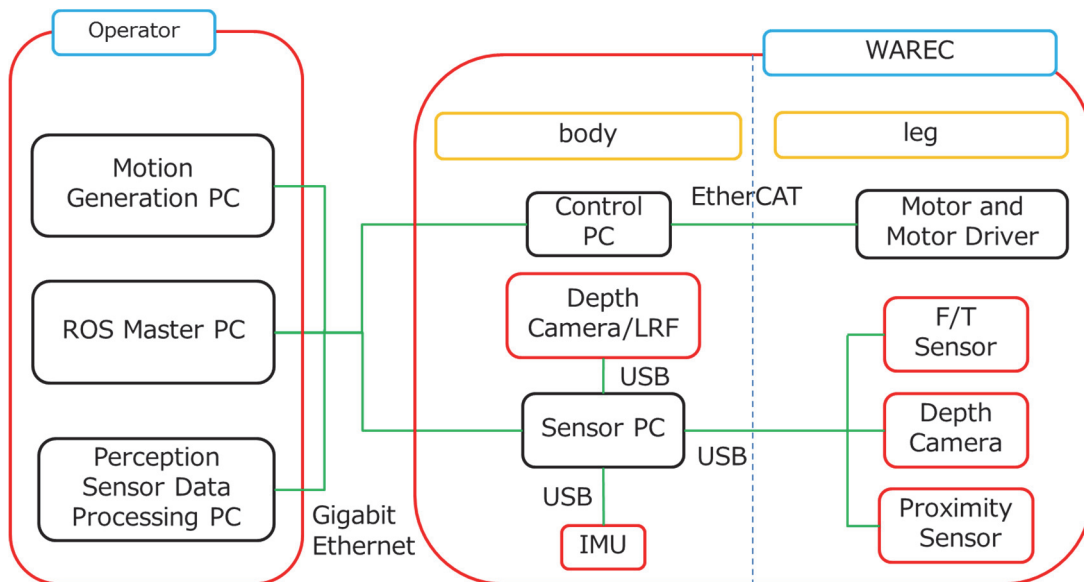


Fig. 2.7 System configuration of WAREC-1.

As the successor of The Prototype, WAREC-1 was designed so that it is capable of not only ladder climbing but also crawling, a locomotion style that the body of the robot and its limbs contact the ground alternately and move forward (Fig. 2.8). Therefore, the improved features above are necessary to make the robot contact the ground and start crawling, which will also be mentioned again in a more detailed manner for the application of error compensation by sensor feedback in Chap. 4.

As for the capability of ladder climbing, of course, is improved as well for WAREC-1. Its slimmer body enables it to climb through safe cage (Fig. 2.9), an attachment that can be often seen on ladders to decrease the risk of falling. Higher output of the actuators also makes WAREC-1 possible to climb faster and longer

limbs allow it to perform ladder climbing with a wider range of available postures.

In this study, results of ladder climbing performed by WAREC-1 are mainly discussed and some results from The Prototype will also be concerned for necessary explanation and for reference.

Table 2-3 Features of WAREC-1 in comparison with The Prototype.

	The Prototype	WAREC-1
Inherited features	Identical design of 4 limbs and end-effectors	
	Same end-effector design for ladder climbing	
	Force/Torque sensors equipped	
Different features (Improved in WAREC-1)	All wirings, encoders, decelerators and related gears exposed to the external environment	Hollow structure of actuator units that (i) allow wirings to go through joints without the exposure and (ii) encoders and decelerators embed inside
	Centralized control with much more wirings required	Decentralized control to decrease the number of necessary wirings greatly
	External PC with much bigger size	Smaller PC hid inside the body
	No contact with external environment available except for end-effectors	Concave body design allowing direct contact with the ground
	Actuator output: 150W for all	Actuator output: 370, 580 and 750W in different joints
	No IMU equipped	IMU sensor added to measure the inclination of the body in ladder climbing and crawling

## 2.4 Summary

This chapter introduces and describes the robot platforms for ladder climbing in this thesis. Their features and designs related to ladder climbing are focused on as the base and prerequisite knowledge to be known in advance before the introduction of the main contents of the study in this thesis start.

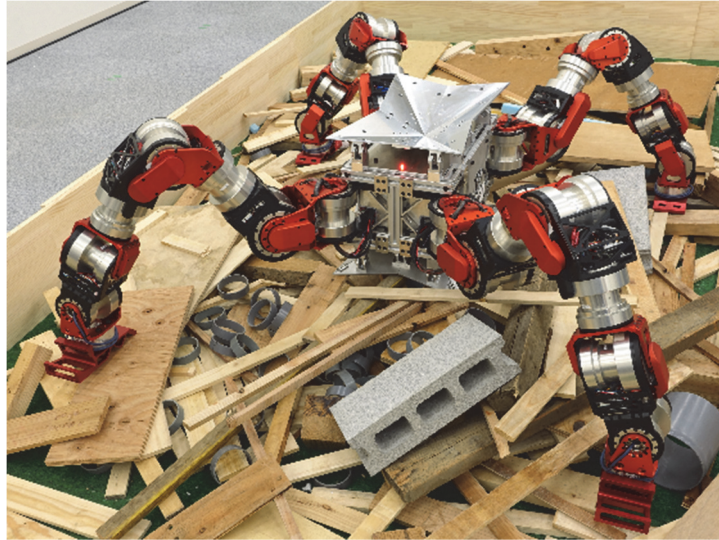


Fig. 2.8 WAREC-1 crawling on uneven terrain.



Fig. 2.9 WAREC-1 climbing a vertical ladder with safety cage.



## Chapter 3. Motion generation system

### 3.1 Introduction

With the consideration of end-effector design in Chap.2, from our perspective first it is necessary to generate motion that enables all end-effectors to move from the current position to the target position (in another word, from a rung to another rung) without colliding with any rung unexpectedly. A successful ladder climbing motion thus can be divided into the following 3 steps:

- 1) The end-effector(s) leaves (leave) the current rung(s) without getting stuck. As the expense of avoiding slip between the end-effectors and rungs of ladder, the hook and groove part of end-effector may get stuck and appropriate motion planning is required;
- 2) The end-effector(s) moves up or down to a position higher to the target rung without colliding with the target rung inappropriately. For instance, when climbing up, if the end-effector moving up collides with the target rung (a higher rung) from the bottom, then it would not be able to reach the target rung from above, which is an appropriate way;
- 3) The end-effector(s) is (are) put on the target rung(s) correctly.

And ladder climbing motion of end-effectors may fail if any one of the steps above cannot be guaranteed, with the failed cases illustrated in Fig. 3.1.

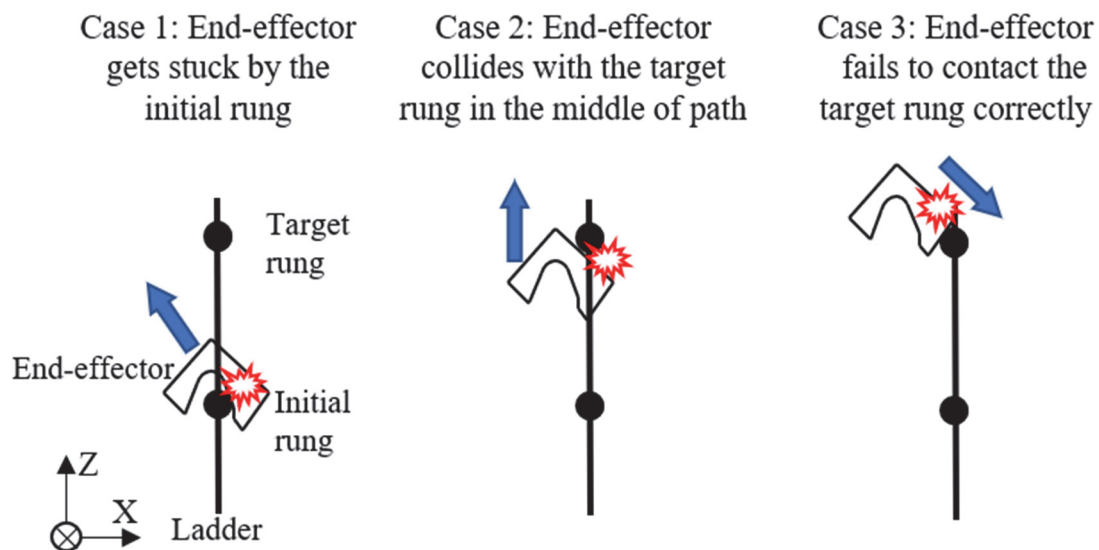


Fig. 3.1 Trouble cases that may happen between the end-effector and rung.  
Blue arrows are the direction that the end-effector is moving towards.

With discussions above, it is not difficult to find that ladder climbing has different features and constraints with multi-legged locomotion styles, such as biped and quadruped walking in the following points, which are also significant bases of the rest of contents in this chapter:

- 1) Constraint of start and end position: Each step of end-effectors must be on a line, not a surface. It is much stricter than multi-legged walking.
- 2) Constraint of path: Besides the point above, the path of end-effectors must guarantee that collision with the target rung would not happen.

To generate whole-body motion of the robot in ladder climbing, 3 crucial components are introduced and explained in the later sections:

- 1) Gaits (climbing patterns) of ladder climbing; It determines the way limbs of robot move in ladder climbing.
- 2) End-effector trajectory planning. It determines the way end-effectors move so that they can reach the target rung from current rung successfully; In this thesis path and time in trajectory are planned individually, which will be explained in Section 3.3.
- 3) Body trajectory planning.

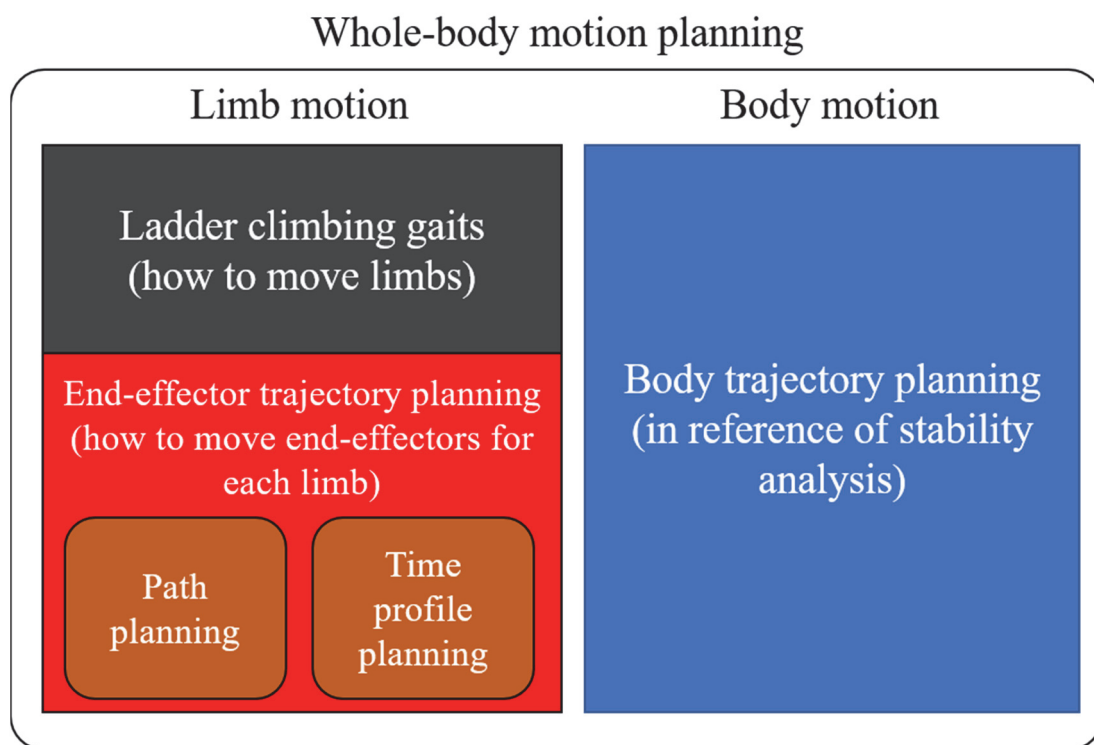


Fig. 3.2 Whole-body motion planning scheme.



And the combination of them finally determines the whole-body motion planning of the robot in ladder climbing. The scheme of whole-body motion planning is depicted in Fig. 3.2.

### 3.2 Gaits of ladder climbing

The word “gait” is often used for describing the order and the number of limbs to move in multi-legged walking. Since our robots both have 4 limbs, in the perspective of quadruped walking ladder climbing patterns of the robot in this thesis can also be considered as quadruped walking gaits, which have also been introduced by the former studies [17].

Although human body is flexible and able to be bent to perform various postures in climbing, such as crossed arms or legs in rock climbing and even reversed posture with legs over the head, these high-difficulty climbing gaits (Fig. 3.3) are not within the scope of this thesis but will be considered in the future for the limit of robots’ material and hardware structure.

Similar to quadruped walking, different choice of gaits in ladder climbing brings huge influence on the ladder climbing motion, mainly in stability (to be discussed in the later sections) and it is the same for strategy of ladder climbing as well. Therefore, in the procedures of whole-body motion planning and generation, gaits of ladder climbing would be determined first.

In this thesis, the following 2 conventional climbing gaits will be mainly discussed: (i) 3-point contact climbing; (ii) 2-point contact climbing. Explicitly, “3-point contact” means that while climbing there are always at least 3 contact points between the robot and ladder, and this is the same for “2-point contact”.



(a) Crossed arms [40]

(b) Legs over the head [41]

Fig. 3.3 Climbing “gaits” with high difficulty.

These 2 climbing gaits can be divided further: 4-step and 5-step types for 3-point contact climbing and trot and pace for 2-point contact climbing. Illustration of them in steps can be seen in Fig. 3.4 ~ Fig. 3.6.

Table 3-1 Comparison of 3-point contact and 2-point contact climbing.

	3-point contact climbing	2-point contact climbing
Advantage(s)	Easy to maintain stability	Faster motion with less steps; 3-point contact: 4 or 5 step/rung; 2-point contact: 1 step/rung.
Disadvantage(s)	Slower motion with more steps required	Proper planning or control of climbing motion may be needed.

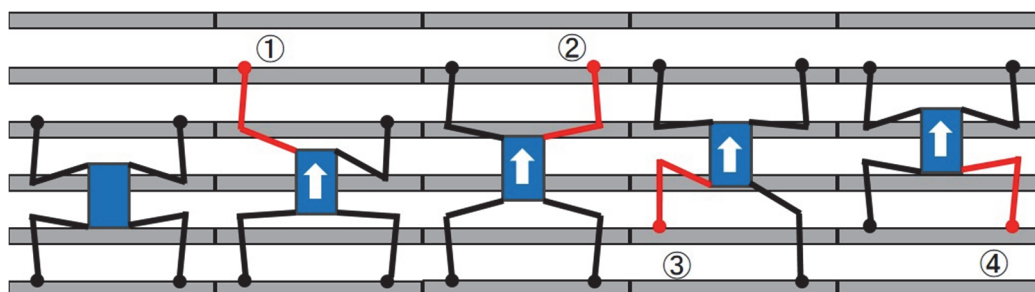


Fig. 3.4 3-point contact climbing (in 4 steps, with body keep moving).

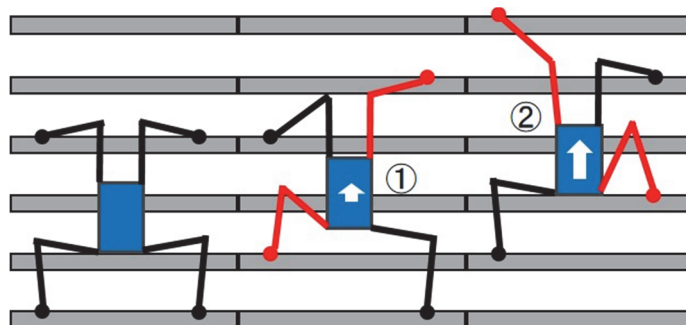


Fig. 3.5 2-point contact climbing (not used in this thesis).  
(trot gait, with 2 limbs in different side move simultaneously)

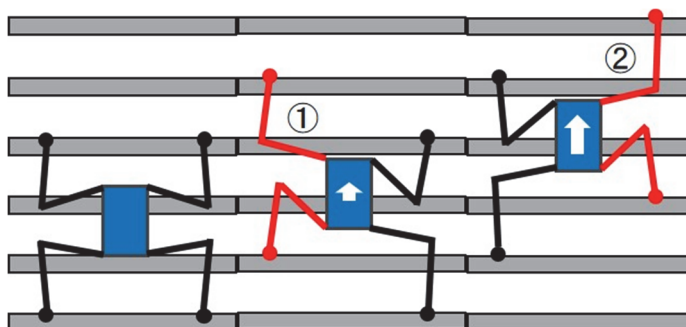


Fig. 3.6 2-point contact climbing.  
(pace gait, with 2 limbs in the same side move simultaneously)

The characteristics of 3-point and 2-point contact climbing gait can be concluded in Table 3-1. Since at least 3 points are required for forming a plane, apparently 3-point contact climbing is more stable than 2-point contact climbing (although this does not mean that 3-point contact climbing is absolutely safe), but it also has the shortcoming that more steps are required for climbing a rung than 2-point contact climbing. On the other hand, 2-point contact climbing needs less steps and is theoretically faster than 3-point contact climbing under the same circumstances but risk of slippery and falling from ladder must be eliminated by appropriate motion planning and/or control methods. In practical application, the choice of these 2 types of climbing gaits depends mainly on the conditions of the target ladder and power supply of the robot itself. Considering the safety of the robot, 2-point contact ladder climbing is chosen if and only if the ladder is wide and tough enough for the robot to make dynamic climbing motion and the power supply cannot support the whole ladder climbing if 3-point contact climbing is chosen. For all other cases, 3-point contact climbing is preferred even if 2-point contact climbing is available.

The details of selection for climbing gaits will be presented further in Section 3.4 as the first step of whole-body motion planning.

### **3.3 End-effector trajectory planning**

After the climbing gait is decided, trajectory planning of end-effectors becomes a significant point in realizing successful steps of climbing motion. As is explained in the beginning of this chapter, constraints of start and end position as well as path in trajectory of end-effector must be considered thoroughly. Meanwhile, the limits in hardware level cannot be ignored as well. Specifically, upper limit of joint angle controlled by inverse kinematics to be introduced in Section 3.6.2, angular velocity, and output torque for each joint must be obeyed while the robot is moving.

To establish a trajectory planning that satisfy both geometric constraints of end-effector and hardware limits, in our opinion it is necessary to separate path (for geometric constraints) and time profile (for hardware limits) in trajectory so that they can be planned individually, which has barely been focused on in the field of ladder climbing robots. With path and time profile separated, it is possible to avoid limit over for respective constraints and limits, even enabling flexible and detailed adjustment according to the need in application. Note that time profile is different from “time scale”.

In path planning, the shape of the path is determined and in time profile planning speed along the given path is given. In this thesis the separation of path and time profile is mathematically processed by the method of arc-length parameterization so that they two can be done independently without influencing each other, which is inspired from the idea of “event-based planning” proposed by Tarn and Xi [28]. However, this idea has rarely been applied on ladder climbing motion. In the following contents of this section, the math knowledge involved will be introduced first and details of our proposed path-time independent trajectory planning method will be described ([24], [29]).

### 3.3.1 Prerequisite math knowledge

Now we will explain the reason why the cubic spline is employed to act the role of the interpolation function in our path planning (Section 3.3.2). According to the characteristics of motor, minimal acceleration will release the burden of motor and is thus desirable in practical application. Based on this consideration, we need to find what type of curve possesses the minimal acceleration. In order to achieve this purpose, the variation method is used in Riemannian manifolds ([30], [31]). Since Euclidean space is a special Riemannian manifold, the results obtained in Riemannian manifolds are also effective in Euclidean space.

Next, let us introduce briefly about Riemannian geometry. It is very known that the theory of general relativity by Einstein is a generalization of the Newton’s mechanics, where Riemannian geometry is used to give the energy-momentum equation. In addition, geodesic, the shortest distance connecting two points of a space gives the motion equation of objects. As the generalization of Euclidean space, Riemannian manifold  $(M, g)$  with the non-trivial metric  $g$  can be seen a symmetric positive-definite matrix. Roughly speaking, a Riemannian manifold in local is a Euclidean space indeed. The difference of Euclidean space and Riemannian space is that the former is a flat space and the latter is a curved space. To describe a curved Riemannian space, we need to give the concept of curvature tensor of a Riemannian manifold. Let  $X$ ,  $Y$  and  $Z$  be vector fields over  $M$ , the curvature tensor is defined by

$$R(X, Y)Z = \nabla_X \nabla_Y Z - \nabla_Y \nabla_X Z - \nabla_{[X, Y]} Z, \quad (3.1)$$

where the symbol  $\nabla$  denotes the covariant derivative. With (3.1) we can obtain the expression of the coefficients  $R_{ijk}^l$  or  $R_{ijkl} = R_{ijk}^m g_{mj}$ , where  $g_{ij}$  is the components

of the Riemannian metric  $g$ . The sectional curvature is defined as

$$K_{ij} = -\frac{R_{ijij}}{g_{ii}g_{jj} - g_{ij}^2}, \quad (3.2)$$

and (3.2) describes how curved a Riemannian manifold is. The fundamental contents about the Riemannian geometry can be seen in Appendix C.

Suppose that  $M$  is a smooth manifold and  $\gamma: [0,1] \rightarrow M$  a smooth curve (the definition of smoothness for manifold and curves on a manifold can be seen in [31]). Denote by

$$F(\gamma) = \int_0^1 \langle \nabla_{\frac{d}{dt}} \dot{\gamma}, \nabla_{\frac{d}{dt}} \dot{\gamma} \rangle dt, \quad (3.3)$$

a functional of  $\gamma$ , where  $\dot{\gamma}$  denotes the speed of the curve  $\gamma$ , and  $\langle \cdot, \cdot \rangle$  denotes the Riemannian metric on  $M$ . When  $M = \mathbf{R}^n$ , i.e., Euclidean space, the curvature tensor  $R$  of  $M$  is zero, and  $\nabla_{\frac{d}{dt}} \dot{\gamma}$  is exactly  $\ddot{\gamma}$ , the second-order derivative of  $\gamma$ . In order to obtain the minimum value of the functional  $F$ , the variation method can be utilized. Now we consider the space  $\{\gamma\}$  of smooth curves,  $\gamma: [0,1] \rightarrow M$ , satisfying

$$\gamma(0) = x_0, \gamma(1) = x_1, \dot{\gamma}(0) = v_0, \dot{\gamma}(1) = v_1. \quad (3.4)$$

In our case, we suppose that start speed and end speed are zero. We have the following proposition [31]:

**Proposition.**  $\gamma \in \{\gamma\}$  is a critical point of  $F(\gamma)$  if and only if  $\gamma$  satisfies

$$\nabla_{\frac{d}{dt}}^3 \dot{\gamma} + R(\nabla_{\frac{d}{dt}} \dot{\gamma}, \dot{\gamma}) \dot{\gamma} = 0 \quad (3.5)$$

for all  $t \in [0,1]$ .

From the proposition above we see that when  $M = \mathbf{R}^n$ , namely, the Riemannian manifold is a flat Euclidean space,  $\gamma^{(4)} = 0$  and  $\gamma$  is therefore a cubic polynomial. In another word,  $\gamma(t) = a_0 + a_1 t + a_2 t^2 + a_3 t^3$  can be given. On the other hand, noting that when  $M = \mathbf{R}^3$ , the functional  $F$  becomes

$$F(\gamma) = \int_0^1 \langle \ddot{\gamma}, \ddot{\gamma} \rangle dt, \quad (3.6)$$

and from the expression of (3.6) it is apparent that the functional  $F$  is minimized by the cubic polynomial. Precisely, among the curve family  $\{\gamma\}$  the cubic polynomial has the minimal acceleration.

**Remark.** The proposition above involves the general case of Riemannian manifold which may be a curved space. In this thesis, we only focus the robot motion on a Euclidean space instead of a curved Riemannian space. In fact, in order to give more precise motion path of robot, the later item including curvature in (3.5) plays important role, and we will consider such situation in the future work.

### 3.3.2 Path planning

For path planning, cubic spline curves are chosen as the path, calculated by spline interpolation connecting given start point, end point and mid-points along the desired path. Besides the reason explained in the last section, spline curves also provide smooth path, which has been verified to be contributive to reducing peak load to motors while climbing the ladder [29]. In addition, cubic spline curve with less orders can also be calculated with less computational resource.

To begin with, set  $s_j(t) = (x(t), y(t), z(t))$  as the expression of each piecewise polynomial for cubic spline interpolation generating the path, where  $x(t)$ ,  $y(t)$  and  $z(t)$  are the coordinate of end-effector in X-axis, Y-axis and Z-axis, respectively. With the definition of cubic spline interpolation curve, we have the following equation:

$$s_j(t) = a_j + b_j(t - t_j) + c_j(t - t_j)^2 + d_j(t - t_j)^3, j = 1, 2, \dots, 5. \quad (3.7)$$

With the given initial point, terminal point and mid-points for spline interpolation, it is not difficult to find that  $s_j(t_j) = a_j, j = 1, 2, \dots, 5$  and  $a_j$  are all given constants as well. The following continuity conditions should be satisfied:

$$s_{j+1}(t_{j+1}) = s_j(t_{j+1}), \quad (3.8)$$

$$\dot{s}_{j+1}(t_{j+1}) = \dot{s}_j(t_{j+1}), \quad (3.9)$$

$$\ddot{s}_{j+1}(t_{j+1}) = \ddot{s}_j(t_{j+1}). \quad (3.10)$$

Setting  $h_j = t_{j+1} - t_j$ , we have

$$b_j = (c_j - c_{j-1})h_{j-1} + 2c_{h-1}h_{h-1} + b_{j-1}, \quad (3.11)$$

$$d_j = -\frac{1}{3} \cdot \frac{(c_j - c_{j-1})}{h_j}. \quad (3.12)$$

With (3.11) and (3.12), (3.8) ~ (3.10) can be written as

$$\mathbf{AC} = \mathbf{b}, \quad (3.13)$$

where

$$\mathbf{A} = \begin{pmatrix} 1 & 0 & 0 & 0 & 0 \\ h_1 & 2(h_1 + h_2) & h_2 & 0 & 0 \\ 0 & h_2 & 2(h_2 + h_3) & h_3 & 0 \\ 0 & 0 & h_3 & 2(h_3 + h_4) & h_4 \\ 0 & 0 & 0 & 0 & 1 \end{pmatrix}, \quad (3.14)$$

$$\mathbf{C} = \begin{bmatrix} c_1 \\ c_2 \\ c_3 \\ c_4 \\ c_5 \end{bmatrix}, \mathbf{b} = \begin{bmatrix} 0 \\ \frac{3a_1}{h_1} - \left(\frac{3}{h_1} + \frac{3}{h_2}\right)a_2 + \frac{3a_3}{h_2} \\ \frac{3a_2}{h_2} - \left(\frac{3}{h_2} + \frac{3}{h_3}\right)a_3 + \frac{3a_4}{h_3} \\ \frac{3a_3}{h_3} - \left(\frac{3}{h_3} + \frac{3}{h_4}\right)a_4 + \frac{3a_5}{h_4} \\ 0 \end{bmatrix}. \quad (3.15)$$

Solving matrix equation of (3.13), the expressions of  $c_1 \sim c_5$  with respect to  $h_1 \sim h_4$  can be obtained. That is

$$c_j = c_j(h_1, h_2, h_3, h_4), j = 1, 2, 3, 4, 5. \quad (3.16)$$

Furthermore, by (3.11) and (3.12) due to the known  $c_j$  we can obtain the expressions of  $b_1 \sim b_5$  and  $d_1 \sim d_5$ . Since

$$x_j(t) = a_{xj} + b_{xj}(t - t_j) + c_{xj}(t - t_j)^2 + d_{xj}(t - t_j)^3, \quad (3.17)$$

$$y_j(t) = a_{yj} + b_{yj}(t - t_j) + c_{yj}(t - t_j)^2 + d_{yj}(t - t_j)^3, \quad (3.18)$$

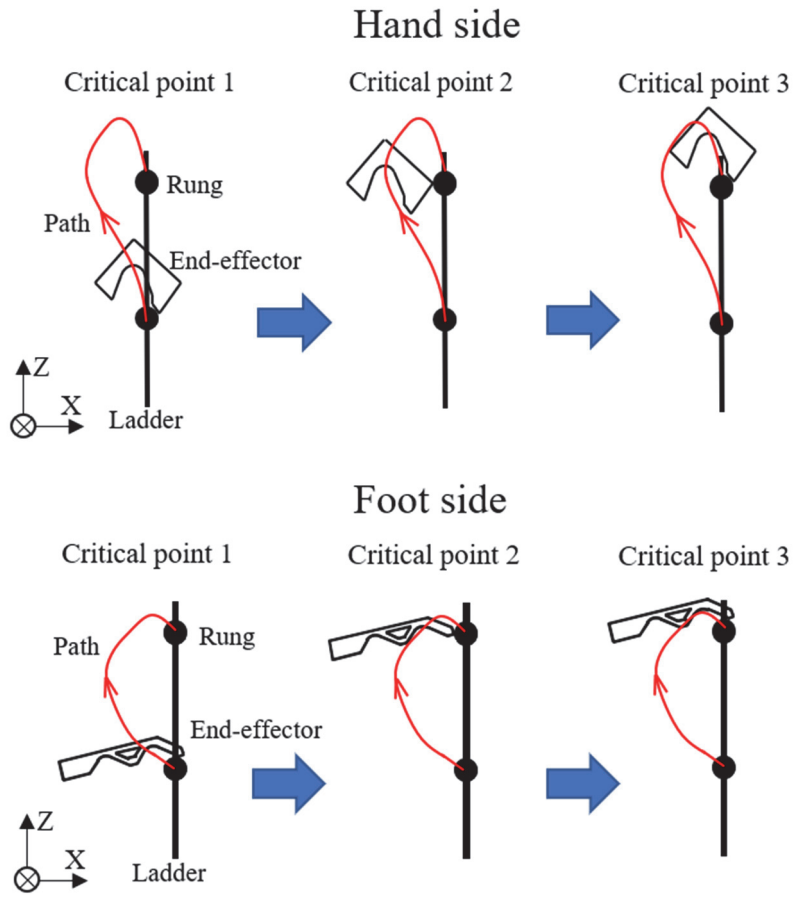


Fig. 3.7 Critical points with risk.

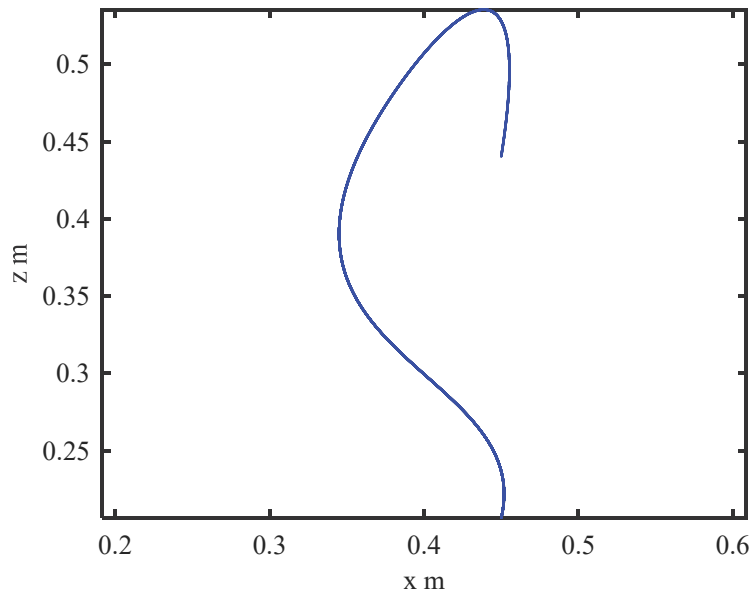


Fig. 3.8 Generated end-effector path of climbing up motion in XoZ space. Coordinates in X and Z-axis is the distance from the origin to end-effector.



$$z_j(t) = a_{zj} + b_{zj}(t - t_j) + c_{zj}(t - t_j)^2 + d_{zj}(t - t_j)^3, j = 1, 2, 3, 4, 5, \quad (3.19)$$

the arc-length of the whole path can be given by

$$l(h_1, h_2, h_3, h_4) = \sum_{j=1}^5 \int_0^{t_j} \sqrt{\dot{x}_j^2(\tau) + \dot{y}_j^2(\tau) + \dot{z}_j^2(\tau)} d\tau. \quad (3.20)$$

### 3.3.2.1 Selection of mid-points in path planning

To deal with the troubles in Fig. 3.1, Fig. 3.7 shows critical points as reference. Apparently, the positions of these critical points are dependent on the shape design of end-effectors, as is explained in Chap. 2. The mid-points of end-effector path are set to be farther to the rungs than critical points with margins empirically determined so that the risk of undesirable collisions can be fully eliminated. An example of generated path (depicted in XoZ plane to make itself easier to see) can be seen in Fig. 3.8.

### 3.3.2.2 Path length minimization (optional)

With mid-points to guarantee appropriate end-effector path in ladder climbing fixed, there is still possibility for further optimization. In this thesis, minimization of path length can be applied optionally. To solve the minimum value of the path length (3.20), we use a sequential quadratic programming (SQP) method [32], which is “fmincon” in MATLAB. In this method, at each iteration the function solves a quadratic programming (QP) subproblem solved by active set strategy. An estimate of the Hessian of the Lagrangian is updated at each iteration with Broyden-Fletcher-Goldfarb-Shanno (BFGS) formula and a line search is performed. With this method, the best combination of  $h_1 \sim h_4$  can be obtained, minimizing the total path length of each segment. This can be contributive to reducing total time spent in ladder climbing.

The comparison of the path before and after length minimization is shown in Fig. 3.9. Before length minimization, the parameters  $h_1 \sim h_4$  of spline curves consisting the path are randomly chosen and after path length minimization  $h_1 \sim h_4$  are uniquely determined by method introduced above. Distinctly, the path after length optimization goes less distance, although they all pass the same mid-points. Their length data are shown in Table 3-2 with parameters shown in Table 3-3. These results prove that the path length with optimization (red curve) is the shortest one among 3 lines. Table 3-3 shows specific values of parameter  $h_1 \sim h_4$  for each curve.

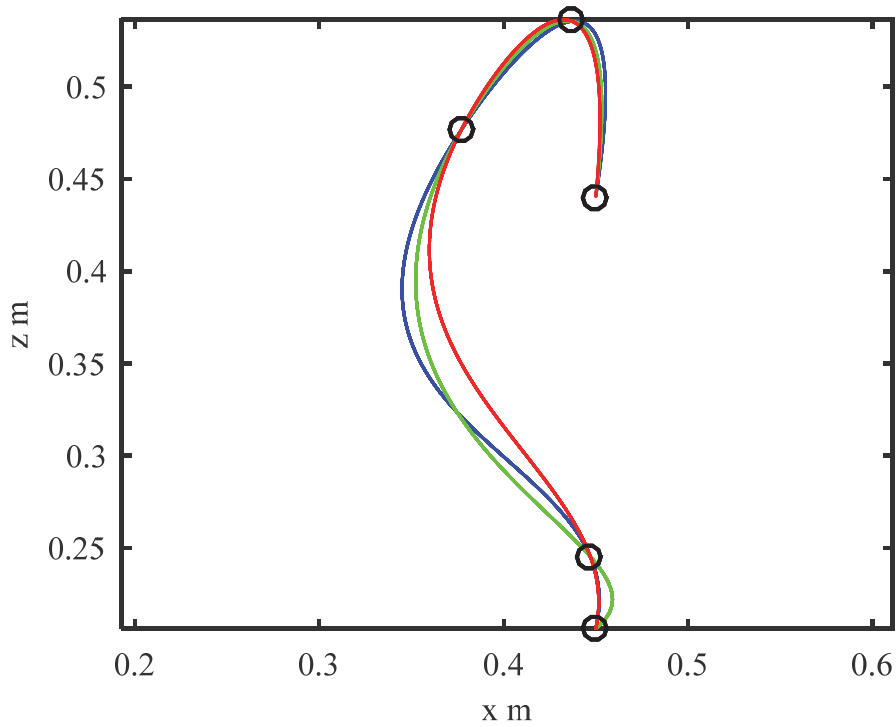


Fig. 3.9 Comparison of path length of climbing up motion.  
(The start, end and mid-points are marked by circles)

Table 3-2 Comparison of path length.

Condition	Path length mm
With path length minimization	488 (the red curve in Fig. 3.9)
Without path length minimization (parameters randomly chosen)	506 (the green curve in Fig. 3.9) 502 (the blue curve in Fig. 3.9)

Table 3-3 Value of parameters in path length comparison.

Condition	Value of parameter				
	$h_1$	$h_2$	$h_3$	$h_4$	$h_5$
Case 1: Green curve	0	4	15.36	18	20.1
Case 2: Blue curve	0	3	10	15	20.1
Case 3: Red curve (optimized)	0	2.28	15.36	17.82	20.1

### 3.3.3 Separation of path and time: Arc-length parameterization

The idea of event-based planning proposed by T. Tarn and N. Xi [28] opened a door to the field of non-time-based planning. In their works idea of individual

planning for path and time profile is provided, but unfortunately no specific methods of separation between path and time profile was given.

In order to realize non-time-based planning, we refer to the approach discussed in [33] and [34], arc-length parameterization, and bring this idea into application [24]. The essential idea of arc-length parameterization is to substitute the variable in former planning, say  $t$ , to arc-length  $s$  here. However, this substitution requires the condition that  $s$  must be the real path length, and its calculation is shown below. Let  $\gamma:[0, 1]\rightarrow\mathbf{R}^3$  be a smooth curve denoted by

$$\gamma(t) = (x(t), y(t), z(t)), \quad (3.21)$$

where  $t \in [0,1]$  is an arbitrary parameter. The arc-length of  $\gamma$  satisfies

$$s(t) = \int_0^t \sqrt{\dot{x}^2(\tau) + \dot{y}^2(\tau) + \dot{z}^2(\tau)} d\tau. \quad (3.22)$$

When  $t=s$ , namely, the parameter  $t$  is adapted as the arc-length parameter of  $\gamma$ , then

$$\sqrt{\dot{x}^2(s) + \dot{y}^2(s) + \dot{z}^2(s)} = 1 \quad (3.23)$$

should be satisfied. It is well known that the arc-length parameterization for cubic spline curves cannot be expressed as a combination of elementary functions, however can be evaluated numerically. In fact, the numerical solution for inverse function  $t=t(s)$  of  $s(t)$  can be obtained, hence we have curve  $\gamma(t(s))$  with the arc-length parameter  $s$  [33]. After introducing arc-length parameter  $s$ , we obtain the new curve

$$\tilde{\gamma}(s) = (\tilde{x}(s), \tilde{y}(s), \tilde{z}(s)), \quad (3.24)$$

with the arc-length parameter

$$s \in [s_j, s_{j+1}], j = 0, 1, \dots, m-1, \quad (3.25)$$

$$\tilde{x}_j(s) = \tilde{a}_{xj} + \tilde{b}_{xj}(s - s_j) + \tilde{c}_{xj}(s - s_j)^2 + \tilde{d}_{xj}(s - s_j)^3, \quad (3.26)$$

$$\tilde{y}_j(s) = \tilde{a}_{yj} + \tilde{b}_{yj}(s - s_j) + \tilde{c}_{yj}(s - s_j)^2 + \tilde{d}_{yj}(s - s_j)^3, \quad (3.27)$$

$$\tilde{z}_j(s) = \tilde{a}_{z_j} + \tilde{b}_{z_j}(s - s_j) + \tilde{c}_{z_j}(s - s_j)^2 + \tilde{d}_{z_j}(s - s_j)^3, \quad (3.28)$$

where  $j=0, 1, 2, \dots, m-1$ . And

$$|\dot{\tilde{\gamma}}(s)| = \sqrt{\dot{\tilde{x}}^2(s) + \dot{\tilde{y}}^2(s) + \dot{\tilde{z}}^2(s)} = 1 \quad (3.29)$$

is satisfied.

### 3.3.4 Time profile planning

After path planning and arc-length parameterization, free time profile planning becomes available because the separation of path and time profile comes from arc-length parameterization and it ensures that path will always stay the same, no matter how we change the time planning  $s(t)$ , making it convenient for us to freely choose the desired time profile.

Excessive acceleration or deceleration would be harmful to motors in robots' joints and thus should be avoided. Viewing from this aspect, the ideal motion plan with least burden to the motor is that the robot should start moving without or with slight initial velocity and acceleration, accelerate gradually until it reaches desired speed, slow down gradually when it gets close to the terminal point and stops without or with slight deceleration as well in the end. To satisfy this plan, we choose the following "s-shaped" piecewise function

$$s(t) = \begin{cases} at^2, & 0 \leq t \leq t_1 \\ bt + c, & t_1 \leq t \leq t_2 \\ s_f - a(t - t_f)^2, & t_2 \leq t \leq t_f \end{cases} \quad (3.30)$$

as the time planning. Three parts refer to acceleration period, constant speed period and deceleration period, where  $t_1$  is the terminal time for acceleration period,  $t_2$  is the initial time for deceleration period,  $t_f$  is the total time of whole motion and  $s_f=s(t_f)$  denotes the total path length traveled. Coefficients  $a$ ,  $b$  and  $c$  are all constants. Note that  $t$  here infers time and it is different from the meaning in path planning and spline interpolation.

To realize minimized burden of motors, our time planning should satisfy the following conditions: (i) Path length  $s(t)$  should always be continuous; (ii) Speed  $\dot{s}(t)$  should always be continuous. According to these 2 conditions,  $a$ ,  $b$  and  $c$  can be calculated as below:

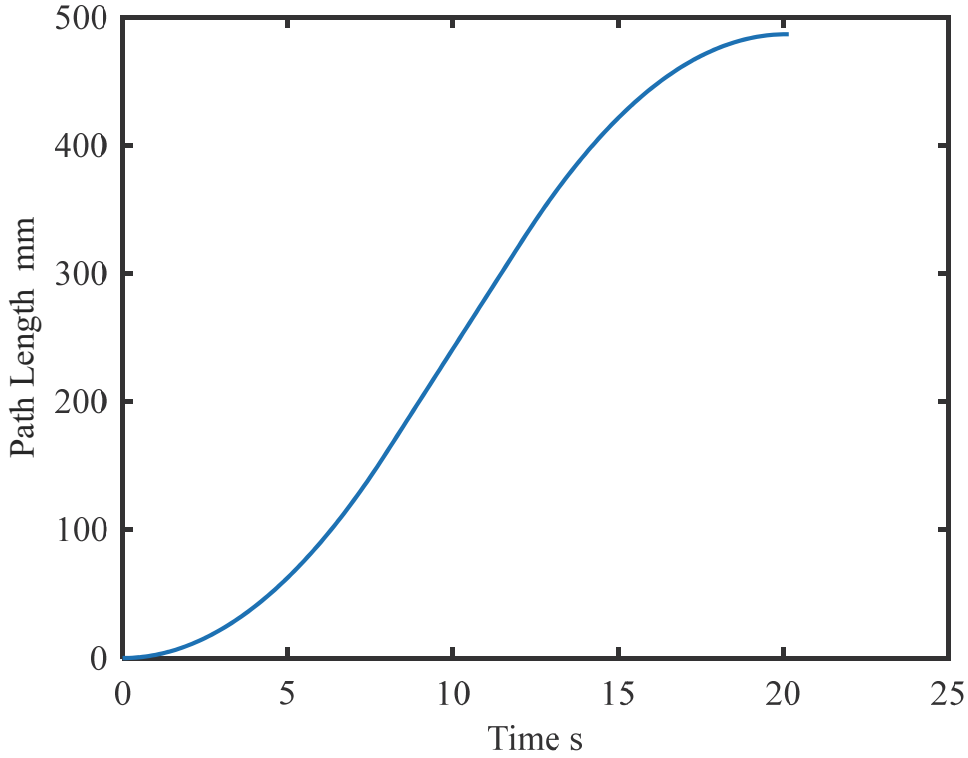


Fig. 3.10 The curve of time profile designed for the robot.

$$a = \frac{s_f}{2t_1t_2}, \quad (3.31)$$

$$b = \frac{s_f}{t_2}, \quad (3.32)$$

$$c = \frac{s_f t_1}{2t_2}. \quad (3.33)$$

An example of the time profile  $s(t)$  designed for our robot and applied in experiments is depicted in Fig. 3.10.

Finally, combining time planning (3.30) with path planning (3.24), we have a complete trajectory planning:

$$\gamma(t) = (x(t), y(t), z(t)). \quad (3.34)$$

And Fig. 3.11 shows the generated end-effector trajectory of climbing up motion in 3D space with time profile in Fig. 3.10. In the figure black dots are plotted for each 0.01s and the origin is the root of the limb where the end-effector is attached. It is not difficult to find that the closer it is to the start and end point of trajectory the denser black dots become and in the middle part of trajectory interval of dots stays almost the same. This feature exactly coincides with time profile of (3.30).

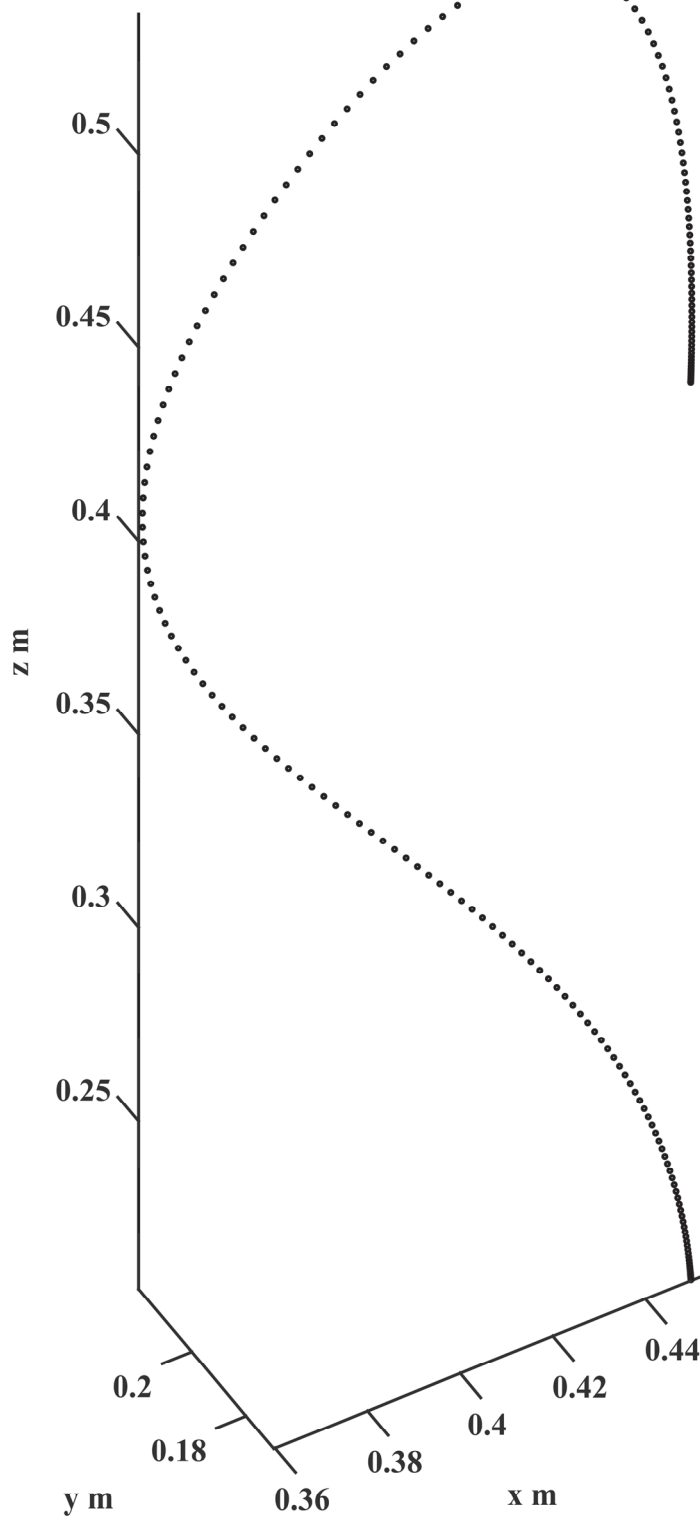


Fig. 3.11 Trajectory of end-effector for climbing up motion in 3D space.  
All coordinates are the distance from origin to end-effector.

### 3.4 Body trajectory planning

In the former sections, gaits of the climbing and end-effector trajectory planning are introduced and discussed in detail. To obtain whole-body motion planning, the only missing piece of puzzle is trajectory planning of the body.

#### 3.4.1 Background: Stability analysis

In Section 3.2, typical gaits of ladder climbing for a four-limbed robot are explained. Calling back the main features of 3-point and 2-point contact climbing, it has been concluded that 3-point contact climbing is much easier to keep stability but slower with more steps required, while 2-point contact climbing is much faster but may be unstable and requires stabilization methods. Therefore, before going through the details of body trajectory planning of the robot, stability conditions will be given first as the base and stability must be considered for whole-body motion planning in 2-point contact climbing gait.

In fact, stability of ladder climbing did not draw sufficient attention in previous researches, because 3-point contact climbing suffices to guarantee stability for a four-limbed robot on a ladder for most of common circumstances. Specifically, the robot on a ladder would keep stable in 3-point contact climbing unless the robot takes an extremely acrobatic posture that the projection of CoM of the robot goes beyond the range of polygon formed by contact points. Take HRP-2 and robot climbers developed by Honda R&D as instances, they climbed ladders only in 3-point contact climbing gait, only a simple static stability condition is given for HRP-2 [20] and stability judgement based on CoM feasible region is given for robots of Honda [21].

However, it is completely different for 2-point contact climbing. For Gorilla-III developed by Fukuda et al. 2-point contact climbing was realized and discussions about its stability are given in [17] and [18], with single-mass model used for robot model. In their stability analysis, the sum of moment (including gravitational moment and external force moment) around AoY (Axis of Yawing, an axis connecting 2 contact points between the robot and ladder) is calculated. It is concluded that if it is zero, then there will be no rotation around AoY, and stable climbing of the robot can be realized. Though illuminative this idea is, unfortunately it and other previous studies have their limits since they used single-mass model for the robot climber. For robots with mass distribution that is not concentrated on its body and long limbs that may cause CoM of the robot changes drastically with the change of robot posture, model error might be too big to be

ignored while calculating gravitational moment, a significantly influential factor to stability in ladder climbing. As a matter of fact, WAREC-1 is exactly the case and its data of mass distribution and length data are listed in Table 3-4.

Table 3-4 Mass distribution and length data of WAREC-1.

	Mass kg	Length mm
One limb	33	1098
Body	23	546
WAREC-1	155	2742 (fully stretched)

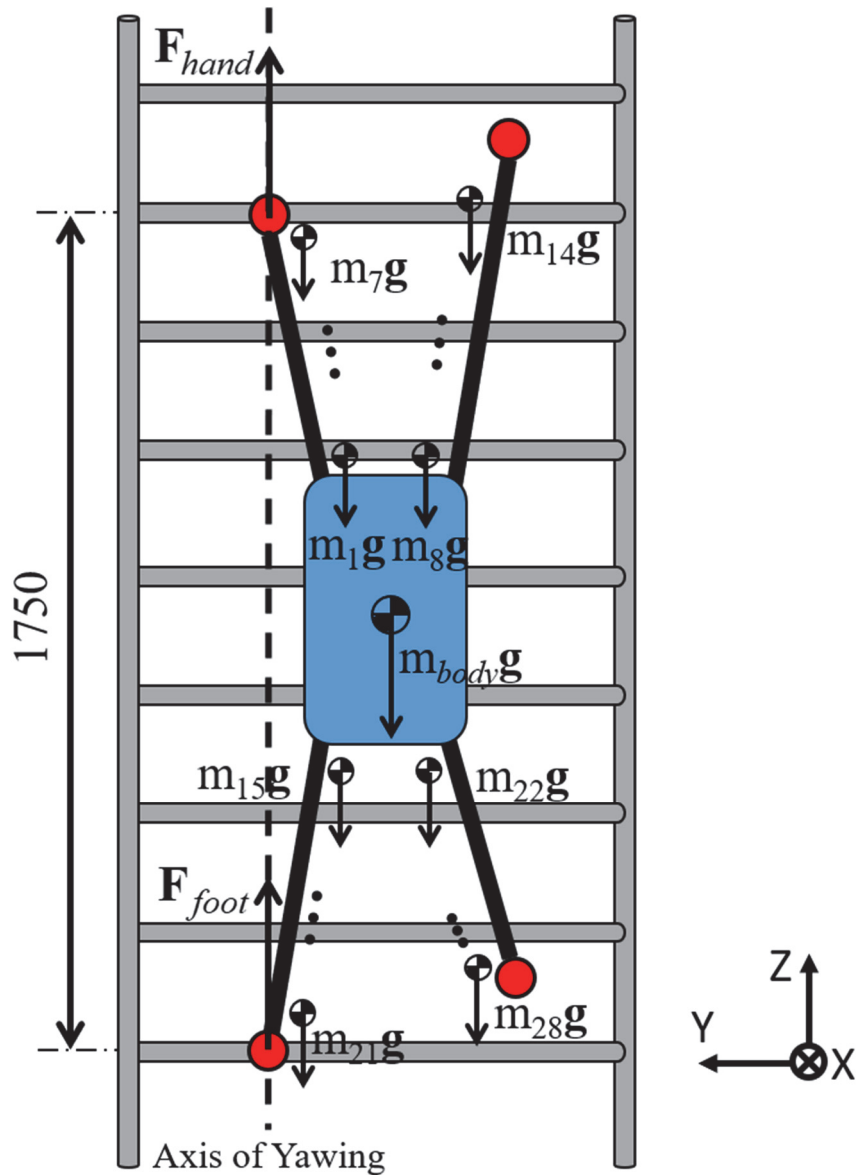


Fig. 3.12 Illustration of WAREC-1 on a ladder.



Apparently, single-mass model lacks reliability if applied to WAREC-1. To solve this issue, in this thesis multi-mass model is chosen for stability analysis. Due to the limit of joint angles, trot gait with 2 limbs on different sides moves at the same time is not within the scope of this thesis and only pace gait is chosen. Stability conditions of ladder climbing in multi-mass model to be proposed will be applicable to not only WAREC-1, but also a wider range of legged robots for ladder climbing.

Fig. 3.12 shows a situation of WAREC-1 climbing a ladder with 2-point contact. In this thesis, the “origin” is defined as the contact point between the foot on ladder and rung of the ladder. If both of 2 feet are on the ladder, then the contact point of right foot will be the origin.

It has been introduced that stable ladder climbing should guarantee that there is no rotation of robot during climbing motion, of which the idea is originated from the studies of Gorilla-III [17]. Therefore, the stability conditions of WAREC-1 can be given as

$$\sum \mathbf{M} = \mathbf{M}_g + \mathbf{M}_{ext} = 0, \quad (3.35)$$

$$\sum \mathbf{M}_{AoY} = \mathbf{R}_\theta (\mathbf{M}_g + \mathbf{M}_{ext}) = 0, \quad (3.36)$$

where

$$\mathbf{R}_\theta = \begin{bmatrix} 1 & 0 & 0 \\ 0 & \cos \theta & -\sin \theta \\ 0 & \sin \theta & \cos \theta \end{bmatrix}, \quad (3.37)$$

$$\mathbf{M}_g = \sum_i (\mathbf{r}_i \times m_i \mathbf{g}), \quad (3.38)$$

$$\mathbf{M}_{ext} = \mathbf{M}_{hand} + \mathbf{M}_{foot}, \quad (3.39)$$

$$\mathbf{M}_{hand} = \mathbf{r}_{hand} \times \mathbf{F}_{hand}, \quad (3.40)$$

$$\mathbf{M}_{foot} = \mathbf{r}_{foot} \times \mathbf{F}_{foot}. \quad (3.41)$$

The definition of variables can be seen in Table 3-5. Equation (3.35) and (3.36) express the equilibrium of moment around the origin and AoY, respectively.

Table 3-5 Explanation of variables.

Variable	Explanation
$\sum \mathbf{M}$	Total sum of moment around the origin of the robot
$\sum \mathbf{M}_{AoY}$	Total sum of moment around AoY
$\mathbf{M}_g$	Total sum of gravity moment
$\mathbf{M}_{ext}$	Total sum of external force (force at contact points between the robot and ladder) moment
$\theta$	Inclination angle of AoY
$\mathbf{R}_\theta$	Rotational matrix of $\theta$
$i$	Number of the link in the robot (the body of robot is also included)
$\mathbf{r}_i$	Displacement vector from the origin to CoM of the $i_{th}$ link
$m_i$	Mass of the $i_{th}$ link
$\mathbf{g}$	Acceleration of gravity
$\mathbf{M}_{hand}$	Moment of force at the supporting hand
$\mathbf{M}_{foot}$	Moment of force at the supporting foot
$\mathbf{r}_{hand}$	Displacement vector from the origin to contact point on the hand
$\mathbf{r}_{foot}$	Displacement vector from the origin to contact point on the foot
$\mathbf{F}_{hand}$	Total force at the supporting hand
$\mathbf{F}_{foot}$	Total force at the supporting foot

In this way, (3.35) and (3.36) can be written as

$$\sum \mathbf{M} = \sum_i (\mathbf{r}_i \times m_i \mathbf{g}) + \mathbf{r}_{hand} \times \mathbf{F}_{hand} + \mathbf{r}_{foot} \times \mathbf{F}_{foot} = 0, \quad (3.42)$$

$$\sum \mathbf{M}_{AoY} = \mathbf{R}_\theta \left( \sum_i (\mathbf{r}_i \times m_i \mathbf{g}) + \mathbf{r}_{hand} \times \mathbf{F}_{hand} + \mathbf{r}_{foot} \times \mathbf{F}_{foot} \right) = 0. \quad (3.43)$$

### 3.4.2 Body trajectory in different climbing gaits

Stability conditions (3.42) and (3.43) reveal that the equilibrium of moment is maintained by the balance of gravity moment  $\mathbf{M}_g$  and reaction force moment  $\mathbf{M}_{ext}$ , with sufficient  $\mathbf{M}_{ext}$  to cancel current  $\mathbf{M}_g$ . Therefore, there are 2 major methods to keep stability for moments: (i) Reduce  $\mathbf{M}_g$  to a level that  $\mathbf{M}_{ext}$  can cancel it; (ii) Increase  $\mathbf{M}_{ext}$  (which are actually  $\mathbf{M}_{hand}$  and  $\mathbf{M}_{foot}$ ) around the contact points to make it sufficient to cancel  $\mathbf{M}_g$ . The former can be realized by the motion planning,

thus is introduced in this chapter. As for the latter, it requires feedback of force sensor and therefore will be introduced in the next chapter.

Considering the stability conditions described above, the body trajectory in ladder climbing motion can be divided into 2 cases depending on climbing gaits:

Case1: For 3-point contact climbing, the body of robot moves only vertically in a constant speed, with the distance of a rung interval that synchronizes the speed of end-effectors so that the move of body and end-effectors starts and stops at the same time. As is explained, since 3-point contact climbing gait requires more steps to climb up or down a rung and stability is much easier to be maintained, body trajectory in this case only involves change of coordinate in Z-axis. In another word, take Fig. 3.4 as instance, the body of robot moves up/down with the distance of 1/4 of rung interval for each step, and finally moves up/down exactly with one rung interval so that the robot can be brought back to the initial state before the ladder climbing and start another climbing cycle.

Case 2: For 2-point contact climbing, the body of robot moves in either Z-axis and X-axis, since for pace gait the gravity moment will be much bigger around AoY and horizontal move of the body can greatly reduce it. To reduce  $\mathbf{M}_g$  significantly, the robot climber takes whole-body movement instead of partial movement. Since this thesis only discusses pace gait for 2-point contact ladder climbing, moving the body horizontally to reduce  $\mathbf{r}_i$  in (3.38) is chosen as an effective and rather easier solution to reduce gravity moment around the origin and along AoY.

Specifically, body move of the robot continues until the CoM of the robot in Y-axis (set as  $y_{body}$ ) is exact at the middle of that for supporting hand (set as  $y_{hand}$ ) and foot (set as  $y_{foot}$ ), which can be written as  $y_{body}=(y_{hand}+y_{foot})/2$ . Especially, in this thesis for the simplicity  $y_{hand}=y_{foot}$  satisfies in pace gait, and thus the body moves until  $y_{hand}=y_{foot}=y_{body}$ , with CoM of the robot and contact points between the robot and ladder form a plane that is parallel to XoZ plane. A similar method was proposed by Ishiguro et al. [45] that the body of robot swings tracking the planned CoM trajectory, but it was not intended and planned for reducing gravity moment around the contact points, and only simulation results of a small-sized robot were provided.

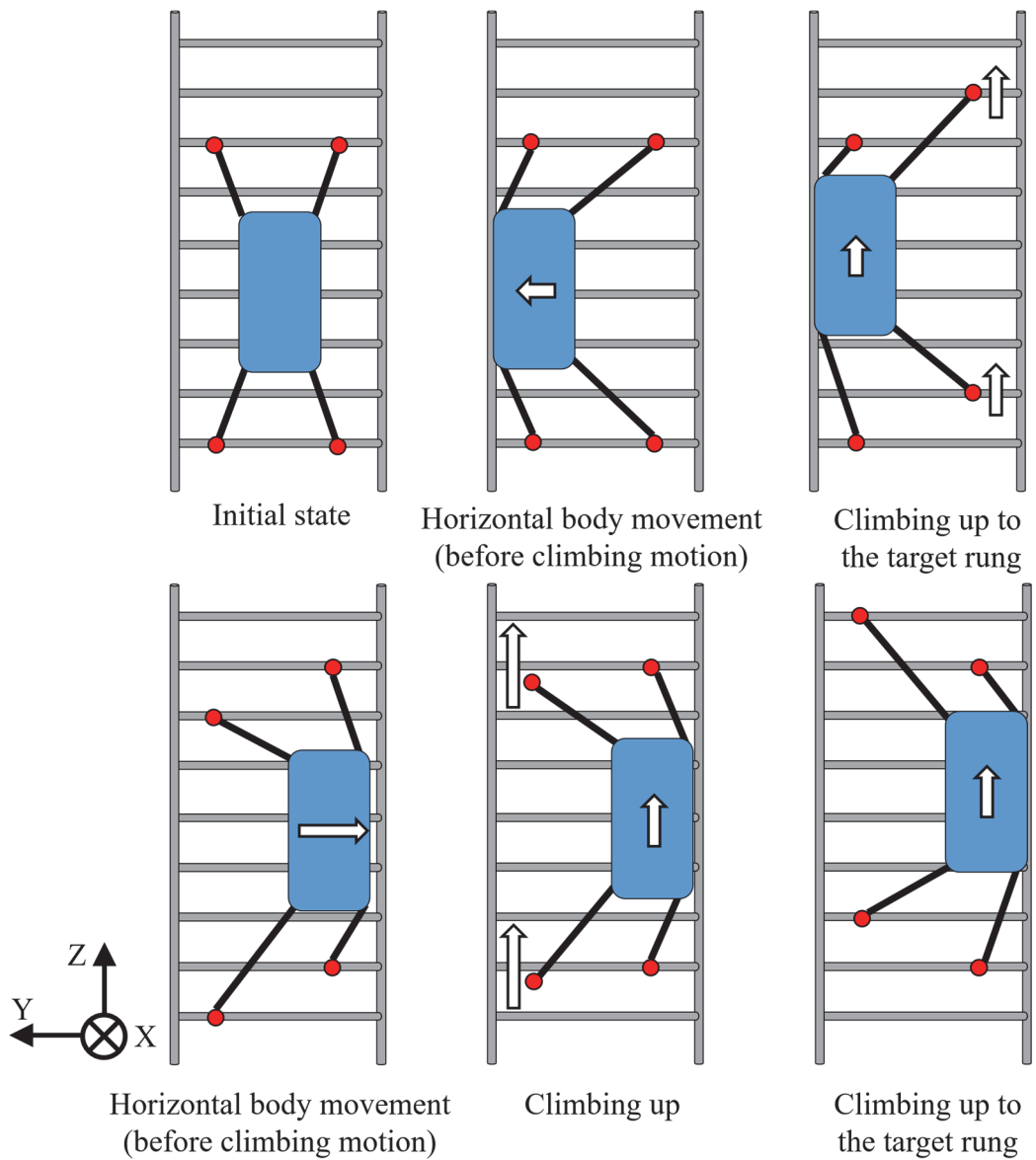


Fig. 3.13 Phases of whole-body motion planning for pace gaits [36].

### 3.5 Whole-body motion planning

Summarizing the former sections in this chapter, whole-body motion planning in this thesis can be concluded by Fig. 3.4 for 3-point contact gait and Fig. 3.13 for 2-point contact gait.

### 3.6 Kinematics

As is well known, kinematics is indispensable to realize motion planning of robot in both simulation and reality. In this section forward and inverse kinematics and their applications are detailedly presented as the base of motion generation.

### 3.6.1 Forward kinematics

To begin with, the definition of coordinate system is depicted in Fig. 3.14. The red arrows refer +X axis direction, green arrows refer +Y and blue arrows refer +Z, which is applicable to not only the robot itself but also all joints in the robot. To

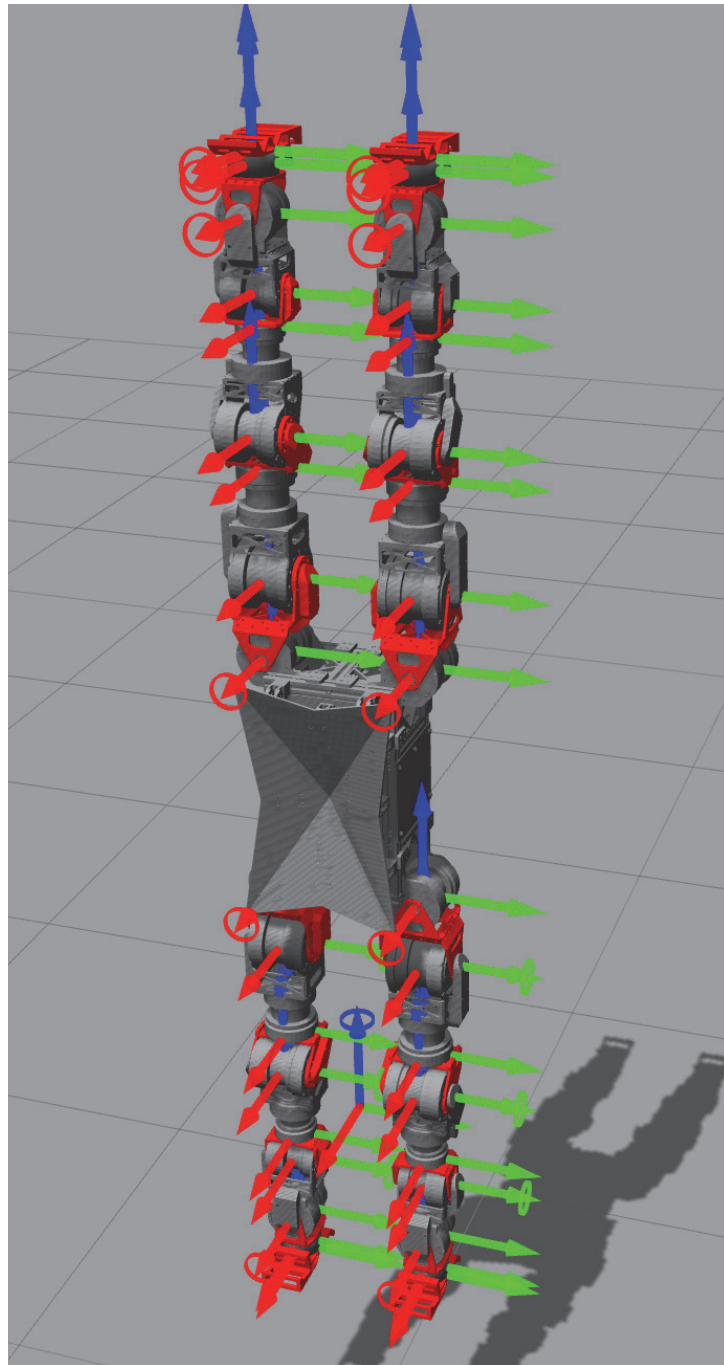


Fig. 3.14 Coordination system of WAREC-1.  
Red arrow: +X; Green arrow: +Y; Blue arrow: +Z.

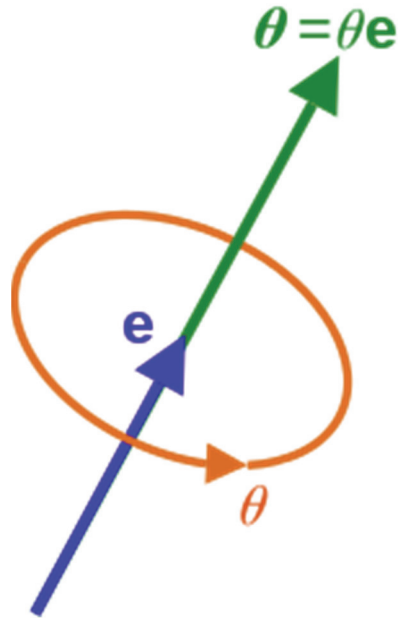


Fig. 3.15 Orientation presentation by Axis-angle ([35], [36]).

avoid gimbal lock and discontinuity of interpolation in motion generation, in this thesis we choose quaternion [37] to express orientation in forward kinematics. Take Axis-angle, a method of orientation presentation illustrated in Fig. 3.15 as reference, 3-dimensional vector  $\mathbf{e}=(e_x, e_y, e_z)$  denotes the rotational axis and scalar  $\theta$  denotes the amount of rotation along  $\mathbf{e}$ . Then the orientation in Fig. 3.15 can be expressed by the quaternion  $\mathbf{q}(x, y, z, w)$  as the following equation with its norm equals 1.

$$\mathbf{q} = \begin{pmatrix} ie_x \sin \frac{\theta}{2} \\ je_y \sin \frac{\theta}{2} \\ ke_z \sin \frac{\theta}{2} \\ \cos \frac{\theta}{2} \end{pmatrix}, \quad (3.44)$$

where  $i, j$  and  $k$  are all unit imaginary with features below

$$i^2 = j^2 = k^2 = l^2 = -1, \quad (3.45)$$

$$j = k, jk = i, ki = j, \quad (3.46)$$

$$ijk = -1, \quad (3.47)$$

and a unit quaternion has the following feature

$$\mathbf{q}^{-1} = \mathbf{q}(-x, -y, -z, -w), \quad (3.48)$$

The point  $\mathbf{p}(x, y, z, 0)$  with rotation of quaternion  $\mathbf{q}$  can be given by

$$\mathbf{p}^{-1} = \mathbf{q}\mathbf{p}\mathbf{q}^{-1}. \quad (3.49)$$

With expressions above, interpolation between orientation  $\mathbf{q}_1$  and  $\mathbf{q}_2$  are given by

$$\mathbf{q} = \frac{\sin(1-t)\theta}{\sin\theta} \cdot \mathbf{q}_1 + \frac{\sin(t\theta)}{\sin\theta} \cdot \mathbf{q}_2, \quad (3.50)$$

where

$$\theta = \cos^{-1}(\mathbf{q}_1 \cdot \mathbf{q}_2). \quad (3.51)$$

Moreover, considering that the norm of quaternion is always 1 and 4 variables  $(x, y, z, w)$  are not independent to each other and thus cannot be utilized in the calculation of Jacobian, conversion of logarithm quaternion [38] is applied. In the expression of logarithm quaternion  $\ln\mathbf{q}=(x_l, y_l, z_l)$  can be converted from quaternion  $\mathbf{q}(x, y, z, w)$  in the following expression

$$x_l = x \cos^{-1}(w), \quad (3.52)$$

$$y_l = y \cos^{-1}(w), \quad (3.53)$$

$$z_l = z \cos^{-1}(w). \quad (3.54)$$

Having established the basic representations about position and orientation above, forward kinematics can be calculated in the steps below. To begin with, all variables used in forward kinematics are defined in Table 3-6. And the position and orientation of each link can be given by

$$\mathbf{b}_{i+1} = \mathbf{q}_i \mathbf{a}_{i+1}, \quad (3.55)$$

$$\mathbf{q}_{i+1} = \mathbf{p}(\theta_{i+1}, \mathbf{b}_{i+1}) \mathbf{q}_i, \quad (3.56)$$

$$\mathbf{r}_{i+1} = \mathbf{q}_{i+1} \mathbf{l}_{i+1} + \mathbf{r}_i. \quad (3.57)$$

Finally, forward kinematics can be given by  $\mathbf{r}_n$  and  $\mathbf{q}_n$ , respectively.

Table 3-6 Explanation of variables related to quaternion.

Variable	Explanation
$n$	Total number of joint in one limb (for WAREC-1, $n=7$ )
$i$	The number of joint, counting from the root of limb to the end
$\theta_i$	Angle of the $i_{\text{th}}$ joint
$\mathbf{l}_i$	Vector of the $i_{\text{th}}$ link for “origin posture” in Fig. 3.14
$\mathbf{q}_i$	Quaternion that shows rotation of the $i_{\text{th}}$ link
$\mathbf{r}_i$	Vector from the root of limb to the end of the $i_{\text{th}}$ link
$\mathbf{a}_i$	Unit vector along the rotation axis of the $i_{\text{th}}$ joint for “origin posture”
$\mathbf{b}_i$	Unit vector along the rotation axis of the $i_{\text{th}}$ joint
$\mathbf{p}(\theta, \mathbf{v})$	Quaternion that shows the rotation with axis vector $\mathbf{v}$ and angle $\theta$

### 3.6.2 Inverse kinematics

In this thesis inverse kinematics based on Jacobian is mainly implemented. The following introduces the basics of Jacobian and its related applications first. After that, details about actual calculation in the computer based on the theories are also given. The detail results and their proofs about inverse kinematics can be found in the Appendix B.

Let  $\mathbf{x} = (x_1, x_2, \dots, x_m)^T \in \mathbf{R}^m$  denote the configuration vector, and  $\boldsymbol{\theta} = (\theta_1, \theta_2, \dots, \theta_n)^T \in \mathbf{R}^n$  denote the joint angle vector, then we have

$$\mathbf{x} = f(\boldsymbol{\theta}). \quad (3.58)$$

From (3.58), we get

$$\dot{\mathbf{x}} = \mathbf{J}(\boldsymbol{\theta}) \dot{\boldsymbol{\theta}}, \quad (3.59)$$



where  $\mathbf{J}(\boldsymbol{\theta}) = \frac{\partial f(\boldsymbol{\theta})}{\partial \boldsymbol{\theta}^T}$  denotes the  $m \times n$  ( $m \leq n$ ) Jacobian matrix and  $\dot{\boldsymbol{\theta}}$  denotes angular velocity of joint. When  $\text{rank}(\mathbf{J})=m$ , we want to solve the following problem

$$\min |\dot{\boldsymbol{\theta}}|^2, \text{ subject to } \dot{\mathbf{x}} = \mathbf{J}(\boldsymbol{\theta})\dot{\boldsymbol{\theta}}, \quad (3.60)$$

and from (3.60) we have

$$\dot{\boldsymbol{\theta}} = \mathbf{J}^+ \dot{\mathbf{x}}, \quad (3.61)$$

where  $\mathbf{J}^+ = \mathbf{J}^T(\mathbf{J}\mathbf{J}^T)^{-1}$  denotes the pseudo-inverse of  $\mathbf{J}$ . Especially, when  $m=n$  and  $\mathbf{J}$  is an invertible matrix, then we have  $\mathbf{J}^+ = \mathbf{J}^T(\mathbf{J}\mathbf{J}^T)^{-1} = \mathbf{J}^{-1}$ . Namely, in this case, the pseudo-inverse  $\mathbf{J}^+$  is exactly the inverse  $\mathbf{J}^{-1}$ .

In order to carry out a number of tasks such as avoid obstacles and so on at the same time as the robot moves, we need the following:

**Proposition.** The velocity of the joint angle can be expressed as

$$\dot{\boldsymbol{\theta}} = \mathbf{J}^+ \dot{\mathbf{x}} + (\mathbf{I} - \mathbf{J}^+ \mathbf{J})\boldsymbol{\xi}, \quad (3.62)$$

where  $\boldsymbol{\xi}$  is an arbitrary  $n$ -dimensional vector.

**Remark.** Taking  $\boldsymbol{\xi} = k \frac{\partial \psi(\boldsymbol{\theta})}{\partial \boldsymbol{\theta}}$ , where  $k$  is a constant and  $\psi(\boldsymbol{\theta})$  is a cost function of  $\boldsymbol{\theta}$ , we can consider the obstacle avoidance problem. In details, by setting  $\boldsymbol{\theta}_o$  as the point ones hope to avoid and choosing

$$\psi(\boldsymbol{\theta}) = \frac{1}{2} (\boldsymbol{\theta} - \boldsymbol{\theta}_o)^T \mathbf{W} (\boldsymbol{\theta} - \boldsymbol{\theta}_o) = d(\boldsymbol{\theta}, \boldsymbol{\theta}_o) \quad (3.63)$$

as the distance function measuring  $\boldsymbol{\theta}$  and  $\boldsymbol{\theta}_o$ , where  $\mathbf{W}$  is a diagonal matrix with positive diagonal entries. Thus, by using

$$\dot{\boldsymbol{\theta}} = \mathbf{J}^+ \dot{\mathbf{x}} + (\mathbf{I} - \mathbf{J}^+ \mathbf{J})k \cdot \frac{\partial \psi(\boldsymbol{\theta})}{\partial \boldsymbol{\theta}}, \quad (3.64)$$

where  $k > 0$ , we can get the maximum of  $\psi(\boldsymbol{\theta})$  so that the distance between  $\boldsymbol{\theta}$  and  $\boldsymbol{\theta}_o$  is far enough to avoid collision.

**Remark.** For the case of  $\text{rank}(\mathbf{J}_{m \times n}) < \min\{m, n\}$ , we need to solve

$$\min\{|\dot{\mathbf{x}} - \mathbf{J}\dot{\boldsymbol{\theta}}| + \lambda^2 |\dot{\boldsymbol{\theta}}|^2\}, \quad (3.65)$$

where  $\lambda \neq 0$  is a real number. The solution of (3.65) gives

$$\dot{\boldsymbol{\theta}} = (\mathbf{J}^T \mathbf{J} + \lambda^2 \mathbf{I}) \mathbf{J}^T \dot{\mathbf{x}}, \quad (3.66)$$

where  $\mathbf{I}$  denotes an identity matrix.

To adapt to ladders with different scales and specifications, such as rung distances and side pole distances, position-based control is utilized in our robot. It is also effective in compensating the error caused by deformation between ladder and the robot. Consequently, joint angles should be given to control end-effectors of the robot to the desired position in space, and inverse kinematics is necessary to convert generated trajectory into joint angles.

In this thesis, taking advantage of redundant DoF, 7-DoF inverse kinematics combined with pseudo-inverse Jacobian is used to calculate the joint angles of the robot. Inverse kinematics in this form enables multiple tasks. Here, the first task is the trajectory tracking of end-effector and the second task is target posture of end-effector to avoid self-collision caused by going beyond the movable range of angle for each joint. The specific equation with pseudo-inverse Jacobian is shown as

$$\dot{\boldsymbol{\theta}} = \mathbf{J}^+ \dot{\mathbf{x}}_1 + (\mathbf{I} - \mathbf{J}^+ \mathbf{J}) [\dot{\mathbf{x}}_{2d} + \mathbf{H}(\mathbf{x}_{2d} - \mathbf{x}_2)], \quad (3.67)$$

where  $\dot{\boldsymbol{\theta}} = \dot{\boldsymbol{\theta}}^{7 \times 1}$  denotes angular velocity of joints,  $\dot{\mathbf{x}}_1 = \dot{\mathbf{x}}_1^{6 \times 1}$  denotes velocity of end-effector,  $\mathbf{H} = \mathbf{H}^{7 \times 7}$  denotes a diagonal gain matrix showing the error between desired and real target posture.  $\mathbf{x}_{2d} = \mathbf{x}_{2d}^{7 \times 1}$  denotes desired target posture in the second task,  $\mathbf{x}_2 = \mathbf{x}_2^{7 \times 1}$  denotes real posture for the second task,  $\mathbf{I} = \mathbf{I}^{7 \times 7}$  denotes an identity matrix,  $\mathbf{J} = \mathbf{J}^{6 \times 7}$  denotes Jacobian and  $\mathbf{J}^+ = \mathbf{J}^{+7 \times 6}$  denotes pseudo-inverse Jacobian. While trajectory can be converted into joints angles, we can give appropriate target posture  $\mathbf{x}_{2d}$  to get rid of self-collision at the same time [39].

As for the actual process in the computer, detailed ideas and calculation are shown below: The inverse kinematics problem for robot that has 7 DoF for one limb like WAREC-1 is the problem of finding 2 points in 7 DoF joint angle space that can be mapped from 2 points in 6 DoF configuration space consists of information of position (in 3 variables) and orientation (in 3 variables). Note that

both joint angle and configuration space has discontinuous sections. For joint angle space there is the constraint of joint angle limits and for configuration space there are constraints of accessible range and avoidance of self-collision.

Actual numerical solution for inverse kinetics to solve joint angles that satisfies desired position and orientation of the end-effector has various types. The author used to choose a method of the most basic one that obtains desired trajectory by interpolation, samples the trajectory for each small “step” and calculate the difference of joint angles for the calculation of Jacobian. However, the shortcomings of this method are that (i) Division of the trajectory to many small sections are necessary; (ii) It is difficult to calculate with multiple initial conditions and (iii) The error in numerical solution accumulates. Therefore, we improved the approach and applied Newton-Raphson method to inverse kinematics expressed as non-linear equations shown below

$$\mathbf{x}_e(\boldsymbol{\theta}) = \mathbf{x}_t - \mathbf{x}(\boldsymbol{\theta}) \doteq \mathbf{0} , \quad (3.68)$$

where  $\boldsymbol{\theta}$  is the present joint angle vector to be updated,  $\mathbf{x}$  is the present configuration vector to be updated,  $\mathbf{x}_t$  is the target configuration vector and  $\mathbf{x}_e$  is the error between the latter two. With

$$\mathbf{x} = \begin{pmatrix} x \\ y \\ z \\ x_l \\ y_l \\ z_l \end{pmatrix} , \quad (3.69)$$

where  $x$ ,  $y$  and  $z$  are coordinates of the end-effector and  $x_l$ ,  $y_l$  and  $z_l$  are the components of logarithm quaternion, inverse kinematics expressed in (3.59) can be solved in the following steps:

- 1) Determine initial joint angles as the initial condition. In most of the cases they are exactly the present joint angles of the robot.
- 2) Solve configuration vector  $\mathbf{x}(\boldsymbol{\theta})$  by forward kinematics with given joint angle vector  $\boldsymbol{\theta}$  to be updated. Then obtain error  $\mathbf{x}_e$  by (3.59).
- 3) Obtain numerical solution of Jacobian. Specifically, set scalar  $h$  as a very small value and solve numerical partial differential of a function  $f(t)$  by

$$\dot{f}(t) = (f(t+h) - f(t-h)) / 2h . \quad (3.70)$$

With (3.59), elements in the desired Jacobian can be obtained.

4) Update joint angle the following 2 equations

$$\dot{\boldsymbol{\theta}} = -\mathbf{W}^{-1} \mathbf{J}^T (\mathbf{J} \mathbf{W}^{-1} \mathbf{J}^T) \mathbf{x}_e , \quad (3.71)$$

$$\boldsymbol{\theta}(t + \Delta t) = \boldsymbol{\theta}(t) + \dot{\boldsymbol{\theta}}(t) \Delta t , \quad (3.72)$$

where  $\mathbf{W}$  is a weight matrix,  $t$  is the present time and  $\Delta t$  is the time elapsed during the section of updating joint angles.

5) Judge convergence. Set a threshold  $\mathbf{x}_{\text{eth}}$  and check whether  $\mathbf{x}_e$  is smaller than this threshold. If it is, end update of joint angles. If  $\mathbf{x}_e$  cannot converge after update back to step “2”) then calculate again. Calculation will be ended if  $\mathbf{x}_e$  cannot converge after certain times of update (10000 in our case).

The update law above has the merits of:

- 1) Reducing error of joint angles in each “step” to the level that can be set freely;
- 2) Since this method interpolates joint angles instead of configuration to make end-effector reach the desired configuration, there is no need to consider the continuity of the path.

## 3.7 Experiments in simulation

### 3.7.1 Conditions

To verify the validity of our climbing motion generation system comprehensively, experiments of the four-limbed robot “WAREC-1” in simulation was made. Specific conditions of the simulator (the same for all other simulations in the following chapters) as well as the ladder and ladder climbing gait in simulation can be seen in Table 3-7.

### 3.7.2 Results

As the integration of all contents this chapter, Fig. 3.16 and Fig. 3.17 show the snapshots of the ladder climbing in both 3-point contact and 2-point contact gait, verifying successful ladder climbing motion is generated for both 2 cases in the simulation.

Table 3-7 Conditions of simulation.

Term	Explanation/Value
Operating System of PC	Ubuntu (Linux)
Simulator	Gazebo
Middleware	ROS (Robot Operation System)
Gaits of ladder climbing	Transverse (3-point contact) and pace (2-point contact)
Rung interval mm	250
Pole distance mm	600

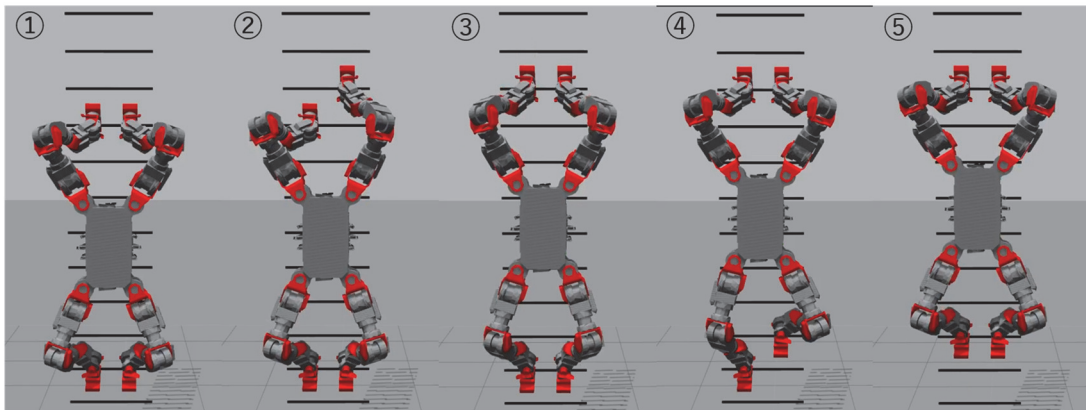


Fig. 3.16 Generated 3-point contact ladder climbing motion in simulator.

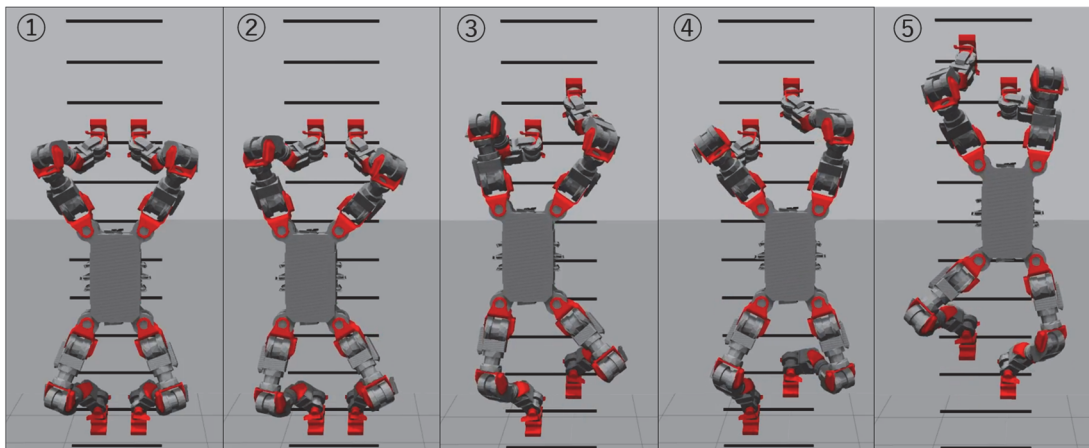


Fig. 3.17 Generated 2-point contact ladder climbing motion in simulator.

### 3.7.3 Discussions

With the simulation results presented above, the motion generation system proposed in this chapter has been validated that it is capable of generate appropriated motion for ladder climbing while obeying the spatial constraints and avoids troubles shown in Fig. 3.1. Note that in simulation we suppose that (i) All objects (the ladder and robot) are considered as rigid bodies; (ii) There is no error in position, orientation or force. However, these conditions may not be satisfied in reality, bringing our concern to the next chapter for the completion of this thesis.

### 3.8 Summary

This chapter describes motion planning and motion generation of ladder climbing that consists of (i) Climbing gaits (ii) End-effector trajectory planning and (iii) Body trajectory planning.

For climbing gaits, basic gaits are introduced because motion planning starts first with the decision of gaits. For end-effector trajectory planning, basic ladder climbing motion planning method used in this thesis is explained: path-time independent trajectory planning. This method is realized by arc-length parameterization and the combination of this method with ladder climbing enables free speed adjustment (i.e., time profile) without bringing influence to planned path, and this point is particularly significant for ladder climbing because of constraints of path to avoid unexpected collision with ladder rungs and constraints of end position of trajectory to guarantee appropriate and accurate contact with rungs. In addition, minimization of path length to be travelled for end-effector is also available if necessary and feasible, realizing the reduction of total time spent in ladder climbing. For body trajectory planning, different strategies are chosen according to different gaits and finally the pattern of whole-body motion planning are presented.

Afterwards, both forward and inverse kinematics are introduced specifically for the base of motion generation of the robot. Basic definitions for position and orientation for WARCE-1 are given as the base of quantitative calculation in the following chapters first. Forward kinematics with quaternion as the orientation presentation is presented and inverse kinematics based on Jacobian and update law of Newton-Raphson are mainly utilized in this thesis as fundamental kinematics.

Finally, experiment results in simulation are given. Based on the features of motion generation methods in this thesis, functions that could be used in real situation are developed and verified, such as self-collision avoidance by the

utilization of redundant DoF and reverse function of motion in the case of unexpected collision, wrong planning, motion generation and so on.





## Chapter 4. Sensor feedback systems

### 4.1 Background and introduction

In the last chapter, planning and generation of appropriate motion customized for ladder climbing of the robots developed are presented and ladder climbing is realized in simulation. Unfortunately, similar to multi-legged robot walking, motion planning alone does not suffice stability in climbing motion in the following points:

- 1) Reaction force distribution at contact points: As is mentioned in Section 3.4.1 as well as former study [21], the bias of reaction force at contact point may cause unstable states that robot rotates around either one of the contact point while climbing in 2-point contact gaits. And the robot keeps stable only if the bias of reaction force is reduced to a level that suffices equilibrium of moment around both 2 contact points.
- 2) Recognition of ladder rungs. Ladders in this world differ from each other in different standards, such as JIS and MIL. So far there is no ladder climbing robot claimed to be capable of climbing a ladder with unknown specification, especially for unknown rung interval, the crucial parameter that determines the start and end point of end-effector trajectory and eventually influences whole-body motion of the robot. However, in the environment where there is no one around the robot, the rung interval must be obtained somehow by the robot itself to perform successful and stable ladder climbing; In addition, besides the change in rung interval rungs of the ladder may also be inclined due to the damage in disaster situations. Therefore, recognition of ladder rungs for not only position but also orientation is required to realize truly stable ladder climbing in this thesis.

Therefore, taking 2 major issues given above into consideration, sensor feedback systems below are developed and utilized in this thesis:

- 1) Force/torque sensor feedback system to measure and reduce the bias of reaction force at contact points as the solution to the former issue.
- 2) Proximity sensor feedback system for measuring relative distance and orientation between the end-effectors and rungs as the solution to the ladder issue.

In the following sections of this chapter, (i) The introduction of each system,

(ii) The mechanism of each system, (iii) The application of each system and (iv) The integration of these 2 sensor feedback systems with motion planning in Chap. 2 will be detailly explained and their validity will be verified in experiments.

## 4.2 Force sensor feedback control

### 4.2.1 Overview

So far, the systems and methods of creating and realizing climbing motion as well as sensor feedback control for guaranteeing appropriate contact between the robot and ladder are proposed and verified. However, unfortunately as Section 3.4.1 explains, they are still not sufficient for stable ladder climbing, especially for the case of 2-point contact ladder climbing for human-sized robots that requires certain conditions that keeps the equilibrium of moment around contact points. Therefore, in this section force sensor feedback control in pace gait is introduced so that besides the stable motion in 3-point contact gaits, stable ladder climbing in 2-point contact gait also becomes available as an option when required, especially for cases that 3-point contact climbing is not fast enough to meet the requirement. In the former studies, although Gorilla-III [17] realized ladder climbing in both pace and trot gait, but it is a pity that Gorilla-III is a little bit small (with the height of 1.0m and weight of 22kg) to be called a human-sized robot. And as for human-sized robots in ladder climbing in recent years, ladder climbers such as HRP-2 [20] and the robot of Honda R&D [21] only climbed the ladder in 3-point contact gait. Thus, it is necessary to propose a complete system to guarantee stable 2-point contact ladder climbing for a human-sized robot.

Recalling the stability analysis and stability conditions (3.42) and (3.43) in Section 3.4.1 and motion planning of the body to reduce gravity moment described in Section 3.4.2, although horizontal body move does make it easier for the robot to stay stable in ladder climbing, there still must be sufficient external force moment  $\mathbf{M}_{ext}$  to cancel  $\mathbf{M}_g$ . In the case that  $\mathbf{M}_{ext}$  is not big enough, reaction force on hand/foot contacting the ladder can be adjusted to increase  $\mathbf{M}_{ext}$ . Detailly, if the external force on either contact point is too small, it is not hard to imagine that rotation of the robot may occur around the other contact point.

Looking back to Fig. 3.12, the state that the robot only has 2 contact points with the ladder: Supporting hand and supporting foot. Note that end-effectors are simplified as points in this thesis. Therefore, there are possibility of rotation for the robot around either one contact point. The solution of body motion planning has been described, and here another solution of reaction force control is introduced.

The idea is simply: if moment of reaction force at hand ( $\mathbf{M}_{hand}$ ) or foot ( $\mathbf{M}_{foot}$ ) is too small to maintain stability, then “push down” the corresponding end-effector to increase the reaction force and obtain reaction force moment sufficient for avoiding rotation of the robot.

#### 4.2.2 Sufficient stability conditions for reaction force norm

Now the main concern is: How much force does it require to maintain stability without rotation around the contact points? The calculation of reaction force required at contact points is presented below:

According to D’Alembert’s Principle, we have

$$\sum_i m_i \mathbf{g} + \mathbf{F}_{hand} + \mathbf{F}_{foot} + \sum_i m_i \mathbf{a}_{gi} = 0, \quad (4.1)$$

where  $\mathbf{a}_{gi}$  is the acceleration of the CoM of the  $i$ th link. The calculation of  $\mathbf{a}_{gi}$  in (4.1) is shown in steps as follows. First, the angular velocity and angular acceleration of each joint can be given as:

$$\boldsymbol{\omega}_{i+1} = \boldsymbol{\omega}_i + \mathbf{s}_{i+1} \dot{\theta}_{i+1}, \quad (4.2)$$

$$\dot{\boldsymbol{\omega}}_{i+1} = \dot{\boldsymbol{\omega}}_i + \mathbf{s}_{i+1} \ddot{\theta}_{i+1} + \boldsymbol{\omega}_{i+1} \times (\mathbf{s}_{i+1} \dot{\theta}_{i+1}), \quad (4.3)$$

where  $\boldsymbol{\omega}_i$  is the angular velocity,  $\dot{\boldsymbol{\omega}}_i$  is the angular acceleration,  $\theta_i$  is the joint angle and  $\mathbf{s}_i$  is the rotation axis vector of the  $i$ th joint.

In this thesis, accumulation expressions like (4.2), (4.3) and others in this paper that will appear are only valid for the joints in the same limb (not including the body of robot). As for the numbering of joint in one limb,  $i$  starts with the number “1” at the root of the limb and increases one by one to the end-effector. Here, based on the definition of forward kinematics,  $\mathbf{s}_i$  can be given as

$$\mathbf{s}_i = [\prod_i \mathbf{R}_i(\theta_i)] \hat{\mathbf{s}}_i, \quad (4.4)$$

where  $\mathbf{R}_i(\theta_i)$  and  $\hat{\mathbf{s}}_i$  are the rotational matrix and initial rotation axis of the  $i$ th joint:

$$\mathbf{R}_i(\theta_i) = \begin{cases} \begin{bmatrix} 1 & 0 & 0 \\ 0 & \cos \theta_i & -\sin \theta_i \\ 0 & \sin \theta_i & \cos \theta_i \end{bmatrix}, & \text{joint } i \text{ is Roll} \\ \begin{bmatrix} \cos \theta_i & 0 & \sin \theta_i \\ 0 & 1 & 0 \\ -\sin \theta_i & 0 & \cos \theta_i \end{bmatrix}, & \text{joint } i \text{ is Pitch} \\ \begin{bmatrix} \cos \theta_i & -\sin \theta_i & 0 \\ \sin \theta_i & \cos \theta_i & 0 \\ 0 & 0 & 1 \end{bmatrix}, & \text{joint } i \text{ is Yaw} \end{cases} \quad (4.5)$$

$$\hat{\mathbf{s}}_i = \begin{cases} (1, 0, 0)^T, & \text{joint } i \text{ is Roll} \\ (0, 1, 0)^T, & \text{joint } i \text{ is Pitch} \\ (0, 0, 1)^T, & \text{joint } i \text{ is Yaw} \end{cases} \quad (4.6)$$

With (4.2) and (4.3) known, we can further solve the velocity and acceleration of each joint by Newton-Euler method [46]

$$\mathbf{v}_{i+1} = \mathbf{v}_i + \boldsymbol{\omega}_i \times \mathbf{l}_i + \dot{\mathbf{l}}_i, \quad (4.7)$$

$$\mathbf{a}_{i+1} = \mathbf{a}_i + \ddot{\mathbf{l}}_i + \dot{\boldsymbol{\omega}}_i \times \mathbf{l}_i + 2\boldsymbol{\omega}_i \times \dot{\mathbf{l}}_i + \boldsymbol{\omega}_i \times (\boldsymbol{\omega}_i \times \mathbf{l}_i), \quad (4.8)$$

where  $\mathbf{l}_i$  is the link vector of the link connecting the  $i$ th joint, denoted by

$$\mathbf{l}_i = [\prod_i \mathbf{R}_i(\theta_i)] \hat{\mathbf{l}}_i, \quad (4.9)$$

and  $\hat{\mathbf{l}}_i$  is the initial link vector of the corresponding link. According to (4.7) and (4.8), the velocity and acceleration at CoM of each link can also be given as the following equations

$$\mathbf{v}_{gi} = \mathbf{v}_i + \boldsymbol{\omega}_i \times \mathbf{l}_{gi}, \quad (4.10)$$

$$\mathbf{a}_{gi} = \mathbf{a}_i + \ddot{\mathbf{l}}_{gi} + \dot{\boldsymbol{\omega}}_i \times \mathbf{l}_{gi} + 2\boldsymbol{\omega}_i \times \dot{\mathbf{l}}_{gi} + \boldsymbol{\omega}_i \times (\boldsymbol{\omega}_i \times \mathbf{l}_{gi}), \quad (4.11)$$

In this way, accelerations of the CoM of each link,  $\mathbf{a}_{gi}$ , can be obtained.

Since the stability condition (3.43) can be satisfied as long as (3.42) holds, from (3.42) we have

$$\mathbf{r}_{hand} \times \mathbf{F}_{hand} + \mathbf{r}_{foot} \times \mathbf{F}_{foot} = -\sum_i \mathbf{r}_i \times (m_i \mathbf{g}), \quad (4.12)$$

and from (4.1), we have

$$\mathbf{F}_{foot} = -\sum_i m_i (\mathbf{g} + \mathbf{a}_{gi}) - \mathbf{F}_{hand}. \quad (4.13)$$

Substituting (4.13) into (4.12), we have

$$\mathbf{r}_{hand} \times \mathbf{F}_{hand} - \mathbf{r}_{foot} \times (\sum_i m_i (\mathbf{g} + \mathbf{a}_{gi}) + \mathbf{F}_{hand}) = -\sum_i \mathbf{r}_i \times (m_i \mathbf{g}), \quad (4.14)$$

$$(\mathbf{r}_{hand} - \mathbf{r}_{foot}) \times \mathbf{F}_{hand} = \sum_i ((\mathbf{r}_{foot} - \mathbf{r}_i) \times m_i \mathbf{g} + \mathbf{r}_{foot} \times m_i \mathbf{a}_{gi}). \quad (4.15)$$

And the norm of both sides in (4.15) satisfies

$$|(\mathbf{r}_{hand} - \mathbf{r}_{foot}) \times \mathbf{F}_{hand}| = \left| \sum_i ((\mathbf{r}_{foot} - \mathbf{r}_i) \times m_i \mathbf{g} + \mathbf{r}_{foot} \times m_i \mathbf{a}_{gi}) \right|. \quad (4.16)$$

Since

$$|(\mathbf{r}_{hand} - \mathbf{r}_{foot}) \times \mathbf{F}_{hand}| = |(\mathbf{r}_{hand} - \mathbf{r}_{foot})| \cdot |\mathbf{F}_{hand}| \cdot |\sin \theta|, \quad (4.17)$$

where  $\theta = \langle \mathbf{r}_{hand} - \mathbf{r}_{foot}, \mathbf{F}_{hand} \rangle$ , with

$$|\sin \theta| \leq 1. \quad (4.18)$$

From (4.16) ~ (4.18) the following inequality satisfies

$$|\mathbf{r}_{hand} - \mathbf{r}_{foot}| \cdot |\mathbf{F}_{hand}| \geq \left| \sum_i ((\mathbf{r}_{foot} - \mathbf{r}_i) \times m_i \mathbf{g} + \mathbf{r}_{foot} \times m_i \mathbf{a}_{gi}) \right|, \quad (4.19)$$

and the inequality about the norm of force at hand can be given as

$$|\mathbf{F}_{hand}| \geq \frac{\left| \sum_i ((\mathbf{r}_{foot} - \mathbf{r}_i) \times m_i \mathbf{g} + \mathbf{r}_{foot} \times m_i \mathbf{a}_{gi}) \right|}{|\mathbf{r}_{hand} - \mathbf{r}_{foot}|}. \quad (4.20)$$

In the same way we also have

$$(\mathbf{r}_{foot} - \mathbf{r}_{hand}) \times \mathbf{F}_{foot} = \sum_i ((\mathbf{r}_{hand} - \mathbf{r}_i) \times m_i \mathbf{g} + \mathbf{r}_{hand} \times m_i \mathbf{a}_{gi}), \quad (4.21)$$

and

$$|\mathbf{F}_{foot}| \geq \frac{\left| \sum_i ((\mathbf{r}_{hand} - \mathbf{r}_i) \times m_i \mathbf{g} + \mathbf{r}_{hand} \times m_i \mathbf{a}_{gi}) \right|}{|\mathbf{r}_{foot} - \mathbf{r}_{hand}|} \quad (4.22)$$

for calculating force required for the foot side.

In addition, set the right side of (4.15) as the vector  $\mathbf{A}$ , we also have

$$\mathbf{A} \cdot (\mathbf{r}_{hand} - \mathbf{r}_{foot}) \times \mathbf{F}_{hand} = \mathbf{A} \cdot \mathbf{A}. \quad (4.23)$$

According to the property of triple product, (4.23) becomes

$$(\mathbf{A} \times (\mathbf{r}_{hand} - \mathbf{r}_{foot})) \cdot \mathbf{F}_{hand} = \mathbf{A} \cdot \mathbf{A}, \quad (4.24)$$

and taking the norm of the both sides of (4.24), we have

$$\left| (\mathbf{A} \times (\mathbf{r}_{hand} - \mathbf{r}_{foot})) \cdot \mathbf{F}_{hand} \right| = |\mathbf{A}|^2. \quad (4.25)$$

According to the definition of dot product of vectors,

$$\left| (\mathbf{A} \times (\mathbf{r}_{hand} - \mathbf{r}_{foot})) \cdot \mathbf{F}_{hand} \right| = |\mathbf{A} \times (\mathbf{r}_{hand} - \mathbf{r}_{foot})| \cdot |\mathbf{F}_{hand}| \cdot |\cos \varphi| \quad (4.26)$$

satisfies, where  $\varphi = \angle \langle \mathbf{A} \times (\mathbf{r}_{hand} - \mathbf{r}_{foot}), \mathbf{F}_{hand} \rangle$ .

Similarly, because

$$|\cos \varphi| \leq 1 \quad (4.27)$$

holds, then the following inequality also satisfies

$$|\mathbf{A}|^2 = \left| (\mathbf{A} \times (\mathbf{r}_{hand} - \mathbf{r}_{foot})) \cdot \mathbf{F}_{hand} \right| \leq |\mathbf{A} \times (\mathbf{r}_{hand} - \mathbf{r}_{foot})| \cdot |\mathbf{F}_{hand}|, \quad (4.28)$$

which leads to another inequality of norm of force at hand:

$$|\mathbf{F}_{hand}| \geq \frac{\left| \sum_i ((\mathbf{r}_{foot} - \mathbf{r}_i) \times m_i \mathbf{g} + \mathbf{r}_{foot} \times m_i \mathbf{a}_{gi}) \right|^2}{\left| \sum_i ((\mathbf{r}_{foot} - \mathbf{r}_i) \times m_i \mathbf{g} + \mathbf{r}_{foot} \times m_i \mathbf{a}_{gi}) \times (\mathbf{r}_{hand} - \mathbf{r}_{foot}) \right|}, \quad (4.29)$$

and the one for foot:

$$|\mathbf{F}_{foot}| \geq \frac{\left| \sum_i ((\mathbf{r}_{hand} - \mathbf{r}_i) \times m_i \mathbf{g} + \mathbf{r}_{hand} \times m_i \mathbf{a}_{gi}) \right|^2}{\left| \sum_i ((\mathbf{r}_{hand} - \mathbf{r}_i) \times m_i \mathbf{g} + \mathbf{r}_{hand} \times m_i \mathbf{a}_{gi}) \times (\mathbf{r}_{foot} - \mathbf{r}_{hand}) \right|}. \quad (4.30)$$

With (4.20), (4.22), (4.29) and (4.30) obtained, the sufficient conditions of the norm of reaction force for both 2 contact points can be given. It means that if at least one of (4.20), (4.22) and at least one of (4.29) and (4.30) are both satisfied, then the robot will not rotate on the ladder. In the case that they are not satisfied, then stability conditions for avoiding rotation (3.42) and (3.43) are checked. If (3.42) and (3.43) are not satisfied, then the robot is not stable and needs reaction force control to bring the robot back to stable states, which leads to the next section.

### 4.2.3 Conditions and distribution of reaction force at contact points

It has been explained and also verified by the former studies that bias of reaction force at contact points may lead to insufficient reaction force moment at contact points. Therefore, appropriate distribution of reaction force at 2 contact points besides the motion planning of the body to reduce gravity moment around the contact points is crucial to avoid rotation of the robot on the ladder.

Here, set  $y_{body}$  as the coordinate of CoM of the robot in Y-axis,  $y_{ori}$  and  $z_{ori}$  as the coordinate of the origin in Y-axis and Z-axis,  $y_{hand}$  and  $z_{hand}$  as the coordinate of hand in Y-axis and Z-axis,  $y_{foot}$  and  $z_{foot}$  as the coordinate of foot in Y-axis and Z-axis, respectively. Also, set  $\mathbf{F}_{hand}=(F_{handx}, F_{handy}, F_{handz})$  and  $\mathbf{F}_{foot}=(F_{footx}, F_{footy}, F_{footz})$  as the reaction force on supporting hand and foot, respectively. According to the characteristic of gravity force that it always pointing the direction of -Z axis in this thesis, then we have the following calculation of moment in scalar:

$$\begin{aligned} \sum M_{roll} = & \sum_i (y_i - y_{ori}) \cdot m_i g + (z_{hand} - z_{ori}) \cdot F_{handy} - (z_{foot} - z_{ori}) \cdot F_{footy} \\ & - (y_{hand} - y_{ori}) \cdot F_{handz} - (y_{foot} - y_{ori}) \cdot F_{footz}. \end{aligned} \quad (4.31)$$

If the origin is set as the contact point at the supporting hand, then  $y_{ori} = y_{hand}$  and  $z_{ori} = z_{hand}$ , thus we have

$$\begin{aligned} \sum M_{rollhand} = & \sum_i (y_i - y_{hand}) \cdot m_i g - (z_{foot} - z_{hand}) \cdot F_{footy} \\ & - (y_{foot} - y_{hand}) \cdot F_{footz} \end{aligned} \quad (4.32)$$

as the total moment in Roll direction around the contact point at supporting hand. Similarly, we have

$$\begin{aligned} \sum M_{rollfoot} = & \sum_i (y_i - y_{foot}) \cdot m_i g + (z_{hand} - z_{foot}) \cdot F_{handy} \\ & - (y_{hand} - y_{foot}) \cdot F_{handz} \end{aligned} \quad (4.33)$$

Now it is clear that both (4.32) and (4.33) should be zero to avoid rotation in Roll direction and keep stable, otherwise rotation around either contact point may happen. Besides, from (4.1) we have

$$F_{handz} + F_{footz} = \sum_i m_i g + \sum_i m_i a_{giz}, \quad (4.34)$$

where  $a_{giz}$  is the acceleration of the  $i_{th}$  link in Z-axis, which means that the sum of reaction force in Z-axis for supporting hand and foot is calculable and the increase of either one directly leads to the decrease of the other one, proving that distribution of reaction force is significant to satisfy both (4.32) and (4.33). Also, assume that

$$F_{handy} = \mu \cdot F_{handz}, \quad (4.35)$$

$$F_{footy} = \mu \cdot F_{footz} \quad (4.36)$$

are satisfied, where  $\mu$  is the friction coefficient between the end-effectors and the ladder. Then (4.32) and (4.33) become

$$\sum M_{rollhand} = \sum_i (y_i - y_{hand}) \cdot m_i g - [(z_{foot} - z_{hand}) \cdot \mu + (y_{hand} - y_{foot})] F_{footz}, \quad (4.37)$$

$$\sum M_{rollfoot} = \sum_i (y_i - y_{foot}) \cdot m_i g - [(z_{foot} - z_{hand}) \cdot \mu + (y_{hand} - y_{foot})] F_{handz}. \quad (4.38)$$

Let (4.37) and (4.38) be zero, then



$$F_{handz} = \left| \sum_i (y_i - y_{foot}) \cdot m_i g / [(y_{hand} - y_{foot}) - (z_{hand} - z_{foot}) \cdot \mu] \right|, \quad (4.39)$$

$$F_{footz} = \left| \sum_i (y_i - y_{hand}) \cdot m_i g / [(y_{hand} - y_{foot}) - (z_{foot} - z_{hand}) \cdot \mu] \right| \quad (4.40)$$

satisfy, which are the minimal target value of reaction force in Z-axis for hand and foot. Therefore, the best distribution of reaction force in Z-axis between  $F_{handz}$  and  $F_{footz}$  can be given as

$$\frac{F_{handz}}{F_{footz}} = \left| \frac{\sum_i (y_i - y_{foot})}{\sum_i (y_i - y_{hand})} \cdot \frac{(y_{hand} - y_{foot}) - (z_{hand} - z_{foot}) \cdot \mu}{(y_{hand} - y_{foot}) - (z_{foot} - z_{hand}) \cdot \mu} \right|. \quad (4.41)$$

The problem of (4.41) is that friction coefficient  $\mu$  has to be known to calculate the best distribution between  $F_{handz}$  and  $F_{footz}$ . However, it may not be practical to obtain  $\mu$  in application. Taking this point into consideration, in this thesis we set  $y_{hand} = y_{foot}$  in 2-point contact ladder climbing. Now we have

$$\frac{F_{handz}}{F_{footz}} = 1 \quad (4.42)$$

from (4.41), which is exactly  $F_{handz} = F_{footz}$ , an equation that is not related to  $\mu$ . In the real application, it is desirable to satisfy the following condition:

$$\left| F_{footz} - F_{handz} \right| \leq F_{tol}, \quad (4.43)$$

where  $F_{tol}$  is the tolerance of the difference of forces that satisfies stability conditions between supporting hand and foot, which is expected to exist inevitably due to the noise of force/torque sensors, response delay of force control and so on. In this thesis  $F_{tol}$  is set to be different values according to different situations. Specifically, if the reaction force in Z-axis of the to-be supporting hand/foot is not sufficient to satisfy (4.43), then force control for the corresponding hand/foot acts until  $F_{handz}$  and  $F_{footz}$  get close enough to satisfy (4.43).

In this thesis, among various types of force controller, we choose PID controller of reaction force with respect to end-effector position in Z-axis to control the force

at contact point of hand and foot. This is because (i) PID controller in this thesis is free from the position error caused by deformation, which will be discussed in the Section 4.3; (ii) PID controller is simple and easy to adjust. The specific equation of PID controller is given as:

$$\Delta r_z = K_p (F_z - F_{zd}) + K_i \int (F_z - F_{zd}) dt + K_d \frac{d(F_z - F_{zd})}{dt}. \quad (4.44)$$

And the definition of variables in (4.44) is listed in Table 4-1. In summary, the flow of reaction force controller for 2-point contact ladder climbing is depicted in Fig. 4.1.

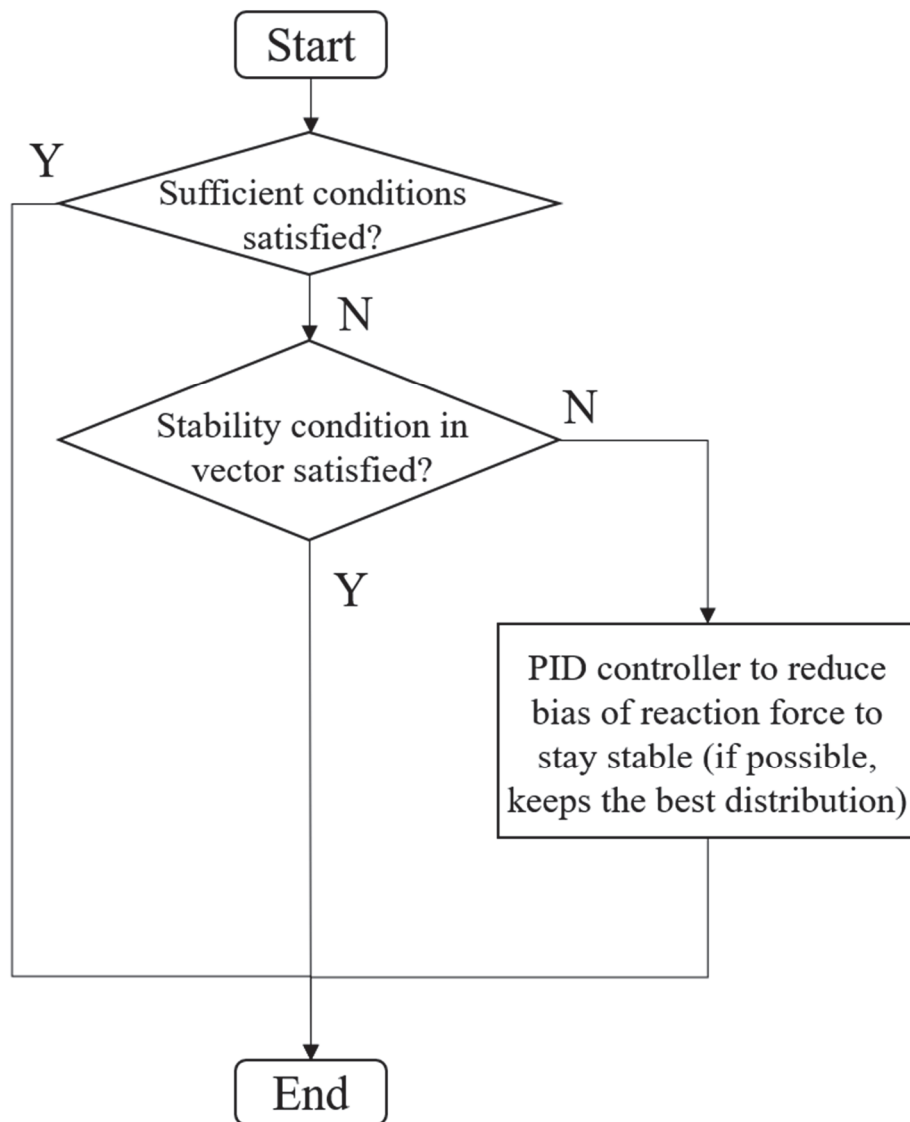


Fig. 4.1 Flowchart of reaction force feedback to maintain stability.

Table 4-1 Definition of variables.

Variable	Definition
$\Delta r_z$	Modification amount of position in Z-axis required for the corresponding end-effector
$K_p$	Proportional gain
$K_i$	Integral gain
$K_d$	Derivative gain
$F_z$	Current value of reaction force in Z-axis
$F_{zd}$	Desired value of reaction force in Z-axis

#### 4.2.4 Experiment: Comparison

##### 4.2.4.1 Conditions

In this section, results of comparative experiment performed by WAREC-1 are presented to validate whether feedback control of reaction force is contributive to enhancing stability of ladder climbing in 2-point contact gait or not. Conditions of the experiment are listed in Table 4-2.

Table 4-2 Conditions in Experiment 1.

Condition	Value
Rung distance mm	250
Pole distance mm	600
$F_{tol}$ for 2-point contact state N	100
Initial force for left hand N (lifted on the air on purpose)	0
Time for 1 climb motion s	10
Time for idling s (inputing command)	6
Total time s	26

Both 2 cases with and without reaction force feedback controller are shown as comparison. Note that in this comparative experiment the initial force at left hand is zero because it is lifted on the air initially on purpose to create bias of the reaction force between supporting hand and foot in 2-point contact ladder climbing. Moreover, for the avoidance of complexity, horizontal move of body is omitted here.

#### 4.2.4.2 Results

Snapshots of comparative experiments can be seen in Fig. 4.2 and Fig. 4.3, reaction force data at hands and feet of WAREC-1 are illustrated in Fig. 4.4 and Fig. 4.5, respectively. For the case with PID reaction force feedback controller the climbing was successful, but for the case without the robot rotated and the climbing motion failed with the rotation of the robot in Roll direction.

#### 4.2.4.3 Discussions

Focusing on force data in Z-axis presented in Fig. 4.4 and Fig. 4.5, averaging by PID controller of reaction force worked well with marks of the red ellipses in Fig. 4.4, It was confirmed that the biggest bias of force in Z-axis between the supporting hand and foot was less than 100N, which completely satisfied the condition of (4.9). However, for the case without PID reaction force feedback controller, the bias of reaction force in Z-axis remained, and when  $t=8s$  the climbing failed.

According to the calculation of required force in Z-axis given in the previous sections, there should be approximately at least 352N in Z-axis for the left hand to maintain stability, while at the moment of  $t=8s$  this condition was no longer satisfied. However, it should be noted that there was actually error between the calculated required force in Z-axis for the left hand and the real reaction force data measured. The reason may be (i) The error of calculation; (ii) The error of force/torque sensor and other factors.

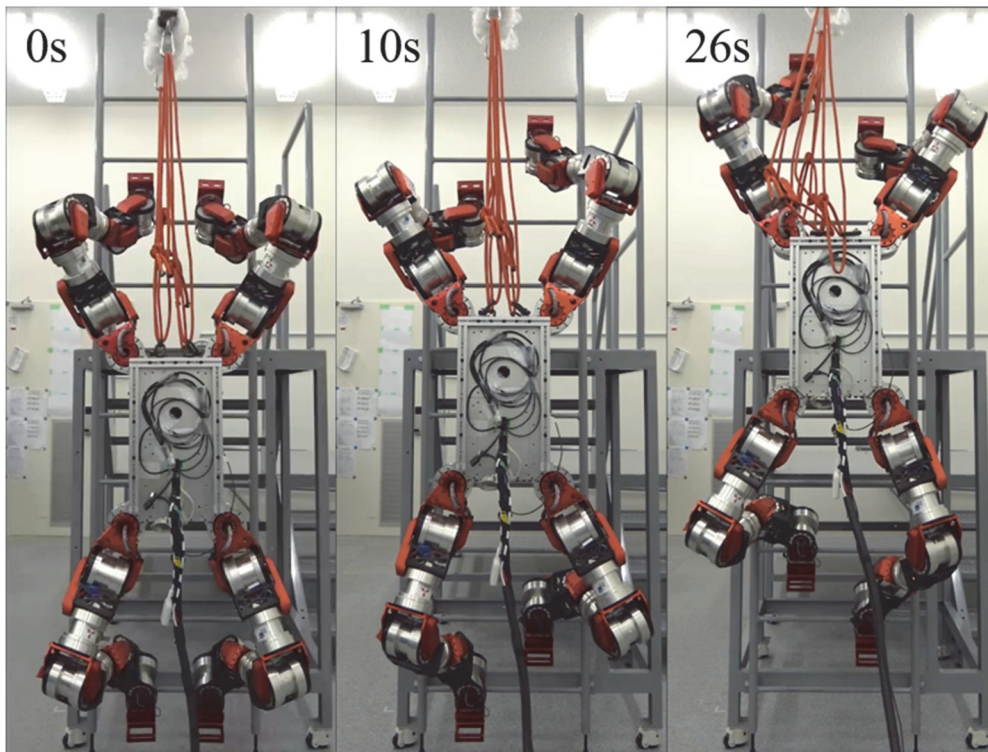


Fig. 4.2 2-point contact ladder climbing by WAREC-1: Successful.  
(with PID reaction force controller)

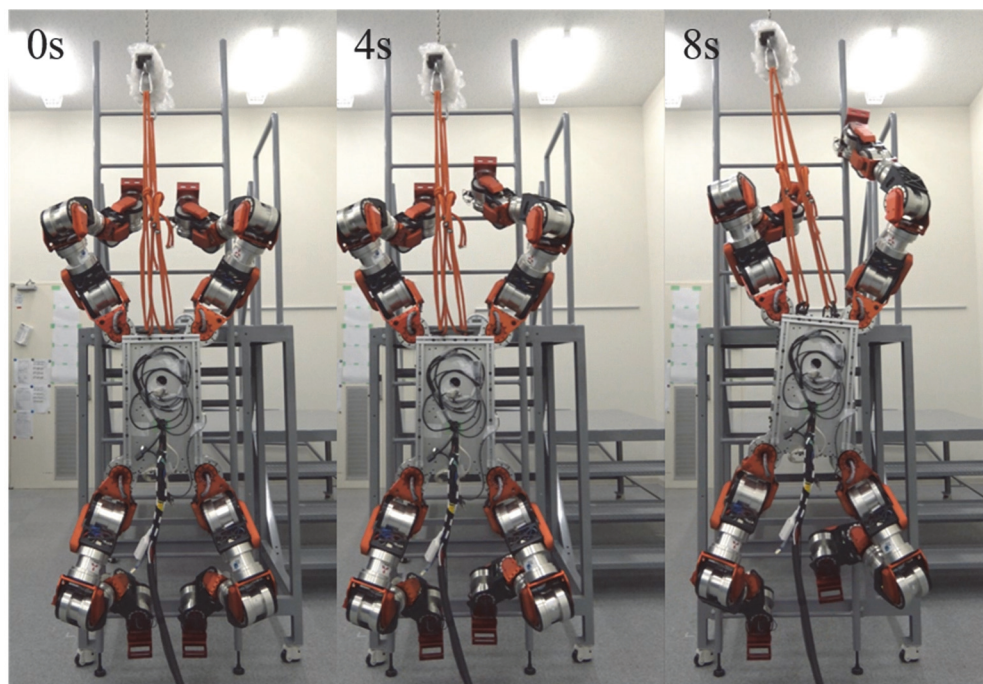


Fig. 4.3 2-point contact ladder climbing by WAREC-1: Failed.  
(without any reaction force feedback control)

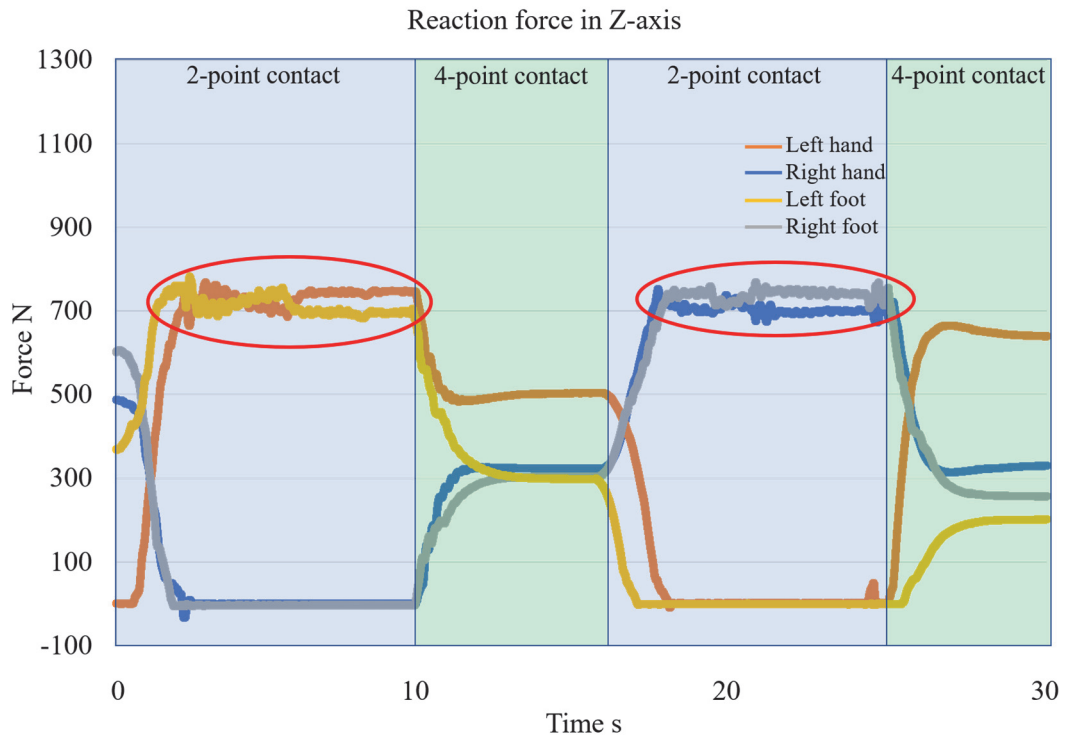


Fig. 4.4 Reaction force in Z-axis measured in 2-point contact ladder climbing. (with PID reaction force controller).

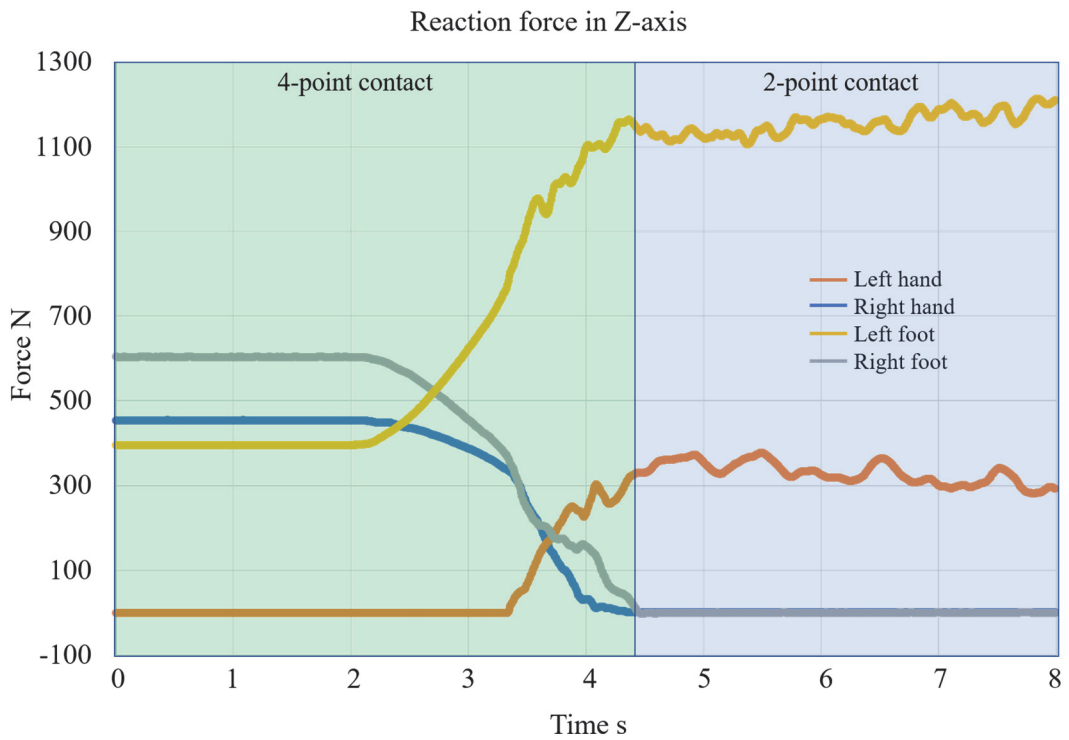





Fig. 4.5 Reaction force in Z-axis measured in 2-point contact ladder climbing. (without any force feedback control)

### 4.3 Proximity sensor feedback system

Due to the size and weight of WAREC-1, error of position and orientation in ladder climbing mainly caused by the deformation of robot as well as ladder and other factors appears inevitably. Although end-effector design in Fig. 2.3 enables error absorption within a certain range, which is up to the width of hook and groove part in Fig. 4.6, the error existing in ladder climbing still may be too big to be fully cancelled by mechanical “compliance” for end-effector and causes failure in ladder climbing. Fig. 4.7 shows typical cases of unsuccessful grabs of rungs that may directly result in failure of ladder climbing. Moreover, this error is complicated, for it may be the mixture of position and orientation and its amount varies for different postures of the robot.

Among the previous studies, Yoneda et al. proposed a recovery motion model for Gorilla-III in the case that the grip of ladder rungs fails, with the judgement of success/failure of grip by output of voltage of the motor in joint [17]. Unfortunately, although it did work with failed contact of the case shown in Fig. 4.2(b), it could neither solve other cases of Fig. 4.2(a) and Fig. 4.2(c) nor correct the wrong contact quantitatively, let along with the recognition of rung with variable specifications.

Table 4-3 Comparison of sensor options.

	Proximity sensor: VL6180X [42]	LRF: Ubg-04lx-f01 [43]	Depth camera: Pico flex [44]
Features			
Size mm	18 × 13 × 2	70 × 60 × 60	68 × 17 × 7.35
Measurable range mm	0~150	60~4000	100~4000
Accuracy	±3%	±1%	±1%
FoV (Field of View) °	±12.5 (horizontal and vertical)	±120 (horizontal)	±31 (horizontal) × ±22.5 (vertical)
Mechanism	ToF (Time of Flight)	LBS (Laser Beam Section)	ToF (Time of Flight)

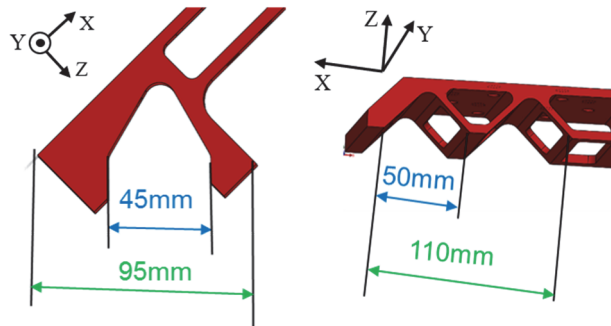
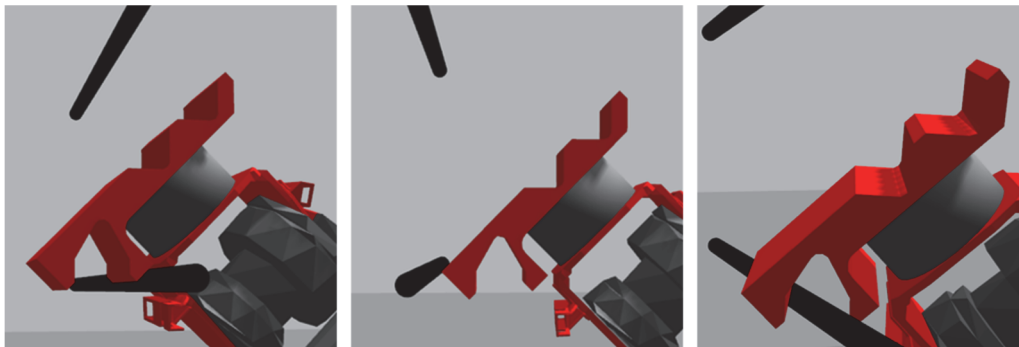


Fig. 4.6 Width of hook and groove on the end-effector.



(a) Too far away      (b) Not enough      (c) Incorrect orientation

Fig. 4.7 Typical cases of failed grab of rungs.

Side poles are omitted for better look.



Fig. 4.8 Proximity sensor VL6180X [42].

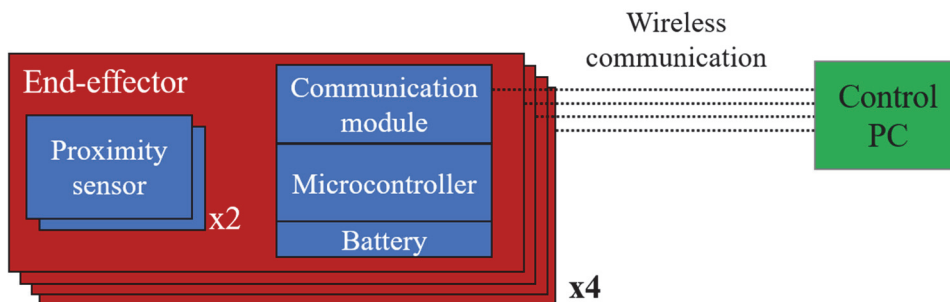


Fig. 4.9 System configuration of proximity sensors.



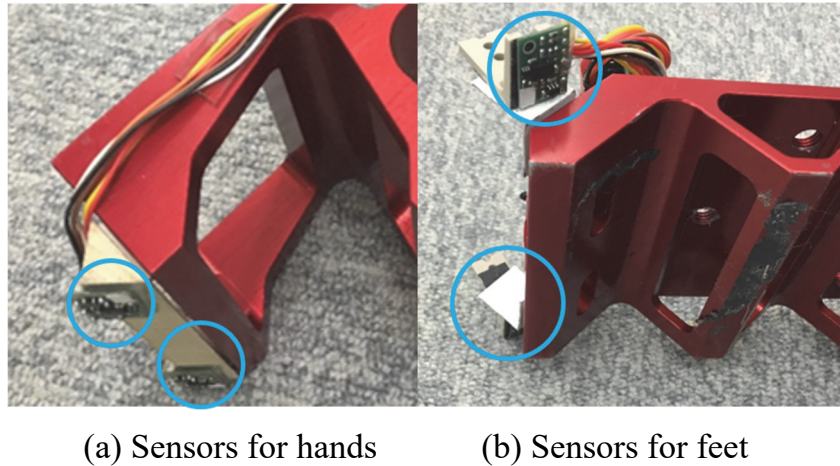


Fig. 4.10 The position and orientation of proximity sensors at the end-effectors. (blue circles).

Consequently, to deal with this issue we developed an environment (rung) recognition system composed by proximity sensors to measure the amount of error. In this thesis, we choose proximity sensor “VL6180X” made by STMicroelectronics shown in Fig. 4.8 among other options of environment recognition sensors listed in Table 4-3, mainly for (i) The shortest measurable range and (ii) Super-small size. The first point is especially significant because in ladder climbing end-effector may get very close to the target rung, even only within millimeters, and the sensor must be able to measure distance in that case. Apparently, LRF and depth camera listed in Table 4-3 do not satisfy this crucial requirement.

In the rung recognition system, sensing data is transmitted via wireless communication. In detail, there are 8 proximity sensors and small-sized batteries in total with 2 sensors equipped at each end-effector and every 2 proximity sensors on the same end-effector are connected to an Arduino Fio (4 in total) as the microcontroller. For each Arduino Fio a Xbee wireless module is connected for sending data to control PC. There is also a master module for wireless communication to transmit and receive data from all 4 Arduino Fios. The whole system configuration for the proximity sensors is depicted in Fig. 4.9. Note that total FoV of VL6180X is as narrow as  $25^\circ$  for enhancing directivity of measuring and avoiding measuring undesired objects to a certain degree. Based on this feature, proximity sensors are attached to end-effectors of WAREC-1 as Fig. 4.10 so that it is in the optimal orientation for recognizing the ladder rungs.

The reason of attaching 2 proximity sensors on each end-effector is that 2

sensors are the minimum requirement for sensing both error in position and orientation in ladder climbing, which can be calculated by the difference of data from 2 sensors, which will be explained detailly in the following section.

### 4.3.1 Error sensing and compensation motion

The following explains (i) how proximity sensors pick up data and calculate relative distance and orientation between end-effectors and rungs and (ii) how the robot moves its end-effectors to compensate the error and hang on rungs correctly.

As is mentioned in Table 4-3, FoV of the proximity sensors is relatively narrow. This feature is contributive to reducing mistakes of measuring wrong target, but also makes it more difficult to adjust the position and orientation of sensors so that

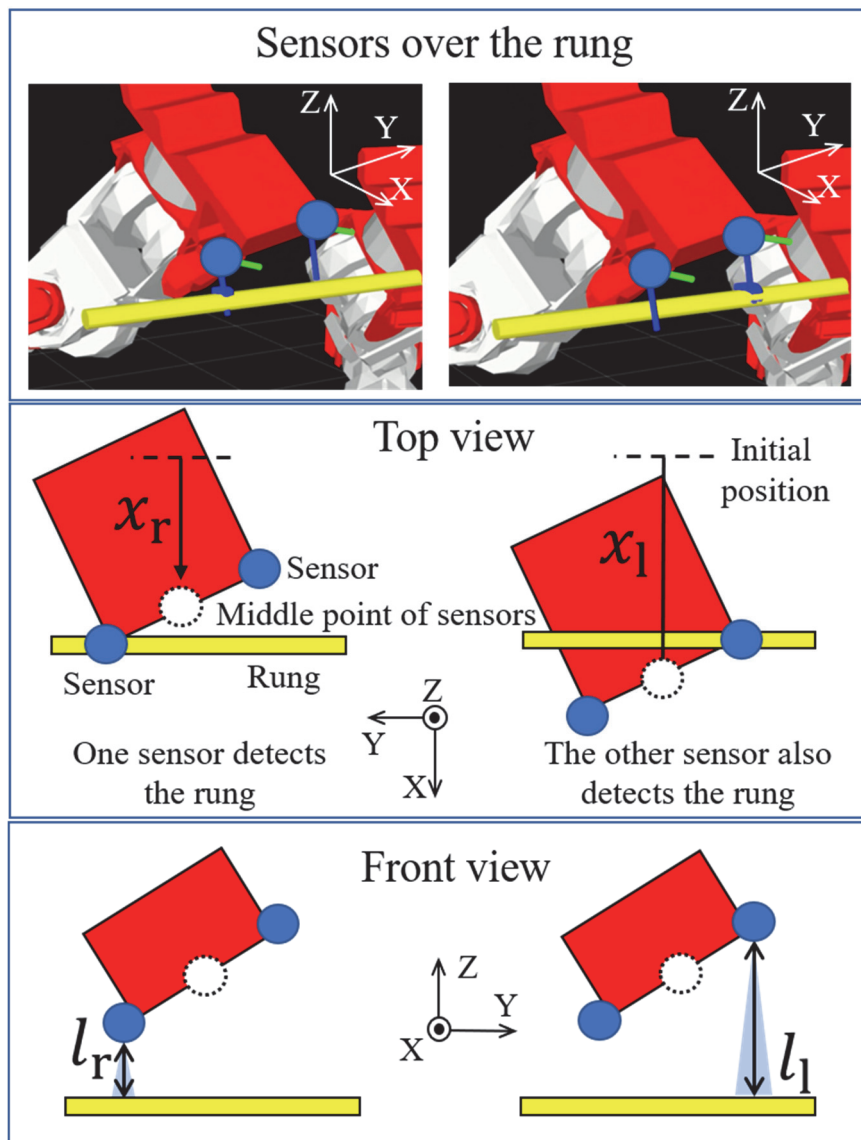


Fig. 4.11 The process of proximity sensors passing the target rung.

the target is within the FoV and measurable range. As a solution, in this thesis a sensing motion called “scan motion” is added for rung recognition. As its name, this motion moves the end-effector forward until it passes over the target rung and with distance moved forward recorded. Apparently, when distance data has reached shortest value and starts to increase again, it indicates that the shortest distance among all measured data is the real distance between the sensor and target rung.

The flow of sensing for proximity sensors and rung recognition goes as follows (Fig. 4.11):

- 1) Start point of “scan motion”: Let end-effector move to the area where 50~150mm higher in Z-axis and 50~200mm less further in X-axis than the target rung;
- 2) “Scan motion”: End-effector moves forward in X-axis. In this procedure both distance data of the sensor and the range of moving forward for 2 sensors calculated by forward kinematics will be recorded. The “scan motion” ends once the end-effector passed over the target rung.
- 3) Calculation of error: With distance data from sensors and moving range data calculated by the robot, it is possible to calculate relative position and orientation now. Specific calculation of distance to move and orientation to adjust are presented in (4.45) ~ (4.52) and definitions of variables in Table 4-4:

$$l_l = \frac{\sum_i (l_{li}/l_{li}^3)}{\sum_i (1/l_{li}^3)}, \quad (4.45)$$

$$l_r = \frac{\sum_i (l_{ri}/l_{ri}^3)}{\sum_i (1/l_{ri}^3)}, \quad (4.46)$$

$$x_l = \frac{\sum_i (x_{li}/l_{li}^2)}{\sum_i (1/l_{li}^2)}, \quad (4.47)$$

$$x_r = \frac{\sum_i (x_{ri}/l_{ri}^2)}{\sum_i (1/l_{ri}^2)}, \quad (4.48)$$

$$x_e = \frac{1}{2}(x_l - x_r) - x_c + x_{offset}, \quad (4.49)$$

$$z_e = \frac{1}{2}(l_l + l_r) + z_{offset}, \quad (4.50)$$

$$\theta_{roll} = \arcsin\left(\frac{l_l - l_r}{s_d}\right), \quad (4.51)$$

$$\theta_{yaw} = \arcsin\left(\frac{x_l - x_r}{s_d}\right). \quad (4.52)$$

Table 4-4 Explanation of variables related to sensor.

Variable	Explanation
$l_l, l_r$	Shortest distance detected by the sensor on the left and right in scan motion
$x_l, x_r$	Coordinate of 2 proximity sensors in X-axis at $l_l$ and $l_r$
$i$	Number of record for data of $l_l, l_r$ and $x_l, x_r$ .
$x_e, z_e$	Calculated relative distance in X-axis and Z-axis
$x_c$	Current coordinate of the end-effector in X-axis after scan motion
$x_{offset}, z_{offset}$	Offset position of the sensor in X-axis and Z-axis
$\theta_{roll}, \theta_{yaw}$	Calculated relative orientation in Roll and Yaw
$s_d$	Distance between 2 sensors at the same end-effector

- 4) Hanging motion to the target rung: the end-effector will first adjust its orientation according to the results of (4.51) and (4.52). After that, with (4.45) ~ (4.48) the end-effector moves horizontally and vertically in order to put itself on target rung smoothly and accurately.

#### 4.3.2 Measures for robustness

To eliminate uncertainty existing in the whole proximity sensor system and reinforce its reliability as much as possible, we also added the following measures:

- 1) Measure for poor wireless communication quality: “wait and repeat”. Since wireless communication in standard of “Zigbee” with frequency of 2.4 GHz is used in transmitting data of measured distances in time series, it is completely possible that in environment filled with radio waves the communication may be interrupted, which did happen in our experiments. Our solutions to this problem are that (i) During the “scan move” in hanging the end-effector to target rung, if no data is returned then stop the motion and wait until data is received. This process is made for the delay of wireless communication, and it lasts for 0.5s, which is longer than the biggest delay that may happen; (ii) After the stage of “wait”, if there is still no data returned from the end-effector, then do the reverse of “scan motion” and go back exactly to the start point and try it

again. Note that (i) and (ii) here may repeat for multiple times until communication quality is good enough to obtain distance data from proximity sensors and continue ladder climbing.

- 2) Measure for incomplete or incorrect data: auto-check and ask for permission. Even if communication quality is good enough to transmit measured data, there are still other cases that are not sufficient to make a successful hanging motion:
  - (i) Data comes back from only one sensor. Since data from both 2 proximity sensors on one end-effector is indispensable for calculating orientation angle required to adjust, in this case scan motion must be done again until complete data from 2 sensors could be collected;
  - (ii) Incorrect data that may cause unreasonable move for the robot. Due to the mechanism of proximity sensor (ToF), when end-effector passes the rung there may be interference of external light or measuring wrong objects that cause incorrect data, which may lead to incorrect calculated orientation angle to adjust as a result. To avoid these cases to happen, an auto-check process is added so that when distance measured from 2 sensors differ too much, warning message and calculated orientation angles to adjust will be displayed to the operator of the robot and the operator will be asked for the permission of continuing hanging motion of end-effector. Never will the end-effector move unless the operator examines actual situation and gives permission. The whole process and flow of hanging an end-effector to rungs of a ladder is depicted in the flowchart of Fig. 4.12.

### **4.3.3 Integration of trajectory planning and proximity sensor feedback**

Although end-effector trajectory in ladder climbing is proposed and introduced in Chapter 3 and error compensation system is constructed in this chapter as well, integration of these two systems is required. Our solution is to divide the trajectory of ladder climbing motion for an end-effector into 2 parts: (i) End-effector trajectory planning from the initial position (usually a rung) to the start point of “scan motion”; (ii) Rung recognition and hanging motion onto the target rung. For (i), trajectory planning described in Chapter 3 is applied. For (ii), motion for error sensing (namely, “scan motion”) and adjustment take over to lead the end-effector to the target rung.

To realize the process above, the actual trajectory planning is designed to be like the one in Fig. 4.13. The position of 3 mid-points of the cubic spline path and terminal point is modified so that the end-effector stops at an appropriate position for starting scan motion. Time profile used in the trajectory planning is the same

pattern as the one shown in Fig. 3.10 so that at the transition point between trajectory planning and rung recognition, the end-effector stops once, switch to rung recognition system and finally hangs on the target rung. The position of transition point is explained in the last section, which is also the best point for WAREC-1 to start rung recognition. This position, of course, can be adjusted freely.

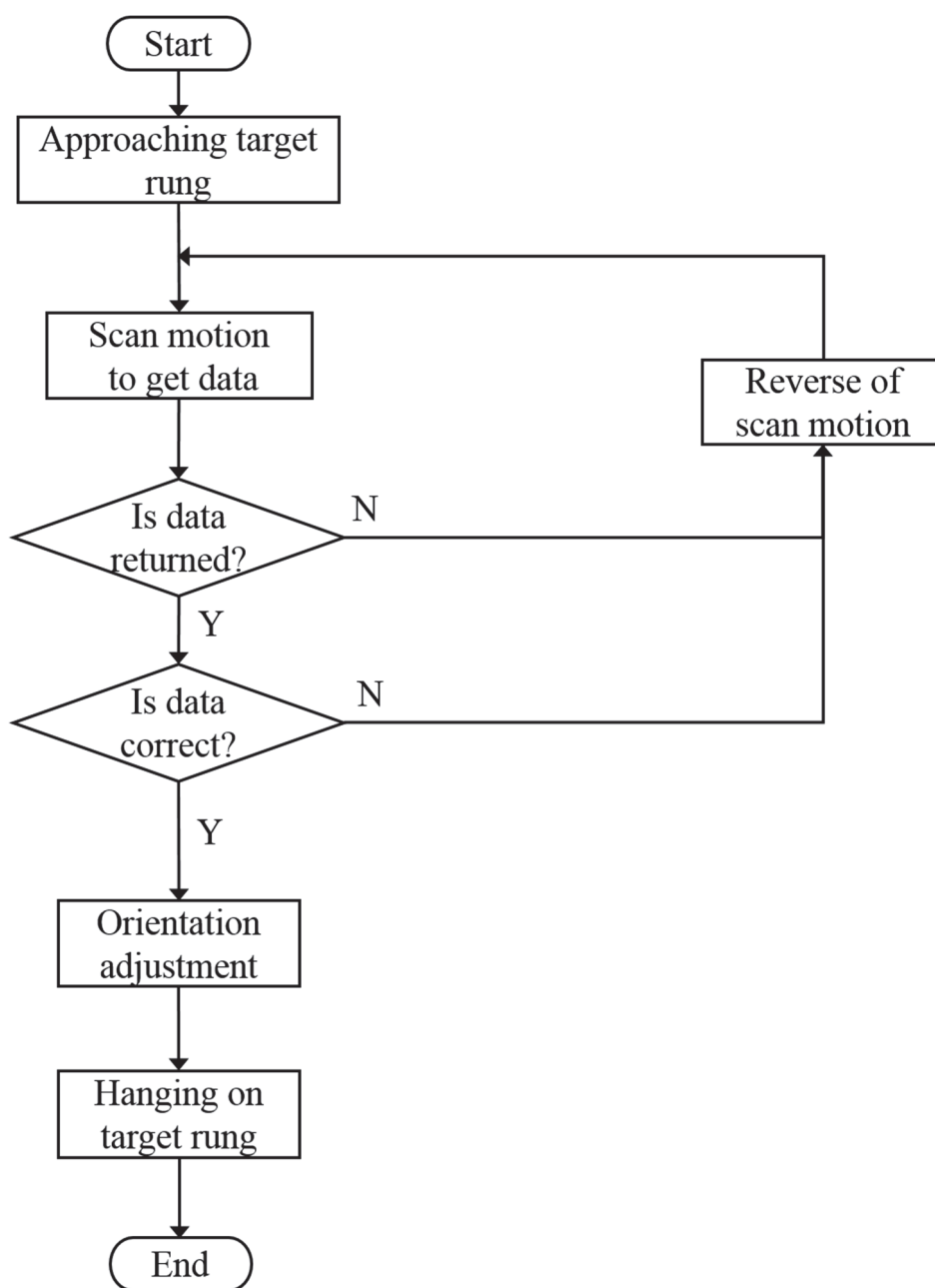


Fig. 4.12 Flowchart of hanging an end-effector on the target rung.

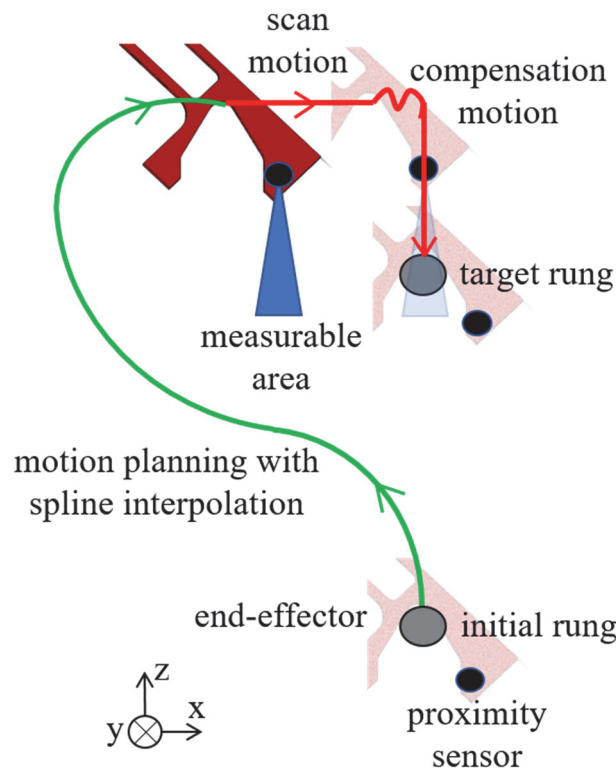


Fig. 4.13 Flowchart of hanging an end-effector on the target rung.

#### 4.3.4 Experiment 1: Reliability and accuracy test

##### 4.3.4.1 Conditions

For the examination of reliability of proximity sensor and accuracy of rung recognition and adjustment, experiments of 3-point contact ladder climbing were made with proximity sensor feedback. The rung interval of the ladder is 250mm, pole distance is 600mm and the diameter of the rungs is 19mm.

##### 4.3.4.2 Results

The statistics of results can be seen in Table 4-5, with success rate of 97.5%, and the rest of 2.5% for unsuccessful cases (5 times) were caused by human error or inappropriate orientation of foot that caused unexpected collision with rungs, for which the inappropriate motion planning made by human should be responsible. Due to the condition of indoor environment filled with electromagnetic waves inside (where there were more than 50 audiences with their cellphones), the interference of wireless communication did cause interruption of wireless data transmission between proximity sensors and the control PC for WAREC-1, which

refers to the case of “With retry” (9 times). Fig. 4.14 ~ Fig. 4.17 pick up the worst case throughout all experiments-it took 4 trails to make a successful hanging on target rung.

Table 4-5 Statistics of error compensation results.

Case		Number of times	Percentage	
Successful (195 in total)	Without retry	186	93%	97.5%
	With retry	9	4.5%	
Failed (5 in total)	Unexpected collision	3	1.5%	2.5%
	Human error	2	1%	
Total	200	200	-	-

#### 4.3.4.3 Discussions

Through the experiment, the reliability and accuracy of the proximity sensor system is partially verified, but the wireless communication is not perfect yet. Thus, we are planning to change it to a wired system to enhance its reliability in future.





Fig. 4.14 Trial 1 for hanging end-effector to rung: Failed.

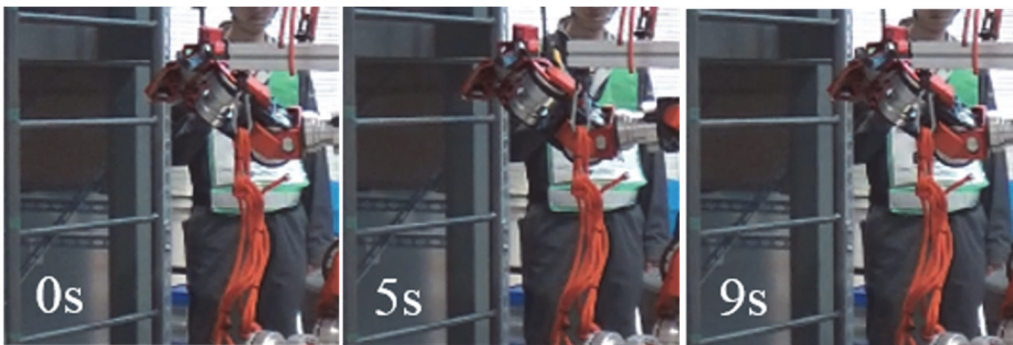


Fig. 4.15 Trial 2 for hanging end-effector to rung: Failed (cannot even finish the whole scan motion).



Fig. 4.16 Trial 3 for hanging end-effector to rung: Failed.

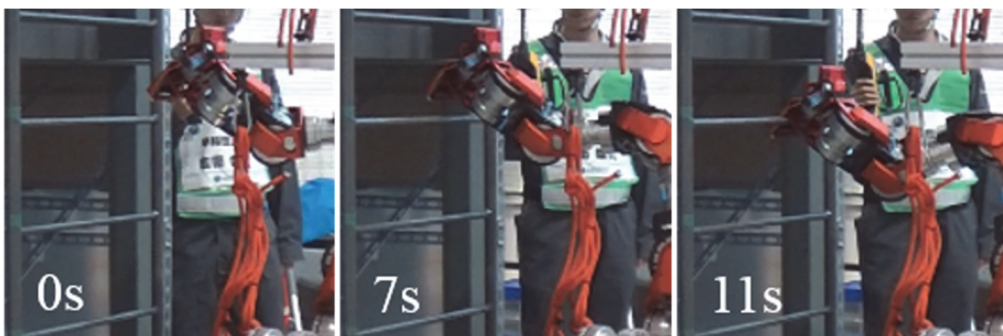


Fig. 4.17 Trial 4 for hanging end-effector to rung: Succeeded.

#### 4.3.5 Experiment 2: Climbing a ladder with a higher rung

Although a ladder is usually manufactured with a certain degrees of tolerance accuracy, the rung interval of a ladder may still change for some reasons. Damage of ladder in disaster situation is an instance. Besides, some handmade temporary ladders equipped in construction sites also may have different rung interval, with an example depicted in Fig. 4.18.



Fig. 4.18 An example of handmade temporary ladder.

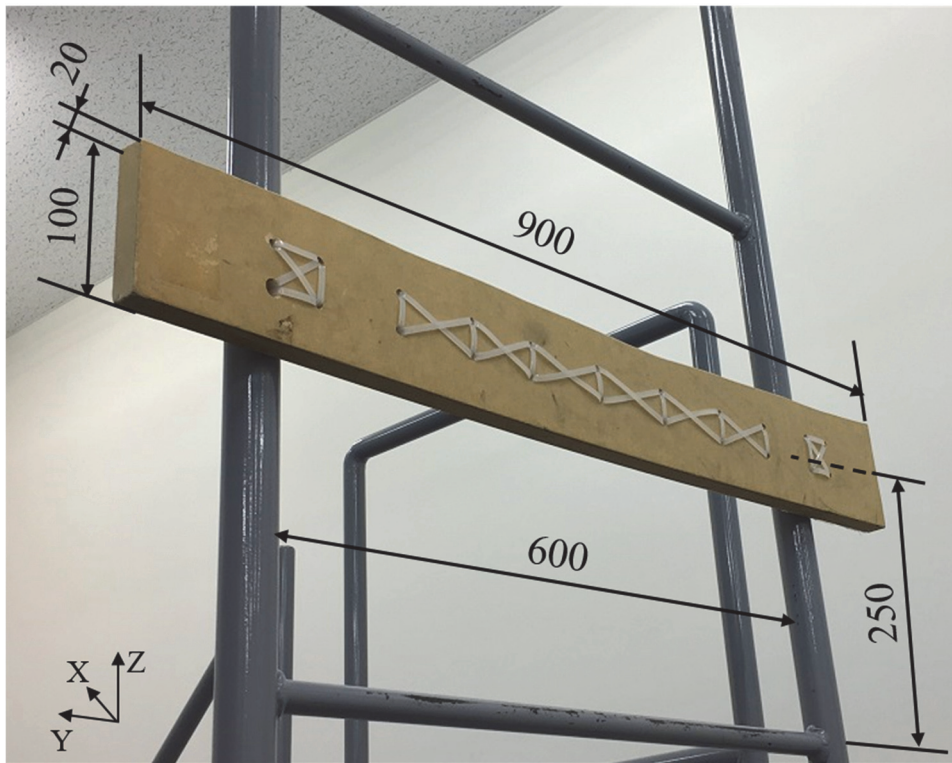


Fig. 4.19 Ladder attachment 1 on the ladder.

Therefore, in our opinion it is desirable that the robot becomes capable of recognizing and climbing a ladder with different rung distances varying within a certain range.

#### 4.3.5.1 Conditions

In this thesis, in the reference of rung interval range in JIS (225mm~300mm), the difference between the longest and shortest rung interval is 75mm. Thus, it is considered to be reasonable that the error of rung interval is within the range of  $\pm 37.5$ mm. According to this idea, we made an attachment to the ladder, which is a wooden plate to simulate a higher rung. For the convenience in this thesis we call it “Ladder Attachment 1”. Its picture with scales marked can be seen in Fig. 4.19. The change of specification for rung after the Ladder Attachment 1 is attached to the ladder is listed in Table 4-6. With Ladder Attachment 1 equipped, ladder climbing experiment was made to examine whether it is possible for WAREC-1 to climb such a ladder without inputting any information about the rung interval.

Table 4-6 Change of specification after equipping Ladder Attachment 1.

Change of specification	Value
Position in X-axis mm	-23
Position in Z-axis mm	+37
Inclination angle °	0

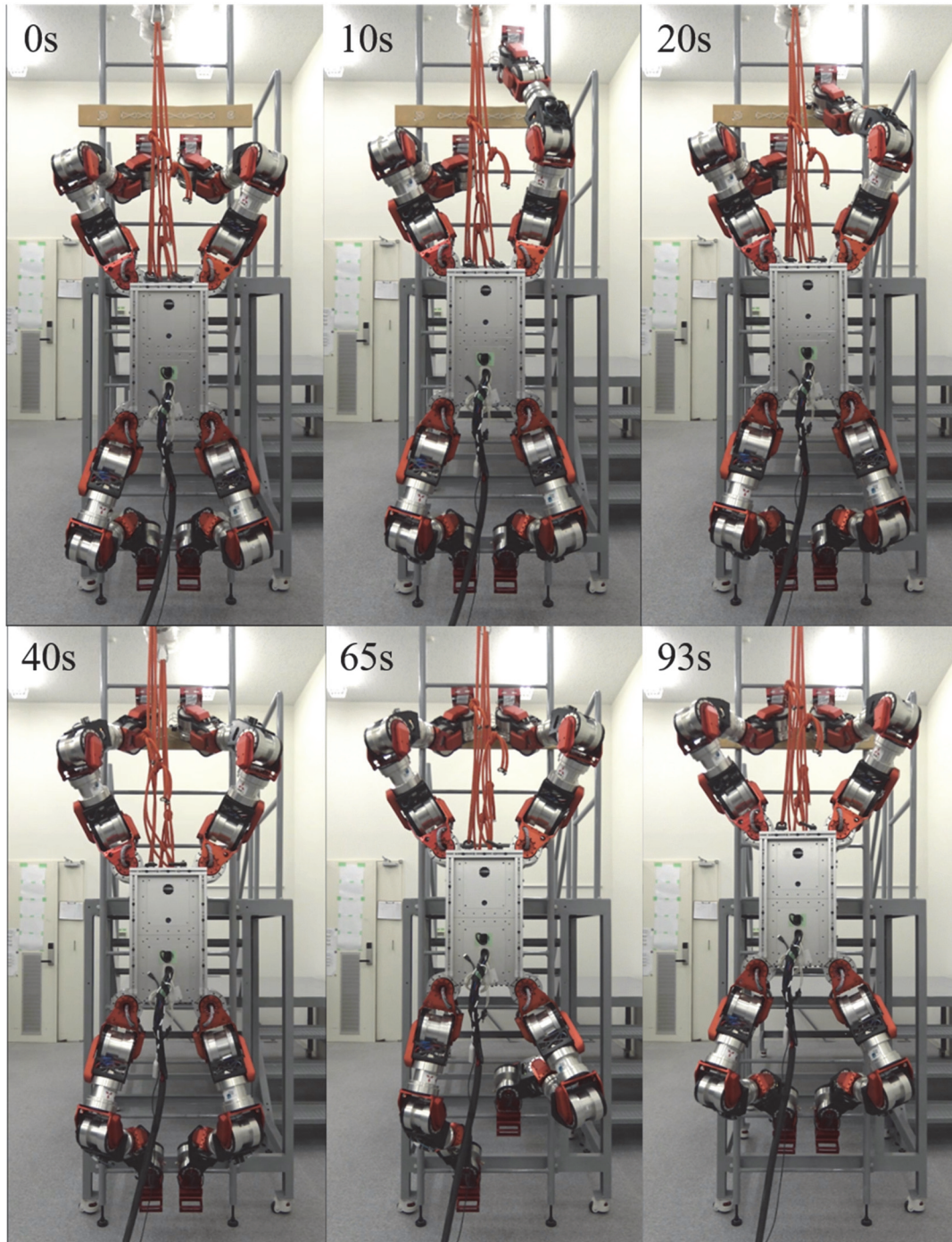


Fig. 4.20 Snapshots of climbing a ladder with Ladder Attachment 1.

Table 4-7 Time data in the experiment of Fig. 4.20.

Term	Time s
Climbing motion	40 (10 for each limb)
Scan and compensation motion	36 (9 for each limb)
Idling (confirming the results and input of commands for safety)	17
Total	93

#### 4.3.5.2 Results

The snapshots of the experiment are depicted in Fig. 4.20 and data about time spent is presented in Table 4-7. The results show that it is possible for WAREC-1 to recognize a rung with the error of +37mm in Z-axis and -23mm in X-axis.

#### 4.3.5.3 Discussions

Although rung recognition was successful, it still took 76s (1min 16s) for the robot to climb up a rung, which is 3.5mm/s in speed. The 3-point contact gait, slow speed of sensing motion are all the cause of being such slow.

#### 4.3.6 Experiment 3: Climbing a ladder with an inclined and higher rung

##### 4.3.6.1 Conditions

In disaster sites, besides the difference of rung interval, inclination of rung may also be seen due to the damage by the external environment. Hence, we made

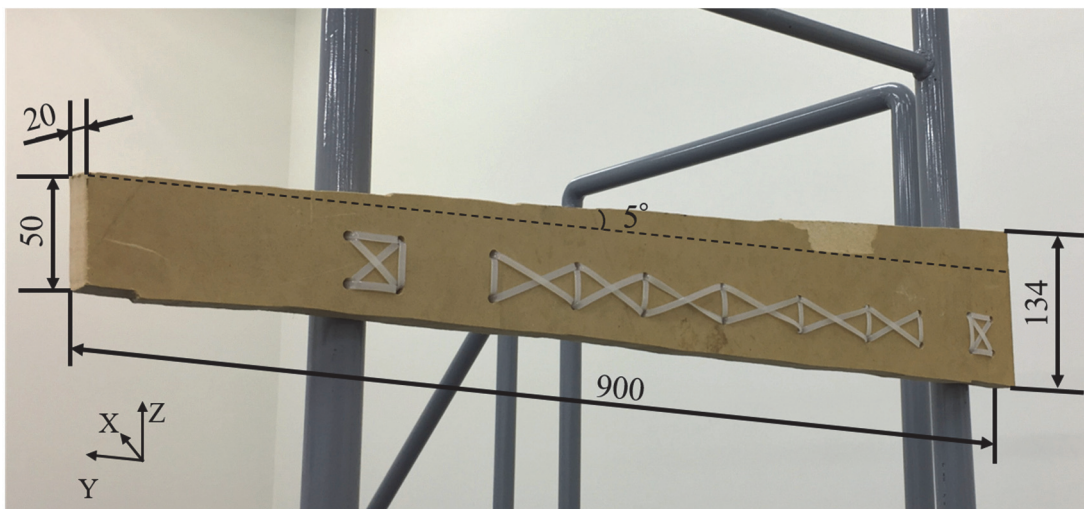


Fig. 4.21 Ladder attachment 2 on the ladder.

another wooden plate called “Ladder Attachment 2” with inclination of  $-5^\circ$  in Roll axis, depicted with scales in Fig. 4.21.

Here, the reason of  $-5^\circ$  for inclination angle is that since the shortest pole distance of ladder in JIS is 400mm, to meet the distance error of  $\pm 37.5\text{mm}$  explained in the last section, the biggest inclination angle possible in the condition of pole distance of 400mm is approximately  $5^\circ$ . Same as the Case 1, The changes of specification are listed in Table 4-8.

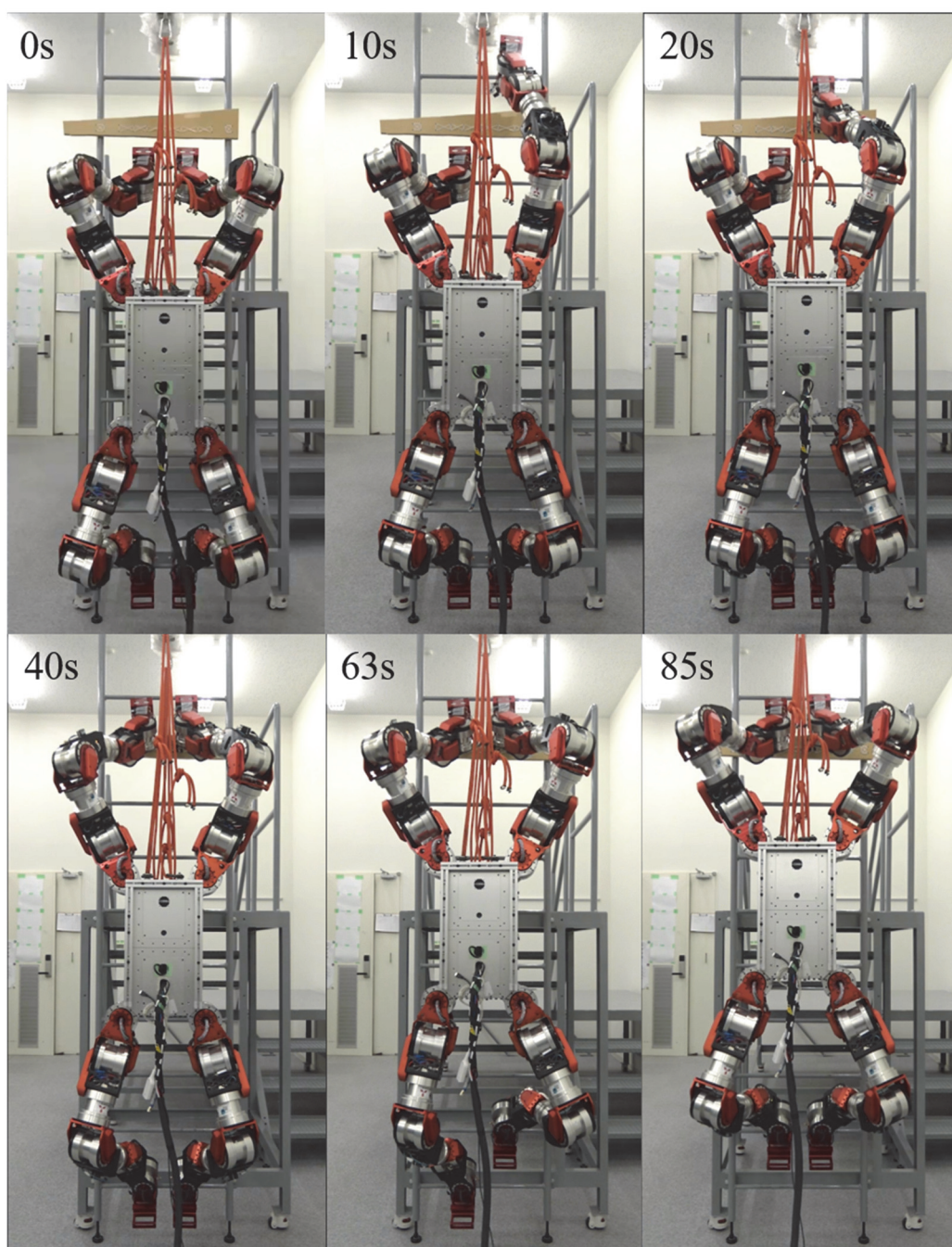


Fig. 4.22 Snapshots of climbing a ladder with Ladder Attachment 2.

Table 4-8 Change of specification after equipping Ladder Attachment 2.

Change of specification	Value
Position in X-axis mm	-23
Position in Z-axis mm	+64 (for right hand) +48 (for left hand)
Inclination angle °	-5 (in Roll axis)

Sensor data of right hand in scan motion for Case 2

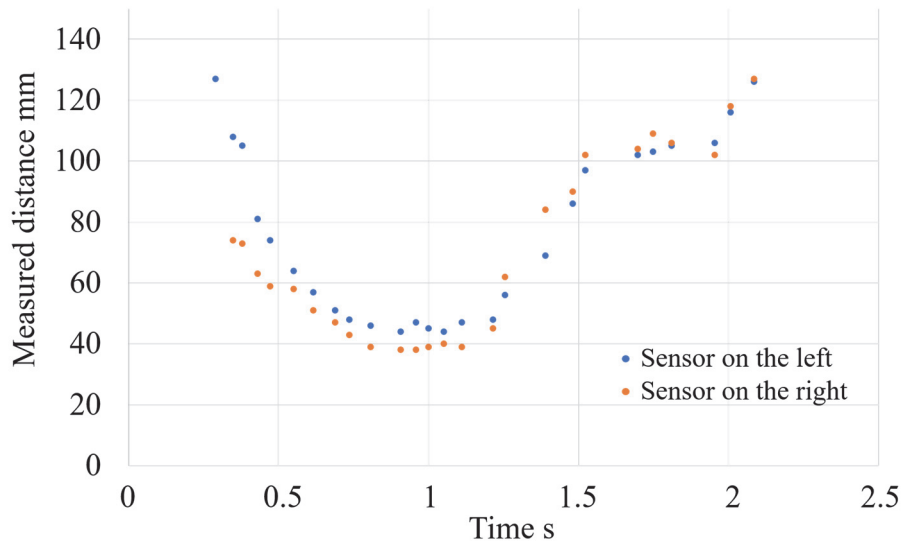


Fig. 4.23 Proximity sensor data of right hand in the Case 2.

Sensor data of left hand in scan motion for Case 2

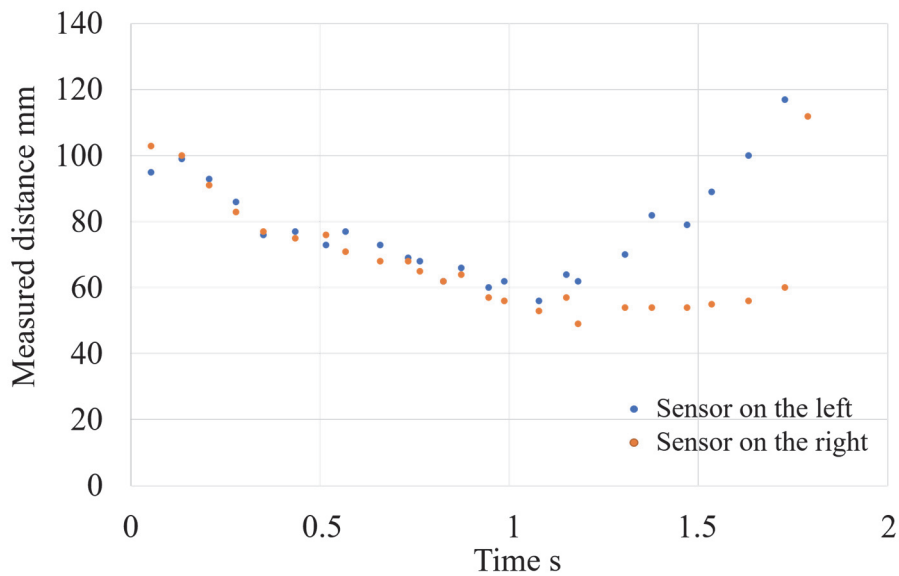


Fig. 4.24 Proximity sensor data of left hand in the Case 2.

### 4.3.6.2 Results

Table 4-9 Time data in the experiment of Fig. 4.22

Term	Time s
Climbing motion	40 (10 for each limb)
Scan and compensation motion	36 (9 for each limb)
Idling	9
Total	85

Time data of the experiment is shown in Table 4-9. The total speed excluding the idling time is also the same: 3.5mm/s. The data of proximity sensor for both left and right hand in scan motion are given in Fig. 4.23 and Fig. 4.24. According to (4.45), (4.46), (4.51) and measured data in these 2 figures, the error angle are calculated to be  $-5^\circ$  and  $-4.2^\circ$  for the left and right hand, respectively. This result is very closed to the real value, proving the accuracy of the whole system.

### 4.3.6.3 Discussions

In addition to the “Experiment 2”, it was also verified that proximity sensor feedback system can recognize a ladder rung with error in X-axis for -23mm and Z-axis for +48 ~ +64mm as well as inclination angle of  $-5^\circ$  in Roll axis, a situation that may happen when the target rung is inclined by deformation, aging, etc.

## 4.3.7 Experiment 4: Comparison in simulation

### 4.3.7.1 Conditions

Finally, we made a ladder with error in both position and orientation that are completely the same with the conditions in the “Experiment 3” in simulator Gazebo. The comparison of ladder climbing performed by WAREC-1 with and without proximity sensor feedback system is made in simulator. All conditions about the simulator and simulation are completely the same as those listed in Table 3-7, thus is omitted here.

### 4.3.7.2 Results

The results are presented in Fig. 4.25 and Fig. 4.26. Apparently, proximity sensor feedback system did avoid falling of WAREC-1 by guaranteeing proper contact between end-effectors and the target rung, while the robot fails to contact the rung correctly and falls directly for the case without it.



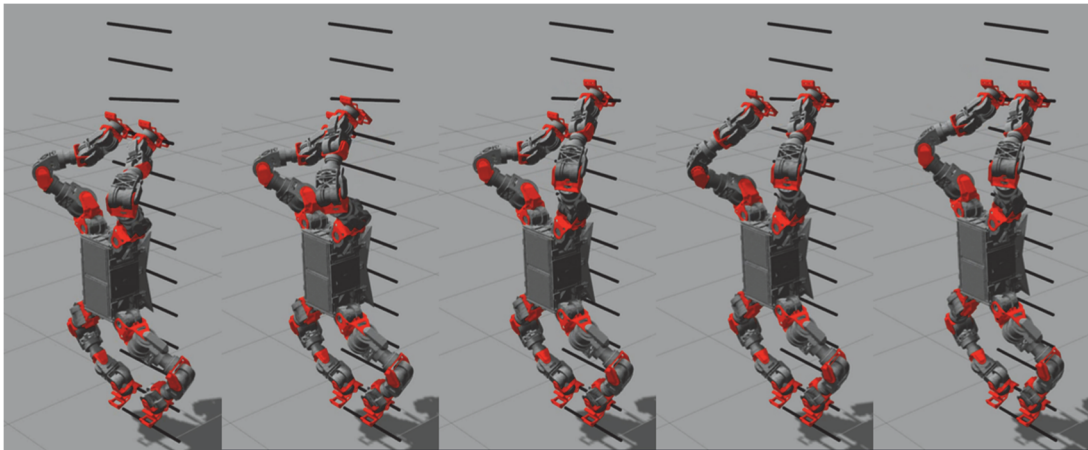


Fig. 4.25 WAREC-1 climbing a ladder with error.  
(with proximity sensor feedback system)

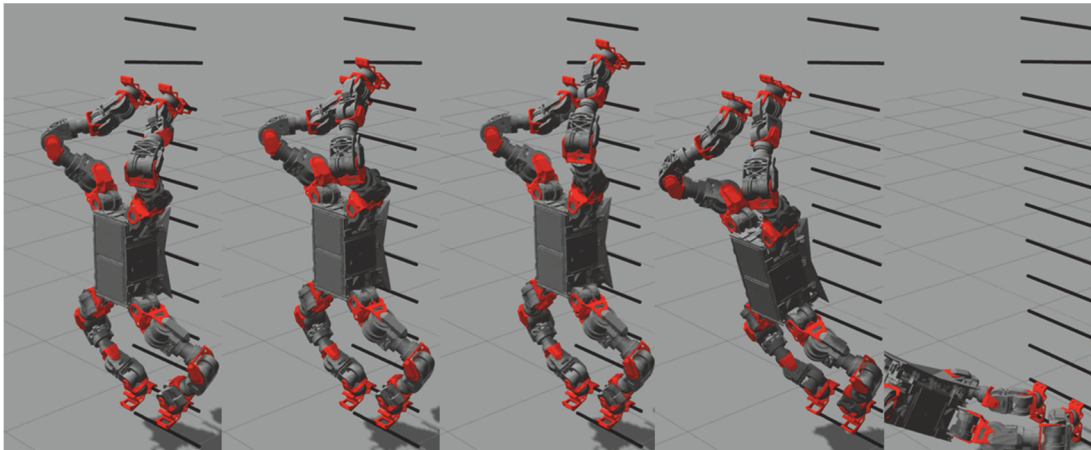


Fig. 4.26 WAREC-1 climbing a ladder with error.  
(without proximity sensor feedback system)

## 4.4 Total integration experiment

### 4.4.1 Total flow of ladder climbing motion

As the integration of all contents in Chap. 2 and Chap. 3, Fig. 4.27 presents a flowchart of ladder climbing for WAREC-1. To begin with, it is required to choose climbing gait: 2-point or 3-point contact climbing. The processes in squares on the straight line connecting “Start” and “End” correspond to the case of 3-point contact climbing and the processes on the right side of them correspond to the case of 2-point contact climbing. Since stability has the highest priority in ladder climbing, 2-point contact climbing will be chosen only if it is feasible and necessary. The point needs to mention is that ladders that cannot be climbed with neither 2-point contact or 3-point contact climbing gaits, like broken ladders, are of course existing

in reality but are not within the range of discuss in flowchart of Fig. 4.27. In that case, locomotion styles other than ladder climbing would be considered.

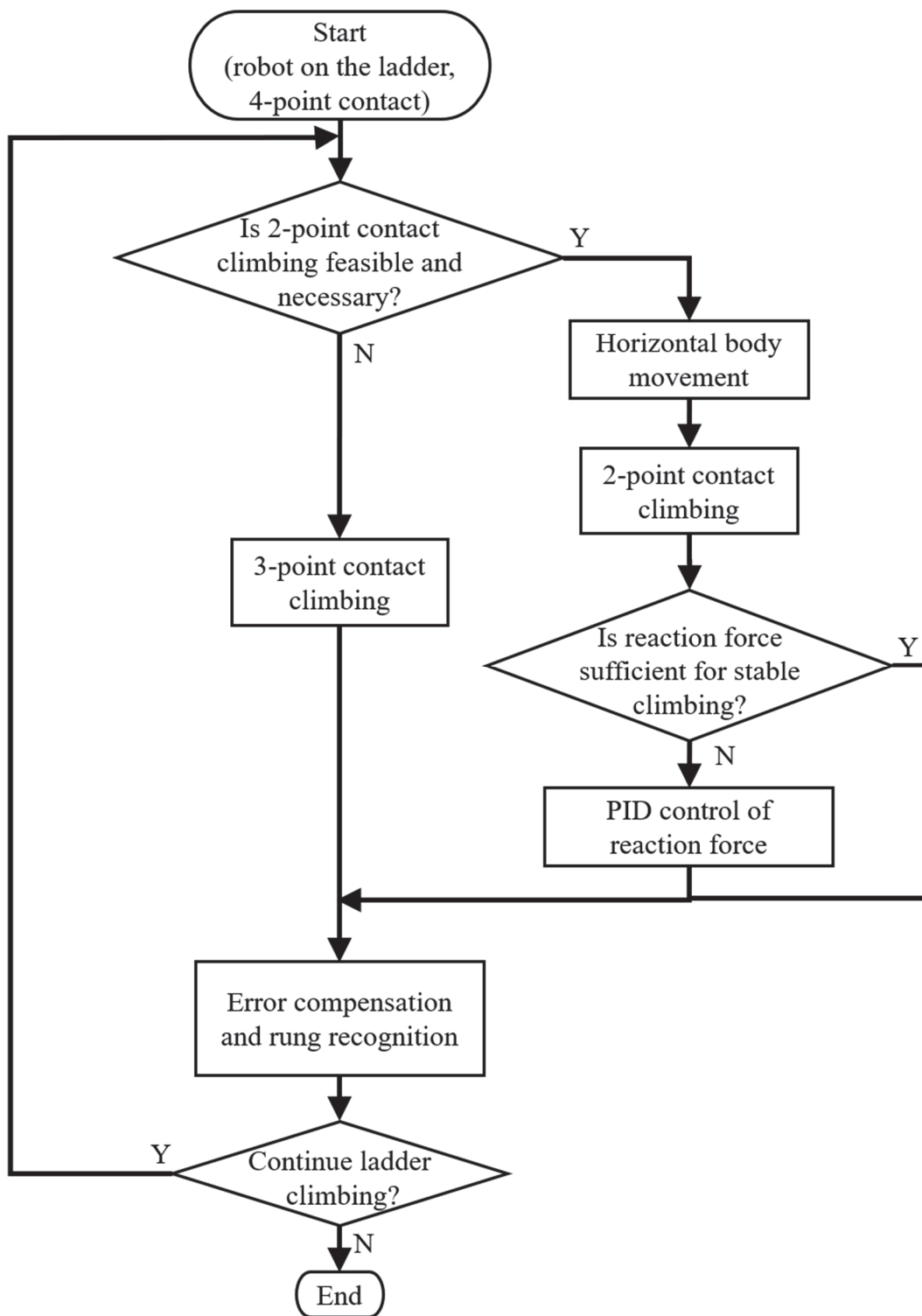


Fig. 4.27 Flowchart of motion generation for WAREC-1.

#### 4.4.2 Conditions

In the last 2 sections (Section 4.2 and 4.3), the solutions to (i) Unstable states caused by the bias of reaction force distribution at contact points and (ii) Recognition of ladder rungs with unknown specification in ladder climbing are described and demonstrated with verification, respectively.

However, from Section 4.3 although it could be seen that although stable ladder climbing is realized with recognition of rungs with error, it takes approximately 76s (3.5mm/s in speed) for the robot to climb up a rung, which is relatively slow in comparison with ladder climbing in 2-point contact gait. Therefore, to improve the speed in climbing a ladder with unknown or variable specification, all systems in Chap. 3 and Chap. 4 are integrated and the experiment results of the integration will be presented in this section. Specifically, the robot climbs the ladder in Section 4.2, while “Ladder attachment 2” in Section 4.3 is equipped at the target rung for simulating inclination of the target rung. Table 4-10 shows the conditions in this integration experiment.

Table 4-10 Conditions of the total integration experiment.

Term	Value/Description
Target rung	With Ladder attachment 2
Pole distance mm	600
Distance of horizontal body move mm	100 (first step) 200 (second step)
Time for 1 climb motion s	5
Time for 1 scan motion and compensation motion s	12
Time for horizontal body move s	2 (first step) 4 (second step)
Time for idling s (inputting command)	6
Total time s	46

#### 4.4.3 Results

Fig. 4.28 presents the snapshots of the experiment. Excluding idling time, total time spent is 40s (12.5mm/s in speed), which did improve the total speed of ladder climbing in comparison with the experiment in Section 4.3.6 (the case in 3-point contact climbing gait). The data of reaction force in Z-axis is shown in Fig. 4.29. In this integration experiment, the threshold of bias of reaction force in Z-axis between

supporting hand and foot is adjusted to 200N, which is of course an acceptable and sufficient value to maintain stability without the risk of unstable state as well. In detail, the biggest reaction force required force for both hand and foot is 321N, which is sufficiently satisfied.

As for the recognition result of the proximity sensor feedback system, it is presented in Fig. 4.30, with the error angle calculated as  $-5^\circ$ , which is in a very good accuracy.

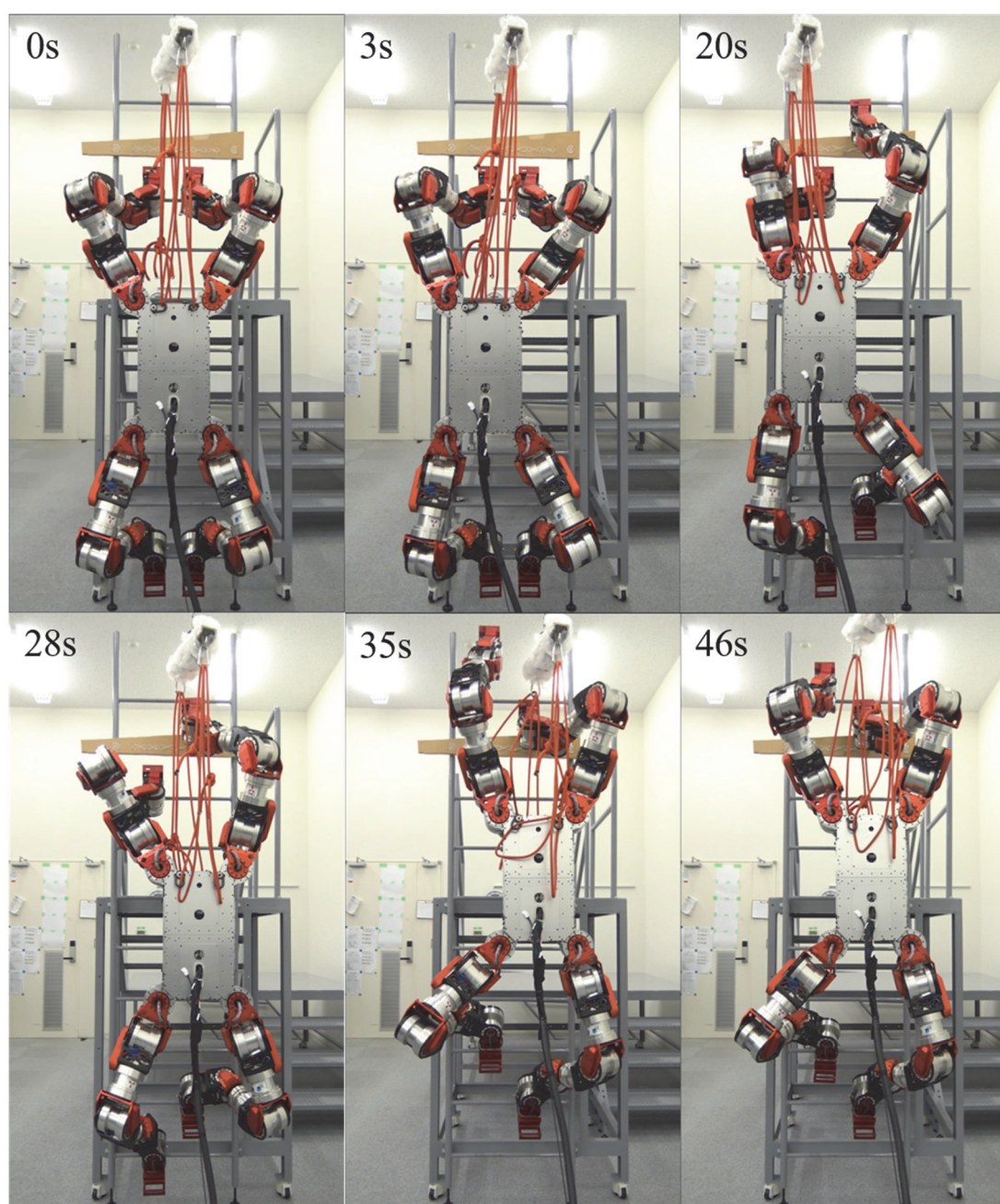


Fig. 4.28 Snapshots of the total integration experiment.

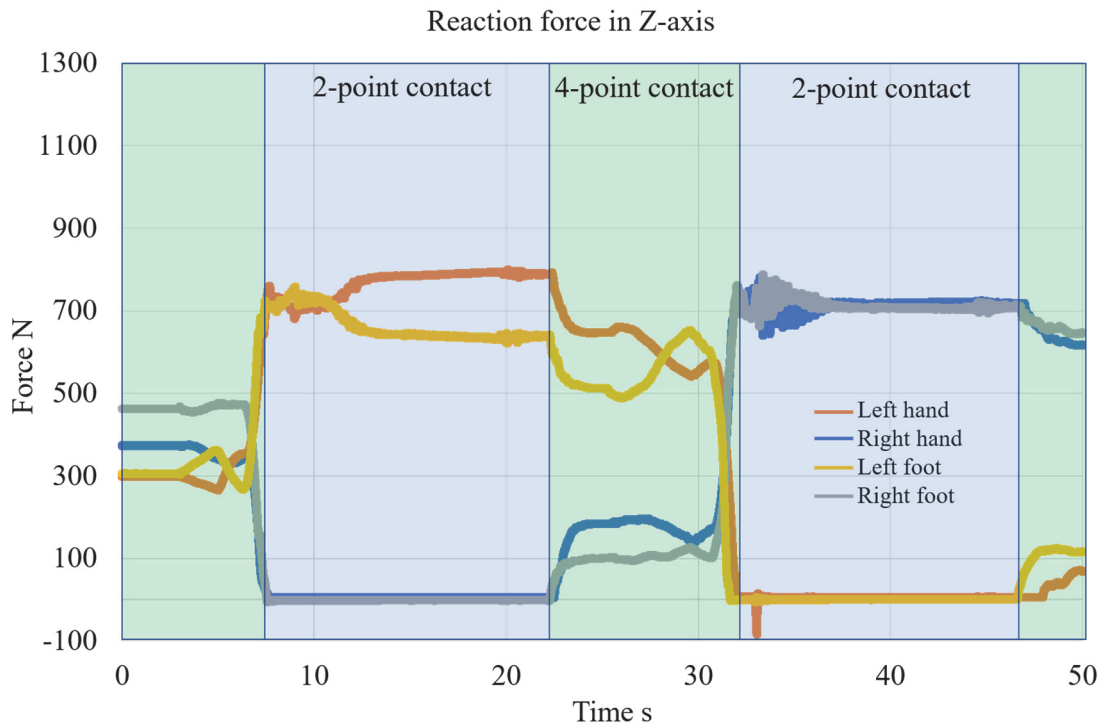


Fig. 4.29 Reaction force in Z-axis in 2-point contact ladder climbing.

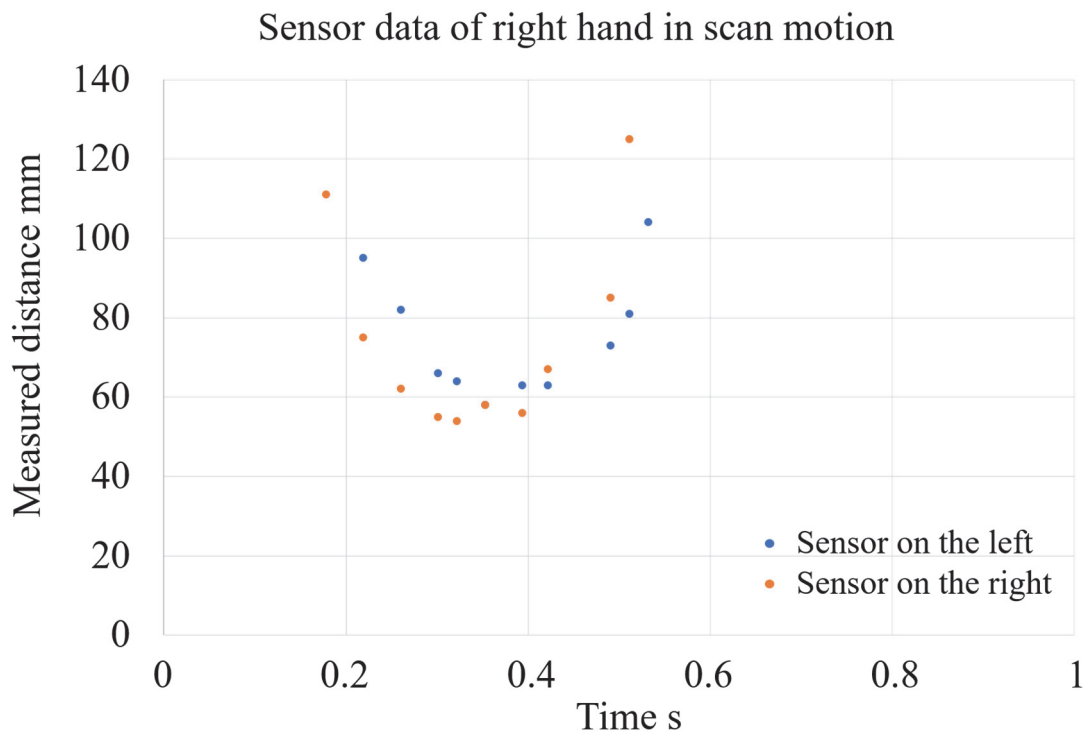


Fig. 4.30 Proximity sensor data of right hand in the total integration.

#### **4.4.4 Discussions**

Results show that the integration is successful in: (i) Reaction force bias between supporting hand and foot is within the threshold of 200N and (ii) Recognition of the inclination of “Ladder attachment 2” with high accuracy. As a result, the speed of climbing a ladder with variable or even unknown specifications becomes much faster (from 3.5mm/s to 12.5mm/s) in comparison with the experiment in Section 4.3.6, which is in 3-point contact climbing gait.

#### **4.5 Summary**

In this chapter, 2 types of sensor feedback system are introduced: (i) Force sensor feedback to control reaction force at supporting hand and foot in 2-point contact climbing gait. It reduces the bias reaction force at 2 contact point between the robot and ladder to avoid rotation of robot on the ladder; (ii) Proximity sensor system for measuring relative position and orientation between the end-effectors of the robot and rungs of ladder to enable recognition of the target rung to climb.

For (i), based on the stability analysis, it is possible to specify the reaction force required for stable ladder climbing at contact points. In this thesis a PID controller with respect to end-effector position is applied to control the reaction force at hand and foot in 2-point contact ladder climbing, reducing the bias of reaction force to keep the climbing motion stable. Strategy for controller is also described. The validity of force sensor feedback system is verified through experiments.

For (ii), the specification and system framework are detailly introduced, with the feature of the proximity sensor system corresponding motion for measuring and compensation motion planning are also designed and described. In the experiment, the proximity sensor feedback system does not only compensate the error of both position and orientation mainly caused by deformation of robot and ladder, but also recognize a higher rung or even an inclined rung with relatively high accuracy in measuring the position as well as inclination of the rung.

Finally, the results of total integration of all contents in Chap. 3 and Chap. 4 are shown and discussed.

## Chapter 5. Conclusions

### 5.1 Contributions

This thesis establishes systems and algorithms that enable the following points that have rarely been realized (or claimed to be realized) before by any human-sized robot:

- 1) Independent planning of path and time profile in end-effector trajectory of ladder climbing enables: (i) Planning ladder climbing motion avoiding unexpected collision between the robot and rungs of the ladder by individual planning of path in trajectory without making any change to time profile and vice versa; (ii) Adjustable time profile that can be given freely contributes to flexible motion adjustment with variable dynamic effects while path planning of motion stays the same. With these features, the complication of the motion planning in ladder climbing can be greatly reduced with the individual consideration of spatial and time constraints becomes available.
- 2) Ladder climbing in 2-point contact gait by human-sized robots. Apparently, 2-point contact ladder climbing is faster than 3-point contact, but is also challenging because appropriate force and moment must be maintained to guarantee stability, otherwise the robot may rotate on the ladder and eventually fall from the ladder. In this thesis the robot realizes stable 2-point contact ladder climbing of our human-sized robots with appropriate motion planning as well as the feedback of force/torque sensor, providing a powerful option of faster ladder climbing in comparison with 3-point contact ladder climbing.
- 3) Rung recognition and error (for both position and orientation) compensation between the robot and ladder rungs realized by the feedback of proximity sensors system. Super-small proximity sensor system and corresponding motion planning are developed for both sensing and compensation motion to make end-effectors “find” and hook on the target rung. This system guarantees that each contact between the robot and ladder is successful and appropriate. Measures prepared for expected error in sensing process enhances the robustness of the whole system. In addition, this system is also validated to be capable of recognizing a ladder rung with error of  $\pm 37$  in Z and X axis and even a rung with the inclination angle of  $5^\circ$ .

With these systems, the range of ladders available for our robots to climb is expanded greatly to ladders in the standard of JIS, even with unknown rung

interval or a rung with inclination to a certain degree. This compatibility to ladder specification greatly reinforces its capability in practical application in future.

## **5.2 Limitations**

### **5.2.1 Developed but incomplete capability of environment recognition**

Although in this thesis the robot is capable of recognizing a rung with offset in X and Z-axis and even an inclined rung in Roll axis with high accuracy, its environment recognition capability is still not complete and limited due to the characteristics of proximity sensors. Their maximum measurable distance is only up to about 150mm and FoV of proximity sensors are also very narrow (25° in total). As a matter of fact, proximity sensor feedback system at present on the robot could only “see” the closest rung to its end-effectors, which may be insufficient in motion planning of ladder climbing, and it is especially the case when the robot is climbing a long ladder. Besides, current proximity sensor feedback system could not recognize side poles. This may be a problem when the robot climbing a ladder is sliding horizontally.

### **5.2.2 No solution to time-variant ladder in different standards**

Moreover, since this thesis only discusses time-invariant ladders with the specifications in JIS, at present the systems in this thesis cannot deal with any ladder that may change in shape during ladder climbing. However, in application there is no guarantee that the target ladders are all in specifications of JIS and will not change their shapes during the ladder climbing.

### **5.2.3 No manipulation capability in ladder climbing**

Although the robots in this thesis are designed and developed to be capable of performing manipulation tasks, it has not been integrated into ladder climbing. However, manipulation in ladder climbing would be highly required when the target of the manipulation is on the wall that the ladder is attached to. Feasibility of manipulation in ladder climbing is also easy to be proved, since the robot is capable of supporting itself and hold on the ladder with only 3 or even 2 end-effectors contacting the ladder. This means that the possibility of one-limb or even 2-limb manipulation does exist.



### 5.3 Future works

According to the problems and discussions described in Section 5.1 and 5.2, we expect that the points below could be realized for the improvement of our present systems applied in ladder climbing:

- 1) Autonomous ladder climbing with the improvement of environment recognition and corresponding motion planning of ladder climbing. Besides the use of existing proximity sensor system, environment recognition by other types of sensors could recognize the whole target ladder as the base of motion planning. For example, at present we have equipped multiple depth cameras to the robot and constructing recognition of the target ladder with sufficient precision to support stable ladder climbing. At the same time, motion planning combined with existing sensor feedback systems to cope with the change of ladder would also be discussed and developed, such as the solution to the destruction or deformation of the rungs during climbing.
- 2) Manipulation tasks in ladder climbing. So far, our robot “WAREC-1” has completed heavy manipulation of turning valves with the torque of 90Nm as well as dexterous manipulation tasks such as button, switch and key operation. The integration of manipulation with ladder climbing would highly improve its capability in practical application. Certainly, feedback of force/torque sensor and other types (like IMU) would also be considered to guarantee the stability of the robot while it is performing manipulation on a ladder.
- 3) Development of hardware that contributes to ladder climbing. Body structure of the robot to enable its hooking to the ladder and corresponding ladder climbing pattern to (i) Accelerate the speed of climbing; (ii) Decrease the energy consumption in ladder climbing and (iii) Guarantee the stability of climbing motion will be a promising and innovative direction.



## References

- [1] 2008 Sichuan earthquake, [https://en.wikipedia.org/wiki/2008\\_Sichuan\\_earthquake](https://en.wikipedia.org/wiki/2008_Sichuan_earthquake), accessed 2017/10/04.
- [2] 2011 Tōhoku earthquake and tsunami, [https://en.wikipedia.org/wiki/2011\\_T%C5%8Dhoku\\_earthquake\\_and\\_tsunami](https://en.wikipedia.org/wiki/2011_T%C5%8Dhoku_earthquake_and_tsunami), accessed 2017/10/04.
- [3] 2014 Mount Ontake eruption, [https://en.wikipedia.org/wiki/2014\\_Mount\\_Ontake\\_eruption](https://en.wikipedia.org/wiki/2014_Mount_Ontake_eruption), accessed 2017/10/04.
- [4] 2016 Kumamoto earthquakes, [https://en.wikipedia.org/wiki/2016\\_Kumamoto\\_earthquakes](https://en.wikipedia.org/wiki/2016_Kumamoto_earthquakes), accessed 2017/10/04.
- [5] 2017 Central Mexico earthquake, [https://en.wikipedia.org/wiki/2017\\_Central\\_Mexico\\_earthquake](https://en.wikipedia.org/wiki/2017_Central_Mexico_earthquake), accessed 2018/08/17.
- [6] 2018 Japan floods, [https://en.wikipedia.org/wiki/2018\\_Japan\\_floods](https://en.wikipedia.org/wiki/2018_Japan_floods).
- [7] DARPA ROBOTICS CHALLENGE FINALS 2015, <https://web.archive.org/web/20160428005028/http://www.darparoboticschallenge.org>, accessed 2017/10/04.
- [8] Impulsing Paradigm Change through Disruptive Technologies Program (ImPACT), <http://www8.cao.go.jp/cstp/sentan/about-kakushin.html>, accessed 2017/10/04.
- [9] K. Hashimoto, X. Sun, K. Uryu, A. Koizumi, S. Hamamoto, T. Teramachi, T. Matsuzawa, A. Takanishi and Y. Kinouchi, “Development of Disaster Response Robot for Extreme Environments 1st Report: Classification of Extreme Environments and Basic Concept of Four-limb Robot”, The Robotics and Mechatronics Conference 2015, 1A1-T03, 2015.
- [10] The 2013 Report of Council on Competitiveness Nippon (COCN), “Establishment plan for a disaster response robot center”, 2013.
- [11] fuRo: Quince, [http://www.rm.is.tohoku.ac.jp/quince\\_eng/](http://www.rm.is.tohoku.ac.jp/quince_eng/), accessed 2017/10/04.
- [12] MHI — MEISTeR, <http://www.mhi.co.jp/news/story/1212065290.html>, accessed 2017/10/04.
- [13] [https://www.mpoweruk.com/wind\\_power.htm](https://www.mpoweruk.com/wind_power.htm), accessed 2018/08/17.
- [14] <https://www.pinterest.es/pin/40884309096155043/>, accessed 2018/08/17.
- [15] <https://blogs.yahoo.co.jp/qhsjn085/41693594.html>, accessed 2018/08/17.
- [16] H. Iida, H. Hozumi, and R. Nakayama, “Development of ladder climbing robot LCR-1,” *Journal of Robotics and Mechatronics*, vol. 1, pp. 311–316, 1989.
- [17] H. Yoneda, K. Sekiyama, Y. Hasegawa, and T. Fukuda, “Vertical ladder climbing motion with posture control for multi-locomotion robot,” in *Proc. 2008 IEEE/RSJ Int. Conf. Intelligent Robots and Systems*, Nice, 2008, pp. 3579-3584.
- [18] T. Fukuda et al., “Multi-Locomotion Robotics Systems,” Springer Press, 2012.

- [19] Z. Lu, K. Sekiyama, T. Aoyama, Y. Hasegawa, T. Kobayashi, and T. Fukuda, "Optimal control of energetically efficient ladder decent motion with internal stress adjustment using key joint method," in Proc. 2012 IEEE/RSJ Int. Conf. Intelligent Robots and Systems, Vilamoura, 2012, pp. 2216–2221.
- [20] J. Vaillant, A. Kheddar, H. Audren, F. Keith, S. Brossette, A. Escande, K. Bouyarmane, K. Kaneko, M. Morisawa, P. Gergondet, E. Yoshida, S. Kajita and F. Kenehiro, "Multi-contact vertical ladder climbing with an HRP-2 humanoid," *Autonomous Robots*, vol. 40, no. 3, pp. 561-580, Feb. 2016.
- [21] S. Nozawa, M. Kanazawa, Y. Kakiuchi, K. Okada, T. Yoshiike and M. Inaba, "Three-dimensional humanoid motion planning using COM feasible region and its application to ladder climbing tasks," in Proc. 2016 IEEE-RAS International Conference on Humanoid Robots, Cancun, 2016, pp. 49-56.
- [22] T. Yoshiike, M. Kuroda, R. Ujino, H. Kaneko, H. Higuchi, S. Iwasaki, Y. Kanemoto, M. Asatani and T. Koshiishi, "Development of Experimental Legged Robot for Inspection and Disaster Response in Plants", in Proc. 2017 IEEE/RSJ International Conference on Intelligent Robots and Systems, Vancouver, 2017, pp. 4869-4876.
- [23] K. Hashimoto, T. Matsuzawa, T. Teramachi, K. Uryu, X. Sun, S. Hamamoto, A. Koizumi and A. Takanishi, "A Four-Limbed Disaster-Response Robot Having High Mobility Capabilities in Extreme Environments", *IEEE/RSJ International Conference on Intelligent Robots and Systems (IROS)*, pp.5398-5405, 2017.
- [24] X. Sun, K. Hashimoto, S. Hamamoto, A. Koizumi, T. Matsuzawa, T. Teramachi and A. Takanishi, "Trajectory Generation for Ladder Climbing Motion with Separated Path and Time Planning," in Proc. 2016 IEEE/RSJ International Conference on Intelligent Robots and Systems, Daejeon, 2016, pp. 5782-5788.
- [25] T. Matsuzawa, K. Hashimoto, T. Teramachi, K. Uryu, X. Sun, S. Hamamoto, A. Koizumi and A. Takanishi, "End-Effector for Disaster Response Robot with Commonly Structured Limbs and Experiment in Climbing Vertical Ladder", *ROMANSY 21-Robot Design, Dynamics and Control.*, Springer International Publishing, pp.311-319, 2016.
- [26] K. Hashimoto, S. Kimura, N. Sakai, S. Hamamoto, A. Koizumi, X. Sun, T. Matsuzawa, T. Teramachi, Y. Yoshida, A. Imai, K. Kumagai, T. Matsubara, K. Yamaguchi, G. Ma and A. Takanishi, "WAREC-1 - A Four-Limbed Robot Having High Locomotion Ability with Versatility in Locomotion Styles", *International Symposium on Safety, Security and Rescue Robotics (SSRR)*, pp. 172-178, 2017.
- [27] X. Sun, K. Hashimoto, S. Hamamoto, T. Teramachi, T. Matsuzawa, S. Kimura, N. Sakai, S. Hayashi, Y. Yoshida and A. Takanishi, "Planning and Control of Stable Ladder Climbing

- Motion for the Four-limbed Robot “WAREC-1”, IEEE/RSJ International Conference on Intelligent Robots and Systems, Vancouver, 2017, pp.6547-6554.
- [28] T. Tarn and N. Xi, “Event-Based Planning and Control for Robotic Systems: Theory and Implementation,” *Essays on Mathematical Robotics*, New York Springer, pp. 31-59, 1998.
- [29] X. Sun, K. Hashimoto, A. Koizumi, S. Hamamoto, T. Matsuzawa, T. Teramachi and A. Takanishi, “Path-Time Independent Trajectory Planning of Ladder Climbing with Shortest Path Length for a Four-limbed Robot”, in Proc. 2016 IEEE RAS/EMBS International Conference on Biomedical Robotics and Biomechatronics, Utown, 2016, pp. 188-194.
- [30] M. Do Carmo, *Riemannian Geometry*. Birkhauser, 1992.
- [31] L. Noakes, G. Heinzinger and B. Paden, “Cubic splines on curves space,” *IMA Journal of Mathematical Control & Information*, vol. 6, pp. 465-473, Jan. 1989.
- [32] T. H. Cormen, C. E. Leiserson and R. L. Rivest, *Introduction to Algorithms*, The MIT Press: McGraw-Hill Book Company, 1990.
- [33] H. Wang, J. Kearney, and K. Atkinson, “Arc-length parameterization spline curves for real-time simulation,” in Proc. 5th Int. Conf. Curves and Surfaces, San Malo, 2002, pp. 387-396.
- [34] J. Gil, D. Keren, “New approach to the arc-length parameterization problem,” 13th Spring Conference on Computer Graphics, 1997, pp. 27-34.
- [35] J. Craig, *Introduction to Robotics — Mechanics and Control*, Addison-Wesley Pub. Co., Reading, MA, 2nd edition, 1989.
- [36] [https://en.wikipedia.org/wiki/Axis%E2%80%93angle\\_representation](https://en.wikipedia.org/wiki/Axis%E2%80%93angle_representation), accessed 2018/08/17.
- [37] [https://en.wikipedia.org/wiki/Quaternions\\_and\\_spatial\\_rotation](https://en.wikipedia.org/wiki/Quaternions_and_spatial_rotation), accessed 2018/08/17.
- [38] <http://momose-d.cocolog-nifty.com/blog/2011/03/exponentialmap-.html>, accessed 2018/08/17
- [39] T. Yoshikawa, *Foundation of Robotics*, Corona Press, 2004.
- [40] <http://www.rock-climbing-for-life.com/rock-climbing-101/>, accessed 2017/10/04.
- [41] <https://shop.frictionlabs.com/collections/accessories/products/signed-climbing-posters-pre-order>, accessed 2017/10/04.
- [42] <https://www.switch-science.com/catalog/2518/>, accessed 2018/08/17.
- [43] <https://www.hokuyo-aut.co.jp/search/single.php?serial=24>, accessed 2018/09/27.
- [44] <https://pmdtec.com/picofamily/flexx/>, accessed 2018/09/27.
- [45] Y. Ishiguro and T. Sugihara, “Dynamic 3-dimensional Locomotion of a Humanoid Robot with Hand-foot Support Coordination,” in Proc. 2014 JSME Conference on Robotics and Mechatronics, Toyama, 2014, 3P1-E06.
- [46] Featherstone, R., *Robot Dynamics Algorithms*, Kluwer Academic Publishers, Norwell, MA, 1987.

- [47] S. Fujii, K. Inoue, T. Takubo, Y. Mae, and T. Arai, "Ladder Climbing Control for Limb Mechanism Robot 'ASTERISK'," in Proc. 2008 IEEE International Conference on Robotics and Automation, Pasadena, 2008, pp. 3052-3057.
- [48] T. Matsuzawa, et al., "Crawling Gait for Four-limbed Robot and Simulation on Uneven Terrain," Proceedings of the 16th IEEE-RAS International Conference on Humanoid Robots, pp. 1270-1275, 2016.
- [49] JISB9713-4, <http://kikakurui.com/b9/B9713-4-2004-01.html>, accessed 2018/10/25.
- [50] M. Kanazawa, S. Nozawa, Y. Kkiuchi, Y. Kanemoto, M. Kuroda, K. Okada, M. Inaba and T. Yoshiike, "Robust vertical ladder climbing and transitioning between ladder and catwalk for humanoid robots." in Proc. 2015 IEEE/RSJ Internation Conference on Intelligent Robots and Systems, Hamburg, 2015, pp. 2202-2209.
- [51] Z. Lu, T. Aoyama, H. Yoneda, K. Sekiyama and T. Fukuda, "Vertical ladder climbing motion of pace gait with body motion control for a multi-locomotion robot," in Proc. 2009 IEEE/SICE International Symposium on System Integration, Tokyo, 2009, pp. 48-53.
- [52] T. Matsuzawa, K. Hashimoto, T. Teramachi, K. Uryu, X. Sun, S. Hamamoto, A. Koizumi and A. Takanishi, "End-Effector for Disaster Response Robot with Commonly Structured Limbs and Experiment in Climbing Vertical Ladder", ROMANSY 21-Robot Design, Dynamics and Control, Springer International Publishing, pp.311-319, 2016.
- [53] J. Vaillant, A. Kheddar, H. Audren, F. Keith, S. Brossette, K. Kaneko, M. Morisawa, E. Yoshida and F. Kanehiro, "Vertical ladder climbing by the HRP-2 humanoid robot," in Proc. 2014 14th IEEE-RAS International Conference on Humanoid Robots, Madrid, 2014, pp. 671-676.
- [54] Y. Ogura, K. Shimomura, H. Kondo, A. Morishima, T. Okubo, S.Momoki, H. O. Lim and A. Takanishi, "Human-like Walking with Knee Stretched, Heel-contact and Toe-off Motion by a Humanoid Robot," in Proc. 2006 IEEE/RSJ Int. Conf. Intelligent Robots and Systems, 2006, Beijing, pp. 3976-3981.
- [55] K. Hashimoto, Y. Takezaki, H. Motohashi, T. Otani, T. Kishi, H. O. Lim and A. Takanishi, "Biped Walking Stabilization Based on Gait Analysis," in Proc. 2012 IEEE Int. Conf. Robotics and Automation, Saint Paul, 2012, pp. 154-159.
- [56] N. Saga and T. Nakamura, "Development of a peristaltic crawling robot using magnetic fluid on the basis of the locomotion mechanism of the earthworm," Smart Materials and Structures, vol. 13, pp. 566, 2004.
- [57] H. Kajima, M. Doi, Y. Hasegawa, and T. Fukuda, "A study on a brachiation controller for a multi-locomotion robot - realization of smooth, continuous brachiation," Advanced Robotics, vol. 18, no.10, pp.1025-1038, Aug. 2004.

- [58] T. H. Cormen, C. E. Leiserson and R. L. Rivest, Introduction to Algorithms, The MIT Press: McGraw-Hill Book Company, 1990.
- [59] R. L. Burden and J. D. Faires, Numerical Analysis, Higher Education Press, 2005.
- [60] H. Geering, L. Guzzella, S. Hepner and C. Onder, "Time-Optimal Motions of Robots in Assembly Tasks," in Proc. 24th IEEE Conf. on Decision and Control, Florida, 1985, pp.982-989.
- [61] K. Hauser, "Fast Interpolation and Time-Optimization on Implicit Contact Submanifolds," Robotics: Science and Systems, 2013.
- [62] P. Pounds, D. Bersak, and A. Dollar, "Grasping From the Air: Hovering Capture and Load Stability," Proceedings of IEEE International Conference on Robotics and Automation, pp. 2491-2498, 2011.
- [63] K. Kondak, F. Huber, M. Schwarzbach, M. Laiacker, D. Sommer, M. Bejar, and A. Ollero, "Aerial manipulation robot composed of an autonomous helicopter and a 7 degrees of freedom industrial manipulator," Proceedings of IEEE International Conference on Robotics and Automation, pp. 2107-2112, 2014.
- [64] B. Yamauchi, "PackBot: a versatile platform for military robotics," In: Defense and Security, International Society for Optics and Photonics, pp. 228-237, 2004.
- [65] T. Yoshida, K. Nagatani, S. Tadokoro, T. Nishimura, E. Koyanagi, "Improvements to the Rescue Robot Quince Toward Future Indoor Surveillance Missions in the Fukushima Daiichi Nuclear Power Plant," Field and Service Robotics, Vol. 92, pp. 19-32, 2013.
- [66] Y. Zhang, et al., "Motion Planning and Control of Ladder Climbing on DRC-Hubo for DARPA Robotics Challenge," Proceedings of IEEE International Conference on Robotics and Automation, pp. 2086, 2014.
- [67] A. Stentz, et al., "CHIMP, the CMU Highly Intelligent Mobile Platform," Journal of Field Robotics, Vo. 32, No. 2, pp. 209-228, 2015.
- [68] M. Schwarz, et al., "NimbRo Rescue: Solving Disaster response Tasks with the Mobile Manipulation Robot Momaro," Journal of Field Robotics, 2016.
- [69] S. Karumanchi, et al., "Team RoboSimian: Semi-autonomous Mobile Manipulation at the 2015 DARPA Robotics Challenge Finals," Journal of Field Robotics, 2016.
- [70] K. Kojima, et al., "Development of Life-Sized High-Power Humanoid Robot JAXON for Real-World Use," Proceedings of IEEE-RAS International Conference on Humanoid Robots, pp. 838-843, 2015.
- [71] F. Negrello, et al., "WALK-MAN Humanoid Lower Body Design Optimization for Enhanced Physical Performance," Proceedings of IEEE International Conference on Robotics and Automation, pp. 1817-1824, 2016.

- [72] T. Fukuda, Y. Hasegawa, M. Doi, and Y. Asano, "Multi-Locomotion Robot - Energy-based Motion Control for Dexterous Brachiation -," Proceedings of IEEE International Conference of Robotics and Biomimetics, pp. 4-9, 2005.
- [73] K. Hashimoto, H. Kondo, H. O. Lim, and A. Takanishi, "Online Walking Pattern Generation Using FFT for Humanoid Robots," Motion and Operation Planning of Robotic Systems: Background and Practical Approaches, pp. 417-438, Springer International Publishing, March, 2015.
- [74] A. Jacoff, A. Downs, A. Virts, and E. Messina, "Stepfield Pallets: Repeatable Terrain for Evaluating Robot Mobility," Proceedings of the 8th Workshop on Performance Metrics for Intelligent Systems, pp. 29-34, 2008.
- [75] A. Jacoff, and E. Messina, "Urban search and rescue robot performance standards: progress update," Proc. SPIE 6561, Unmanned Systems Technology IX, 65611L, pp. 29-34, 2007.
- [76] T. Yoshikawa, "Analysis and control of robot manipulators with redundancy," in Robotics research: the first international symposium. Cambridge, MA: Mit Press, pp. 735-747, 1984.



## Appendix

### A. Pseudo-inverse matrix

It is well known that in many situations we need to obtain the inverse of a matrix, which is a square matrix. However, in some cases, we must face the case that the matrix we will deal with is not a square matrix. In order to obtain the inverse of a non-square matrix, we introduce the concept of pseudo-inverse. Here we introduce briefly about the properties of inverse matrix, which are often used in robotics.

Let  $\mathbf{A}$  be an  $m \times n$  real matrix. There exists only one pseudo inverse  $\mathbf{A}^+$  of  $\mathbf{A}$  satisfying the following conditions:

$$\mathbf{A}\mathbf{A}^+\mathbf{A} = \mathbf{A}, \quad (\text{a1})$$

$$\mathbf{A}^+\mathbf{A}\mathbf{A}^+ = \mathbf{A}^+, \quad (\text{a2})$$

$$(\mathbf{A}\mathbf{A}^+)^T = \mathbf{A}\mathbf{A}^+, \quad (\text{a3})$$

$$(\mathbf{A}^+\mathbf{A})^T = \mathbf{A}^+\mathbf{A}. \quad (\text{a4})$$

Furthermore, from the equations above, we have the following properties:

$$(\mathbf{A}^+)^+ = \mathbf{A}, \quad (\text{a5})$$

$$(\mathbf{A}^T)^+ = (\mathbf{A}^+)^T, \quad (\text{a6})$$

$$(\mathbf{A}\mathbf{A}^T)^+ = (\mathbf{A}^+)^T\mathbf{A}^+, \quad (\text{a7})$$

$$(\mathbf{A}\mathbf{B})^+ = \mathbf{B}^+\mathbf{A}^+, \quad (\text{a8})$$

where  $\mathbf{A}$ ,  $\mathbf{B}$  are square matrices with the same order

$$\mathbf{A}^+ = (\mathbf{A}^T\mathbf{A})^+\mathbf{A}^T = \mathbf{A}^T(\mathbf{A}\mathbf{A}^T)^+. \quad (\text{a9})$$

Suppose that  $\mathbf{A}$  is an  $m \times n$  matrix. When  $\text{rank}(\mathbf{A})=m$ , then

$$\mathbf{A}^+ = \mathbf{A}^T(\mathbf{A}\mathbf{A}^T)^{-1}, \quad (\text{a10})$$

and when  $\text{rank}(\mathbf{A})=n$ , then

$$\mathbf{A}^+ = (\mathbf{A}^T\mathbf{A})^{-1}\mathbf{A}^T. \quad (\text{a11})$$

From (a10) and (a11), it can be found that in both cases the pseudo inverse matrix  $\mathbf{A}^+$  is exactly  $\mathbf{A}^{-1}$  when  $\mathbf{A}$  is an invertible matrix.



## B. Inverse kinematics

Inverse kinematics plays a significant role in the robot motion. Here we briefly introduce the main contents used in this thesis. For the forward kinematics, we have

$$\mathbf{x} = f(\boldsymbol{\theta}), \quad (\text{b1})$$

where the vector  $\mathbf{x}$  means the posture including the positions and the orientations, and the vector  $\boldsymbol{\theta}$  denotes the joint angle. By using this formula through the given joint angles, the desired posture can be obtained. Compared with the forward kinematics, the inverse kinematics becomes more complicated. It is rather difficult to obtain joint angles from the desired posture. To solve this issue, by derivative with respect to  $t$  from (b1) we get

$$\dot{\mathbf{x}} = \mathbf{J}(\boldsymbol{\theta})\dot{\boldsymbol{\theta}}, \quad (\text{b2})$$

where  $\mathbf{J}(\boldsymbol{\theta}) = (\frac{\partial f(\boldsymbol{\theta})}{\partial \boldsymbol{\theta}})^\top$  is the Jacobian, an  $m \times n$  ( $m \leq n$ ) matrix. In order to obtain the expression of  $\boldsymbol{\theta}$  from (b2), the following lemma is needed:

**Remark b1:** When  $\text{rank}(\mathbf{J}(\boldsymbol{\theta}))=m$ , the matrix  $\mathbf{J}\mathbf{J}^\top$  is invertible.

In fact, since  $\mathbf{J}\mathbf{J}^\top$  is an  $m \times m$  matrix,  $\mathbf{X}^\top \mathbf{J}\mathbf{J}^\top \mathbf{X} = (\mathbf{J}^\top \mathbf{X})^\top (\mathbf{J}^\top \mathbf{X}) \geq 0$  for any  $\mathbf{X} \in \mathbf{R}^m$ , and the equation holds if and only if  $\mathbf{J}^\top \mathbf{X} = \mathbf{0}$ . Furthermore,  $\text{rank}(\mathbf{J}^\top) = \text{rank}(\mathbf{J}) = m$  implies that  $\mathbf{X} = \mathbf{0}$ . This proves that the quadratic form is positive definite and the matrix  $\mathbf{J}\mathbf{J}^\top$  is a positive definite matrix so that it is an invertible matrix. Now, with the assumption that  $\mathbf{J}\mathbf{J}^\top$  is invertible, we have the following:

**Proposition b1:** For the problem

$$\min |\dot{\boldsymbol{\theta}}|^2, \text{ subject to } \dot{\mathbf{x}} = \mathbf{J}(\boldsymbol{\theta})\dot{\boldsymbol{\theta}}, \quad (\text{b3})$$

we have  $\dot{\boldsymbol{\theta}} = \mathbf{J}^\top (\mathbf{J}\mathbf{J}^\top)^{-1} \dot{\mathbf{x}}$ .

To solve this problem, we use the Lagrange multiplier method

$$L(\dot{\boldsymbol{\theta}}, \boldsymbol{\lambda}) = \frac{1}{2} |\dot{\boldsymbol{\theta}}|^2 + \boldsymbol{\lambda}^\top (\dot{\mathbf{x}} - \mathbf{J}(\boldsymbol{\theta})\dot{\boldsymbol{\theta}}), \quad \boldsymbol{\lambda} \in \mathbf{R}^m. \quad (\text{b4})$$

From (b4) we get

$$\frac{\partial L(\dot{\boldsymbol{\theta}}, \boldsymbol{\lambda})}{\partial \dot{\boldsymbol{\theta}}} = \dot{\boldsymbol{\theta}} - \mathbf{J}(\boldsymbol{\theta})\boldsymbol{\lambda} \quad (\text{b5})$$

and

$$\frac{\partial L(\dot{\boldsymbol{\theta}}, \boldsymbol{\lambda})}{\partial \boldsymbol{\lambda}} = \dot{\mathbf{x}} - \mathbf{J}(\boldsymbol{\theta})\dot{\boldsymbol{\theta}}. \quad (\text{b6})$$

Let right sides of (b5) and (b6) be zero, we get  $\mathbf{J}\dot{\boldsymbol{\theta}} = \mathbf{J}\mathbf{J}^T\boldsymbol{\lambda}$ ,  $\boldsymbol{\lambda} = (\mathbf{J}\mathbf{J}^T)^{-1}\dot{\mathbf{x}}$  and further

$$\dot{\boldsymbol{\theta}} = \mathbf{J}^T(\mathbf{J}\mathbf{J}^T)^{-1}\dot{\mathbf{x}}, \quad (\text{b7})$$

where  $\mathbf{J}^+ = \mathbf{J}^T(\mathbf{J}\mathbf{J}^T)^{-1}$  is called the pseudo inverse of  $\mathbf{J}$ . Equation (b7) means that for pointed posture, we can obtain joint angles.

**Corollary b1:** In (b3),  $|\dot{\boldsymbol{\theta}}|^2 = \dot{\boldsymbol{\theta}}^T\dot{\boldsymbol{\theta}}$  is the Euclidean length. However, in many cases we need weighted length  $|\dot{\boldsymbol{\theta}}|_M^2 = \dot{\boldsymbol{\theta}}^T\mathbf{M}\dot{\boldsymbol{\theta}}$ , where  $\mathbf{M}$  is a positive definite matrix, and for some cases we just assume that  $\mathbf{M}$  is a diagonal matrix with all positive entries. Thus, for the following problem:

$$\min |\dot{\boldsymbol{\theta}}|_M^2, \text{ subject to } \dot{\mathbf{x}} = \mathbf{J}(\boldsymbol{\theta})\dot{\boldsymbol{\theta}}, \quad (\text{b8})$$

by constructing the Lagrange function

$$L(\dot{\boldsymbol{\theta}}, \boldsymbol{\lambda}) = \frac{1}{2} |\dot{\boldsymbol{\theta}}|_M^2 + \boldsymbol{\lambda}^T(\dot{\mathbf{x}} - \mathbf{J}(\boldsymbol{\theta})\dot{\boldsymbol{\theta}}), \quad (\text{b9})$$

and letting  $\frac{\partial L(\dot{\boldsymbol{\theta}}, \boldsymbol{\lambda})}{\partial \dot{\boldsymbol{\theta}}} = \frac{\partial L(\dot{\boldsymbol{\theta}}, \boldsymbol{\lambda})}{\partial \boldsymbol{\lambda}} = \mathbf{0}$  from (b9) we can obtain  $\dot{\boldsymbol{\theta}} = \mathbf{M}^{-1}\mathbf{J}^T\boldsymbol{\lambda}$ ,  $\boldsymbol{\lambda} = (\mathbf{J}\mathbf{M}^{-1}\mathbf{J}^T)^{-1}\dot{\mathbf{x}}$ . Therefore,

$$\dot{\boldsymbol{\theta}} = \mathbf{M}^{-1}\mathbf{J}^T(\mathbf{J}\mathbf{M}^{-1}\mathbf{J}^T)^{-1}\dot{\mathbf{x}}. \quad (\text{b10})$$

For simplicity, we write  $\mathbf{J}_M^+ = \mathbf{M}^{-1}\mathbf{J}^T(\mathbf{J}\mathbf{M}^{-1}\mathbf{J}^T)^{-1}$  so that (b10) can be written as

$\dot{\boldsymbol{\theta}} = \mathbf{J}_M^+\dot{\mathbf{x}}$ . It is obvious that when  $\mathbf{M}$  is an identity matrix as the same order as  $\mathbf{M}$ , (b10) becomes (b7).

**Remark b2:** When  $\text{rank}(\mathbf{J}(\boldsymbol{\theta})) = n$ , (b7) and (b10) become

$$\dot{\boldsymbol{\theta}} = (\mathbf{J}^T\mathbf{J})^{-1}\mathbf{J}^T\dot{\mathbf{x}}, \quad (\text{b11})$$

and

$$\dot{\boldsymbol{\theta}} = (\mathbf{J}^T \mathbf{M}^{-1} \mathbf{J})^{-1} \mathbf{M}^{-1} \mathbf{J}^T \dot{\mathbf{x}}. \quad (\text{b12})$$

On the other hand, noticing that

$$\mathbf{J}(\mathbf{I} - \mathbf{J}^+ \mathbf{J}) = \mathbf{J} - \mathbf{J} \mathbf{J}^+ \mathbf{J} = \mathbf{J} - \mathbf{J} \mathbf{J}^T (\mathbf{J} \mathbf{J}^T)^{-1} \mathbf{J} = \mathbf{0} \quad (\text{b13})$$

and

$$\dot{\mathbf{x}} = \mathbf{J} \mathbf{J}^+ \dot{\mathbf{x}} + \mathbf{J}(\mathbf{I} - \mathbf{J}^+ \mathbf{J}) \mathbf{X} = \mathbf{J}(\mathbf{J}^+ \dot{\mathbf{x}} + (\mathbf{I} - \mathbf{J}^+ \mathbf{J}) \mathbf{X}), \quad \mathbf{X} \in \mathbf{R}^m, \quad (\text{b14})$$

we have

**Proposition b2:**

$$\dot{\boldsymbol{\theta}} = \mathbf{J}^+ \dot{\mathbf{x}} + (\mathbf{I} - \mathbf{J}^+ \mathbf{J}) \mathbf{X}. \quad (\text{b15})$$

From the analysis above it can be found that (b15) is also a solution of (b7), and the second term of (b15) is useful so that we can complete two works at the same time, namely, when we obtain the joint angles for given posture, we also can complete another work like obstacle avoidance and so on.

**Remark c3:** To obtain the optimal value of a cost function  $H(\dot{\boldsymbol{\theta}}) = \frac{1}{2} \|\dot{\boldsymbol{\theta}}\|_{\mathbf{W}}^2 = \frac{1}{2} \dot{\boldsymbol{\theta}}^T \mathbf{W} \dot{\boldsymbol{\theta}}$ , where  $\mathbf{W}$  is a positive definite matrix or even a diagonal matrix with all positive entries. We want to obtain minimum of  $H(\dot{\boldsymbol{\theta}})$ , while solving the solution of (b7). Since  $\frac{\partial H(\dot{\boldsymbol{\theta}})}{\partial \dot{\boldsymbol{\theta}}} = \mathbf{W} \dot{\boldsymbol{\theta}}$ , substituting  $\mathbf{X} = k \mathbf{W} \dot{\boldsymbol{\theta}}$ ,  $k \in \mathbf{R}$  into (b15) we get

$$\dot{\boldsymbol{\theta}} = \mathbf{J}^+ \dot{\mathbf{x}} + k(\mathbf{I} - \mathbf{J}^+ \mathbf{J}) \mathbf{W} \dot{\boldsymbol{\theta}}. \quad (\text{b16})$$

From (b16) we find that when  $k > 0$ , we can get the maximum and when  $k < 0$  we can get the minimum of  $H(\dot{\boldsymbol{\theta}})$ , while solving joint angles based on the desired posture.

Above theories are under the assumption that  $\text{rank}(\mathbf{J}) = m$  or  $\text{rank}(\mathbf{J}) = n$  so that the matrices  $\mathbf{J} \mathbf{J}^T$  or  $\mathbf{J}^T \mathbf{J}$  are invertible. Unfortunately, in many cases the conditions above are not satisfied, precisely,  $\text{rank}(\mathbf{J}) = r < \min\{m, n\}$ . As a result, the methods above are not effective. To deal with such issue, we introduce the following ‘‘damped least-squares method’’ for inverse kinematics.

**Proposition b3:** The solution of damped least-squares methods for inverse kinematics problem

$$\min \{|\dot{\mathbf{x}} - \mathbf{J}\dot{\boldsymbol{\theta}}|^2 + \lambda^2 |\dot{\boldsymbol{\theta}}|^2\}, \lambda \in \mathbf{R} \quad (\text{b17})$$

is given by

$$\dot{\boldsymbol{\theta}} = (\mathbf{J}^T \mathbf{J} + \lambda^2 \mathbf{I})^{-1} \mathbf{J}^T \dot{\mathbf{x}}, \quad (\text{b18})$$

where  $\mathbf{I}$  denotes the  $n \times n$  identity matrix.

In fact, setting

$$F(\dot{\boldsymbol{\theta}}) = \frac{1}{2} \{|\dot{\mathbf{x}} - \mathbf{J}\dot{\boldsymbol{\theta}}|^2 + \lambda^2 |\dot{\boldsymbol{\theta}}|^2\}, \quad (\text{b19})$$

by calculation we get

$$\frac{\partial F(\dot{\boldsymbol{\theta}})}{\partial \dot{\boldsymbol{\theta}}} = \frac{\partial}{\partial \dot{\boldsymbol{\theta}}} \frac{1}{2} \{(\dot{\mathbf{x}} - \mathbf{J}\dot{\boldsymbol{\theta}})^T (\dot{\mathbf{x}} - \mathbf{J}\dot{\boldsymbol{\theta}}) + \lambda^2 \dot{\boldsymbol{\theta}}^T \dot{\boldsymbol{\theta}}\} = -\mathbf{J}^T \dot{\mathbf{x}} + (\mathbf{J}^T \mathbf{J} + \lambda^2 \mathbf{I}) \dot{\boldsymbol{\theta}}, \quad (\text{b20})$$

and  $\frac{\partial F(\dot{\boldsymbol{\theta}})}{\partial \dot{\boldsymbol{\theta}}} = \mathbf{0}$  implies that  $-\mathbf{J}^T \dot{\mathbf{x}} + (\mathbf{J}^T \mathbf{J} + \lambda^2 \mathbf{I}) \dot{\boldsymbol{\theta}} = \mathbf{0}$ . Since for any  $\lambda \neq 0$ , the matrix  $\mathbf{J}^T \mathbf{J} + \lambda^2 \mathbf{I}$  is invertible, thus, we get  $\dot{\boldsymbol{\theta}} = (\mathbf{J}^T \mathbf{J} + \lambda^2 \mathbf{I})^{-1} \mathbf{J}^T \dot{\mathbf{x}}$ .

**Corollary b3:** The solution of damped least-squares methods for inverse kinematics problem

$$\min \{|\dot{\mathbf{x}} - \mathbf{J}\dot{\boldsymbol{\theta}}|^2 + \lambda^2 |\dot{\boldsymbol{\theta}}|_{\mathbf{M}}^2\}, \lambda \in \mathbf{R} \quad (\text{b21})$$

is given by

$$\dot{\boldsymbol{\theta}} = (\mathbf{J}^T \mathbf{J} + \lambda^2 \mathbf{M})^{-1} \mathbf{J}^T \dot{\mathbf{x}}, \quad (\text{b22})$$

where  $\mathbf{M}$  is a positive definite matrix.

The proof is similar to proposition b3, and here we omit it.

**Remark b4:** For problem (b17), we have

$$\dot{\boldsymbol{\theta}} = \mathbf{J}^T (\mathbf{J}\mathbf{J}^T + \lambda^2 \mathbf{I})^{-1} \dot{\mathbf{x}}. \quad (\text{b23})$$

In fact, only check that  $\mathbf{J}^T (\mathbf{J}\mathbf{J}^T + \lambda^2 \mathbf{I})^{-1} = (\mathbf{J}^T \mathbf{J} + \lambda^2 \mathbf{I})^{-1} \mathbf{J}^T$ , we can get the result in (b23).

**Remark b5:** When  $m < n$ ,  $\mathbf{J}\mathbf{J}^T + \lambda^2 \mathbf{I}$  is an  $m \times m$  matrix, and in this case, the complexity of  $(\mathbf{J}\mathbf{J}^T + \lambda^2 \mathbf{I})^{-1}$  is lower. Similarly, when  $n < m$ , the complexity of  $(\mathbf{J}^T \mathbf{J} + \lambda^2 \mathbf{I})^{-1}$  is lower. Thus, one can choose the different form depending size of

m and n.

**Remark b6:** In real operation of robot, there are some singularities of the matrix  $\mathbf{J}\mathbf{J}^T + \lambda^2\mathbf{I}$  when  $\lambda$  approaches to zero, therefore one needs to choose suitable  $\lambda$  to use.





### C. Riemannian manifold

The Euclidean space is a linear space which is flat and the shortest distance connecting two points is a straight line. Different from the Euclidean space such as sphere, which is no longer flat and the shortest distance connecting two points is no longer a straight line. The reason is simple that the space is curved, and the curvature describes how curved the space is. As the generalization of curves and surfaces in Euclidean space, the abstract manifold appears. The concept of manifold is complicated and here we only give a simple introduction. A manifold first is a topological space and is locally Euclidean so that at any point of manifold, the inner product (metric) on the tangent space like the one in Euclidean space can be defined. By using the metric, the curvature of manifold can be defined. Furthermore, the geodesic, which is the shortest curve connecting two points on manifold can be defined as well. Here the fundamental concepts involved in this thesis are introduced briefly.

**Definition c1:** Let  $M$  be an  $n$  dimensional manifold. The affine connection defined by

$$\nabla : T_p M \times T_p M \rightarrow T_p M , \quad (\text{c1})$$

satisfying the Leibnitz's rule and the linearity, where  $T_p M$  denotes the tangent space at point  $p \in M$ .

**Definition c2:** Let  $M$  be an  $n$  dimensional manifold. The Riemannian metric is defined by

$$g : T_p M \times T_p M \rightarrow \mathbf{R} , \quad (\text{c2})$$

satisfying

$$g(X, Y) = g(Y, X) , \quad (\text{c3})$$

$$g(kX + Y, Z) = kg(X, Z) + g(Y, Z) , \quad (\text{c4})$$

$$g(X, X) \geq 0 , \quad (\text{c5})$$

and the equality holds if and only if  $X=0$ . Where  $X, Y, Z \in T_p M$  are the tangent vectors,  $k \in \mathbf{R}$ .

Before introducing the concept curvature of manifold, the concept curvature tensor will be given first:

**Definition c3:** The curvature tensor of a manifold is defined as

$$R : T_p M \times T_p M \times T_p M \rightarrow T_p M ,$$

or precisely,

$$R(X, Y)Z = \nabla_X \nabla_Y Z - \nabla_Y \nabla_X Z - \nabla_{[X, Y]} Z , \quad (c6)$$

where  $[\cdot, \cdot]$  denotes the Lie bracket satisfying  $[X, Y]f = X(Yf) - Y(Xf)$ ,  $X$ ,  $Y$  and  $Z$  are over  $M$  and  $f \in C^\infty(M)$ .

By a direct calculation from (c6) we can get the component expression of the curvature tensor as

$$R_{ijk}^l = \frac{\partial \Gamma_{kj}^l}{\partial x^i} - \frac{\partial \Gamma_{ki}^l}{\partial x^j} + \Gamma_{kj}^h \Gamma_{hi}^l - \Gamma_{ki}^h \Gamma_{hj}^l , \quad (c7)$$

where  $\{x^i\}_{i=1}^n$  are the coordinate of the point  $p$  and the connection coefficients  $\Gamma_{ij}^k$  satisfy  $\nabla_{\frac{\partial}{\partial x^i}} \frac{\partial}{\partial x^j} = \Gamma_{ij}^k \frac{\partial}{\partial x^k}$ . Especially, for the Riemannian manifold  $M$  with the Riemannian metric  $g$ , we have

$$\Gamma_{ij}^k = \frac{1}{2} \left( \frac{\partial g_{ik}}{\partial x^j} + \frac{\partial g_{jk}}{\partial x^i} - \frac{\partial g_{ij}}{\partial x^k} \right) , \quad (c8)$$

which are called the Riemannian connection coefficients. Set  $R_{ijkl} = R_{ijk}^m g_{ml}$ . The sectional curvature of  $M$  is defined by

$$K(i, j) = - \frac{R_{ijij}}{g_{ii} g_{jj} - g_{ij}^2} . \quad (c9)$$

From (c9) by computation it can be found that the curvature of the plane is zero, the curvature of a sphere is 1 and the curvature of hyperbolic space is negative. By (c7) Ricci curvature and the scalar curvature can be defined as follows:

$$R_{ij} = R_{ijkl} g^{jl} , \quad (c10)$$

where

$$g^{jl}g_{li} = \delta_i^j = \begin{cases} 1, & i = j \\ 0, & i \neq j \end{cases}, \quad (\text{c11})$$

$$R = R_{ij}g^{ij}. \quad (\text{c12})$$

The sectional curvature, Ricci curvature and the scalar curvature are 3 kinds of curvatures describing how curved a manifold is. As a very famous example, the Einstein equation consists of curvatures. For instance, the curvature of the Euclidean space  $\mathbf{R}^n$  is zero, the curvature of the sphere  $S^n$  is 1, and the curvature of a hyperbolic space is negative. For a flat Euclidean space, it is well known that the shortest distance of two points on Euclidean space is exactly the straight line connecting them. However, in the curved space like sphere  $S^2$ , the shortest distance of two points on  $S^2$  is the minor arc of the great circle on  $S^2$ . We call this shortest distance “geodesic distance” and the curve connecting these points “geodesic”. It is obvious that on the curved space, the curve with shortest distance is no longer a straight line like it is in Euclidean space.

Now, let us recall the concepts of geodesic and geodesic distance. There are several ways to give the concept of geodesic. Among them the critical point of energy functional along curves with fixed original point and the end point derives the shortest curve, geodesic, and the corresponding distance is the geodesic distance. Generally speaking, the motion of an object should move along the geodesic, the shortest path. However, for the robot motion minimizing the acceleration for reduction of energy consumption is necessary. Similar to the energy functional, we consider the acceleration functional to search for a curve that along which the acceleration is minimal. The curve we want is the path of robot motion.

Now, let us introduce the concept of geodesic. It is known that geodesic in a curved manifold is not a straight line, but a curve. In geometry, geodesic is a curve which length is shortest locally. On the other hand, in physics geodesic is curve which is a critical value of energy functional, and precisely along geodesic the energy is the minimum. For a cost function defined on a Riemannian manifold, the geodesic distance will be the distance to get the optimal values.

**Definition c4:** Let  $\gamma: (-\varepsilon, \varepsilon) \rightarrow M$  be a smooth curve. If the following condition is satisfied

$$\nabla_{\dot{\gamma}(t)}\dot{\gamma}(t) = 0, \quad (\text{c13})$$

from (c13) we can get the expression of the coefficients

$$\ddot{\gamma}^k(t) + \Gamma_{ij}^k \dot{\gamma}^i(t) \dot{\gamma}^j(t) = 0. \quad (\text{c14})$$

Since in the Euclidean space, the Riemannian metric  $g_{ij} = \delta_{ij}$ , combining with (c8)

$$\Gamma_{ij}^k = 0 \quad (\text{c15})$$

is satisfied. And from (c14) it can be seen that

$$\ddot{\gamma}^k(t) = 0 \quad (\text{c16})$$

so that

$$\gamma^k(t) = a^k + b^k t, \quad a^k, b^k \in \mathbf{R} \quad (\text{c17})$$

and

$$\gamma(t) = a + bt, \quad a, b \in \mathbf{R}^n \quad (\text{c18})$$

are straight lines.

## **D. Application of proximity sensor system**

### **D.1 Introduction: Continuous motion from the ground to a ladder**

The whole continuous sequential motion from the ground to ladder for a robot climber has not been concerned in the former studies but is indispensable for practical use, where there is no human for assist near the robot. In this part, the motion in 2 sequences of approaching and transition for vertical ladder is explained respectively.

**(1) Approaching.** In this thesis the robot approaches the ladder on a flat ground without obstacles as a preliminary attempt and verification, considering the application in complicated situations of disaster sites we choose crawling, the most stable locomotion with the lowest CoM and biggest area of support polygon that WAREC-1 can perform as the locomotion style for approaching the target ladder.

To make WAREC-1 crawl to the target ladder, first it is necessary to plan the path of the robot. There are at least 2 parameters required for the path planning of crawling: the difference of position for body center and the orientation between the present values and desired ones. In this paper these parameters are measured and input to the system by human. With 2 parameters known crawling motion of WAREC-1 is planned as follows:

**Stage 1:** When the ladder is not within the range of one crawling motion, which is approximately 300mm for WAREC-1, the robot would first take a pivot turn so that it is faced towards target ladder. Then the robot starts crawling motion with the biggest stride possible to realize straight move towards the target ladder with max speed available. Finally, when the center of body reaches the desired point, the robot will take another pivot turn to adjust the orientation of the robot to desired value. This stage can be skipped if the ladder is within the range of one crawling motion and goes to the Stage 2 directly. The details of crawling motion are detailly described in [48]. Basically, it is the repetition of the following in order: (i) lifting body off the ground; (ii) moving body towards the desired direction; (iii) putting down body until it contacts the ground and limbs floating in the air and (iv) moving limbs towards the desired direction.

**Stage 2:** Considering that there may be deviation in moving distance and direction in Stage 1. In this stage the error between desired and real position and orientation are measured again. According to the amount of error, there will be another crawling motion for adjustment to reduce the error to the biggest degree.

The trajectory of pivot turns in both Stage 1 and 2 can be given by

$$\mathbf{x}_{id} = \mathbf{q}\mathbf{x}_i\mathbf{q}^* + \mathbf{d}, \quad (d1)$$

where  $\mathbf{x}_i$  is vector from rotation center point (body center point here) to the  $i$ th end-effector,  $\mathbf{q}$  is relative target orientation quaternion of crawling,  $\mathbf{d}$  is relative target position of crawling. The illustration of strategies described above and snapshots of corresponding simulation are depicted in Fig. D.1 and Fig. D.2, respectively.

Note that crawling motion not only enables pivot turn for adjustment of robot's

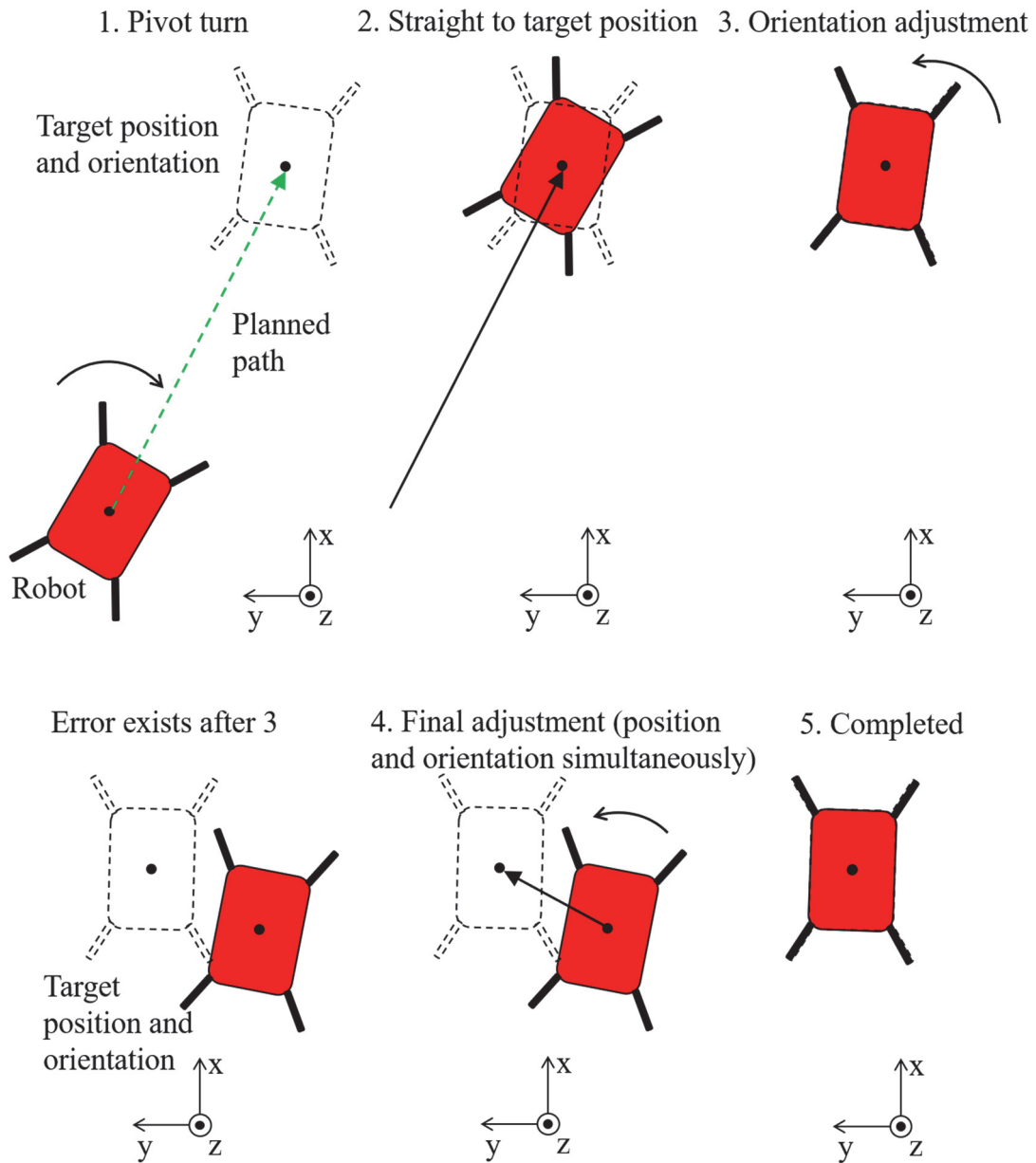


Fig. D.1 Motion planning for 2 stages in approaching the target ladder.

orientation but also supports omnidirectional movement simultaneously (Fig. D.3). This feature makes the approaching motion planning more efficient, flexible and requires less space than traditional wheeled robots and robots with caterpillars.

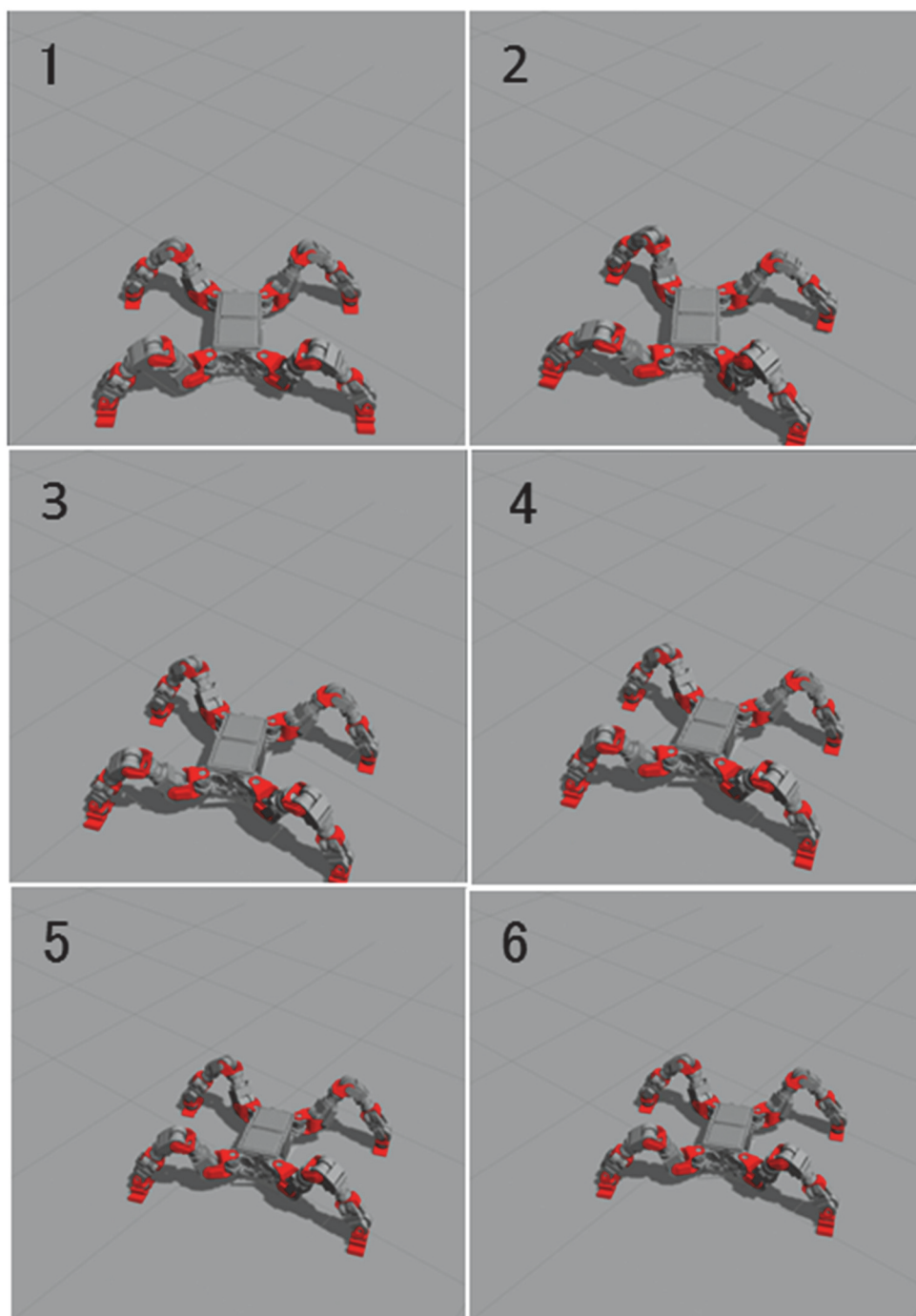


Fig. D.2 Approaching motion, stages 1.

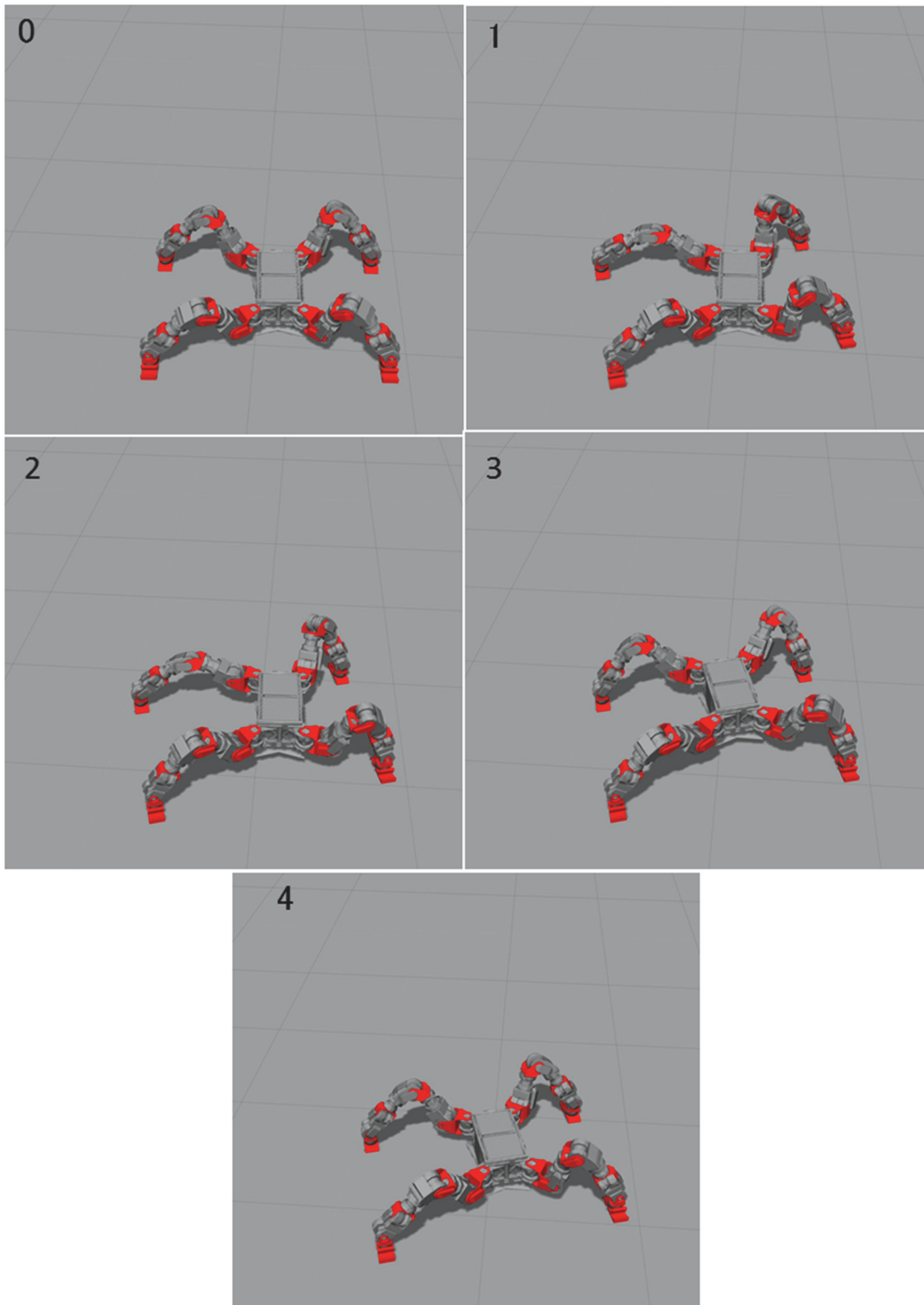


Fig. D.3 Approaching motion, stage 2.



**(2) Transition.** Until now, no robot has been claimed to be capable of transition to a ladder autonomously before climbing it from the state on the ground. However, being faced with a ladder in actual application, especially in extreme environment where there is nobody putting the robot on the ladder so that the robot can start climbing, like the situation in laboratory, attaching to ladder is indispensable because it is a process that can never be omitted before ladder climbing.

The attempt of transition to a ladder starting from biped standing has been realized by The Prototype in 2015, but it can only be done when the robot is standing on the specified position. And even slight error in the standing position (in

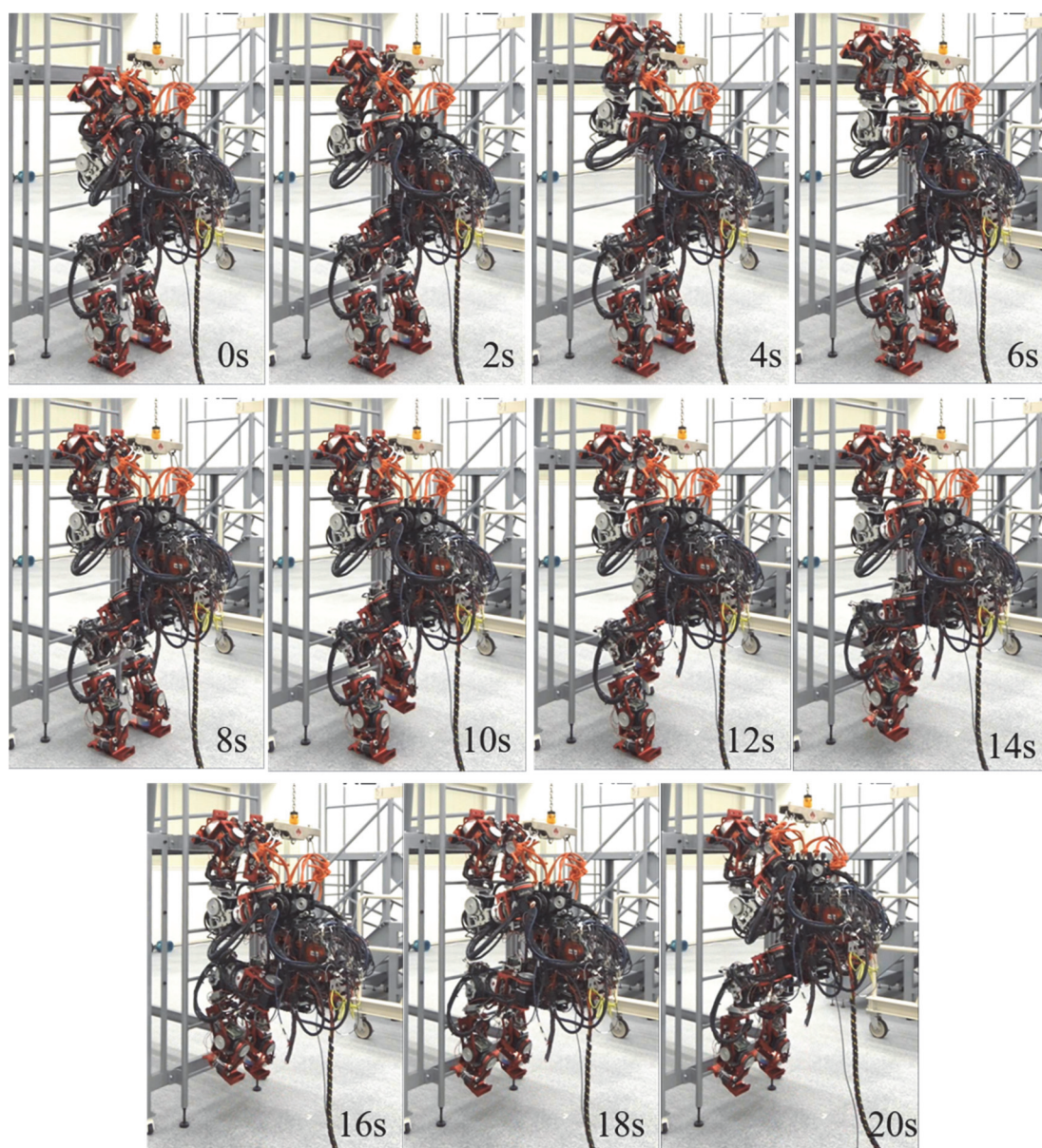


Fig. D.4 Ladder attaching of The Prototype.

millimeters) would cause failure in ladder attaching. Fig. D.4 shows the snapshots of attaching to a ladder by The Prototype. It starts with biped stance and first put its 2 hands simultaneously on a rung, then puts its 2 feet on another rung in orders to finish attaching.

With preliminary attempts of ladder attaching, our robot managed to attach to the ladder “independently” but it is still far from genuine autonomous ladder attaching because the robot could only freely attach to the ladder with no need of human help after being put on the right position, but this process itself still requires support of human.

Through our challenges described above, it is clear that:

(i) The relative distance and orientation between the robot and ladder are crucial for ladder attaching;

(ii) Besides the attaching itself, the posture before attaching should also be considered if necessary. For the case of The Prototype, it is biped stance but high CoM position and small area of support polygon in biped stance makes it a rather difficult posture to maintain stability before ladder attaching;

(iii) Expanding ladder attaching further and prior, the locomotion style for approaching the ladder should also be designed appropriately so that with the step of (a) Approaching (b) Preparation (posture change if necessary) and (c) Attaching, a continuous and practical ladder attaching finally completes.

As for the transition to ladder by WAREC-1 after the attempt by The Prototype, in consideration of stability and reducing interval steps with change of contact point, we choose a pose called “Gorilla stance” depicted in Fig. D.5 for the initial state of transition from ground to target ladder. Biped stance and quadruped stance that are more difficult in guaranteeing stability are not chosen.

To shorten the total time of attaching and make whole attaching motion smooth, there is a preparation phase before 4 limbs are attached to the ladder. The body of robot leaves the ground and rotates in Pitch axis until it is perpendicular to ground while all 4 end-effectors of the robot keep contacting the ground, which looks like a gorilla standing on the ground with all 4 limbs.

With “Gorilla stance” in Fig. D.5, transition to the ladder starts in the order of (i) one arm; (ii) the other arm and (iii) 2 legs at the same time. This order can guarantee as big support polygon as possible, for there are always at least 3 contact points between the robot and ladder or on the ground. After 2 arms attached to the ladder, body approaches and contacts the ladder so that 2 legs of the robot can float in the air and attached to the ladder simultaneously.

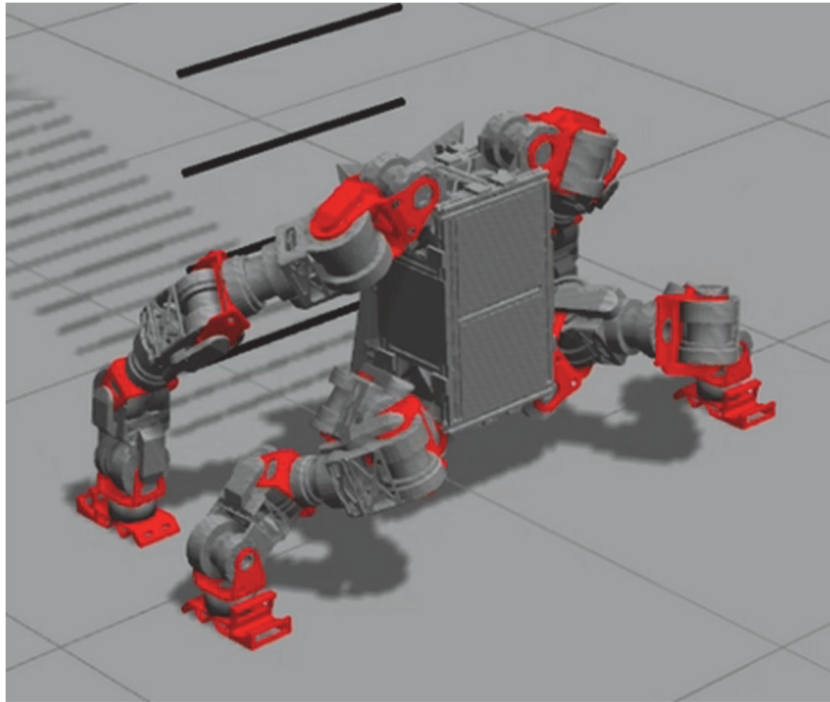


Fig. D.5 Gorilla stance.

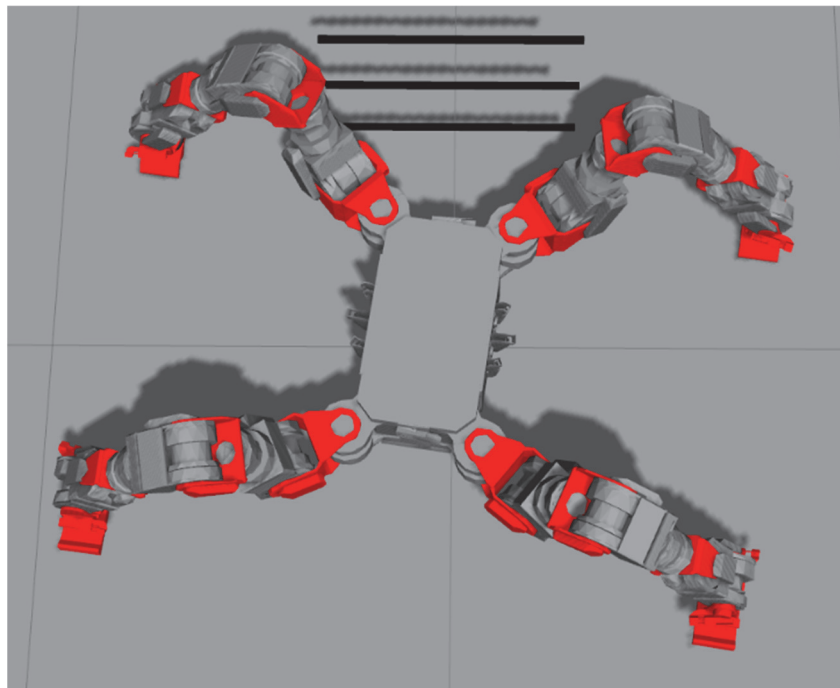


Fig. D.6 Initial position and orientation with error before transition.

## D.2 Posture adjustment after transition

Unfortunately, proximity sensor system in Section 4.3 can only eliminate the error between end-effectors and rungs of ladder and cannot deal with undesired change in whole-body level. Thus, additional approach is required for error in whole-body motion.

First, due to various factors, error may still exist (and it did in experiments) after Stage 1 and Stage 2 of approaching target ladder, which influences the result of transition. Fig. D.6 shows an example for this type of error.

Although there is no problem for transition from ground to ladder, it is apparent

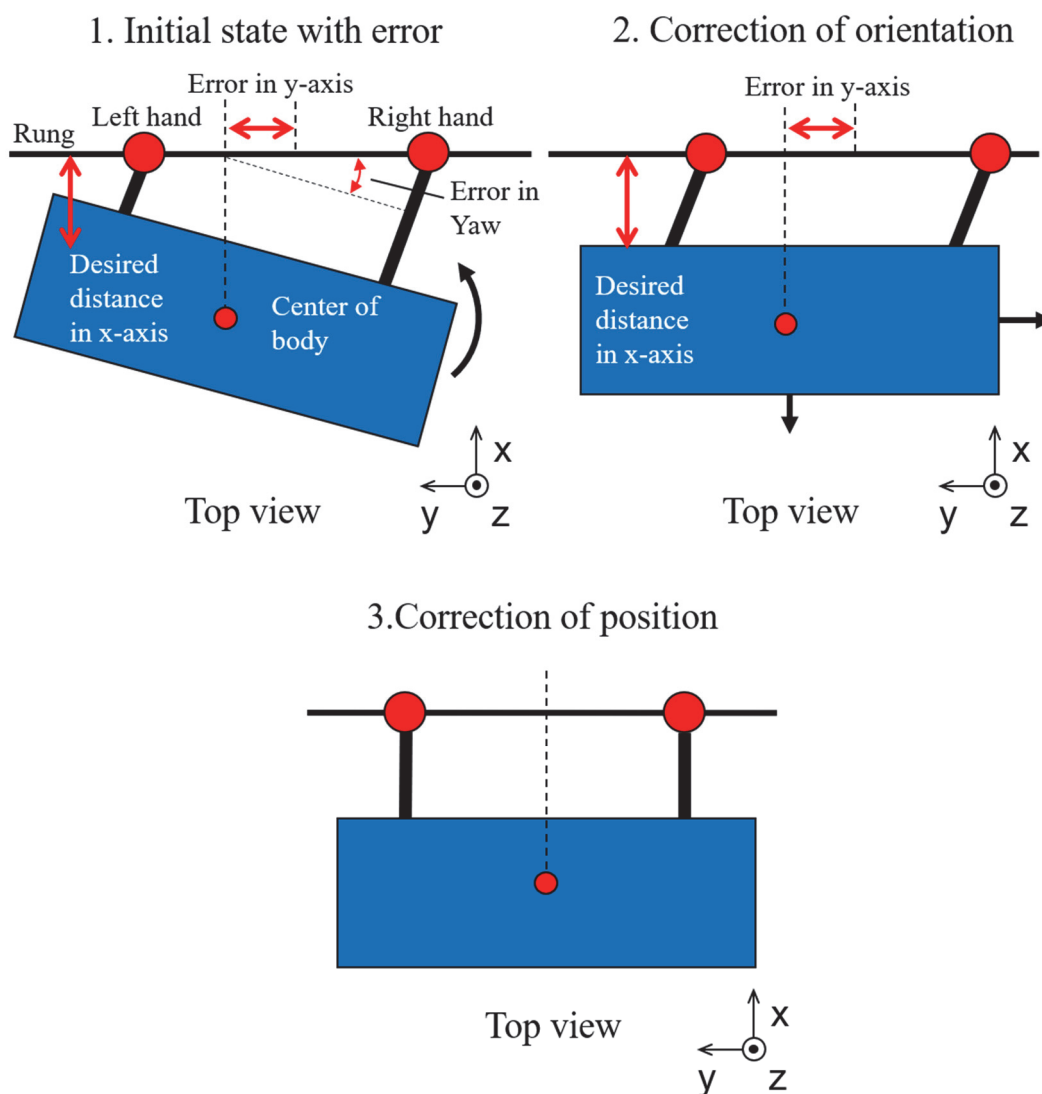


Fig. D.7 Posture adjustment after transition.

Red arrows are error existing and black arrows are the direction of correction.

that error will remain and may even lead to failure for subsequent ladder climbing. Depicted in Fig. D.7, our solution is to utilize forward kinematics combined with joint angles of WAREC-1 to calculate the amount of error in both position and orientation and their corresponding compensation motion will be done with all end-effectors on the rungs of ladder. Note that error in z-axis, Roll and Pitch is not considered because it is too small to make a difference.

### D.3 Experiment

In this part the experiments in an indoor field of Tohoku University, Japan are presented. The rung interval, diameter and side pole distance of the ladder are 250mm, 19mm and 600mm, respectively. To make it easier to see the snapshots of continuous motion of approaching, transition and ladder climbing are divided into 2 different angles: For approaching, snapshots taken from WAREC-1’s back are shown in Fig. D.8 and for transition and ladder climbing, snapshots in Fig. D.9 are taken from WAREC-1’s side. In Fig. D.8, ①~⑥ correspond to “Stage 1” (approaching) and ⑦~⑧ correspond to “Stage 2” (adjustment for error compensation). In Fig. D.9, ⑨~⑯ are the process from crawling posture to “Gorilla stance”, ⑰~⑳ are the transition from “Gorilla stance” to target ladder. Note that in ㉔~㉖ the body of WAREC-1 contacts the ladder so that its feet can float in the air and close to the state in ㉖. The whole motion takes 9min48s in total and details of time spent are shown in Table D-1.

Table D-1 Time spent in each sequence.

Phase	Time
Approaching	1min46s
Transition	8min2s
Total	9min48s

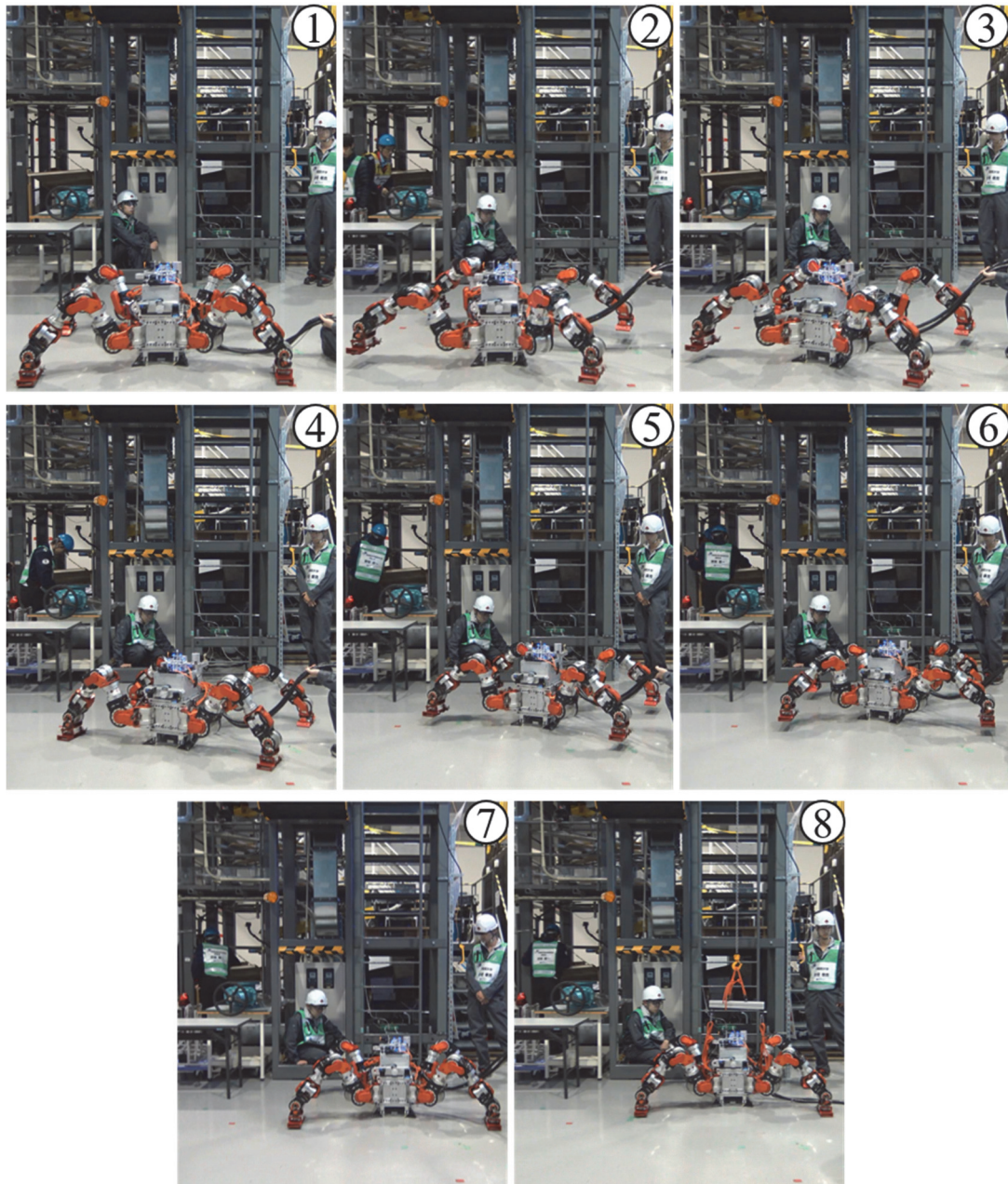


Fig. D.8 Snapshots of the sequence of “approaching”.

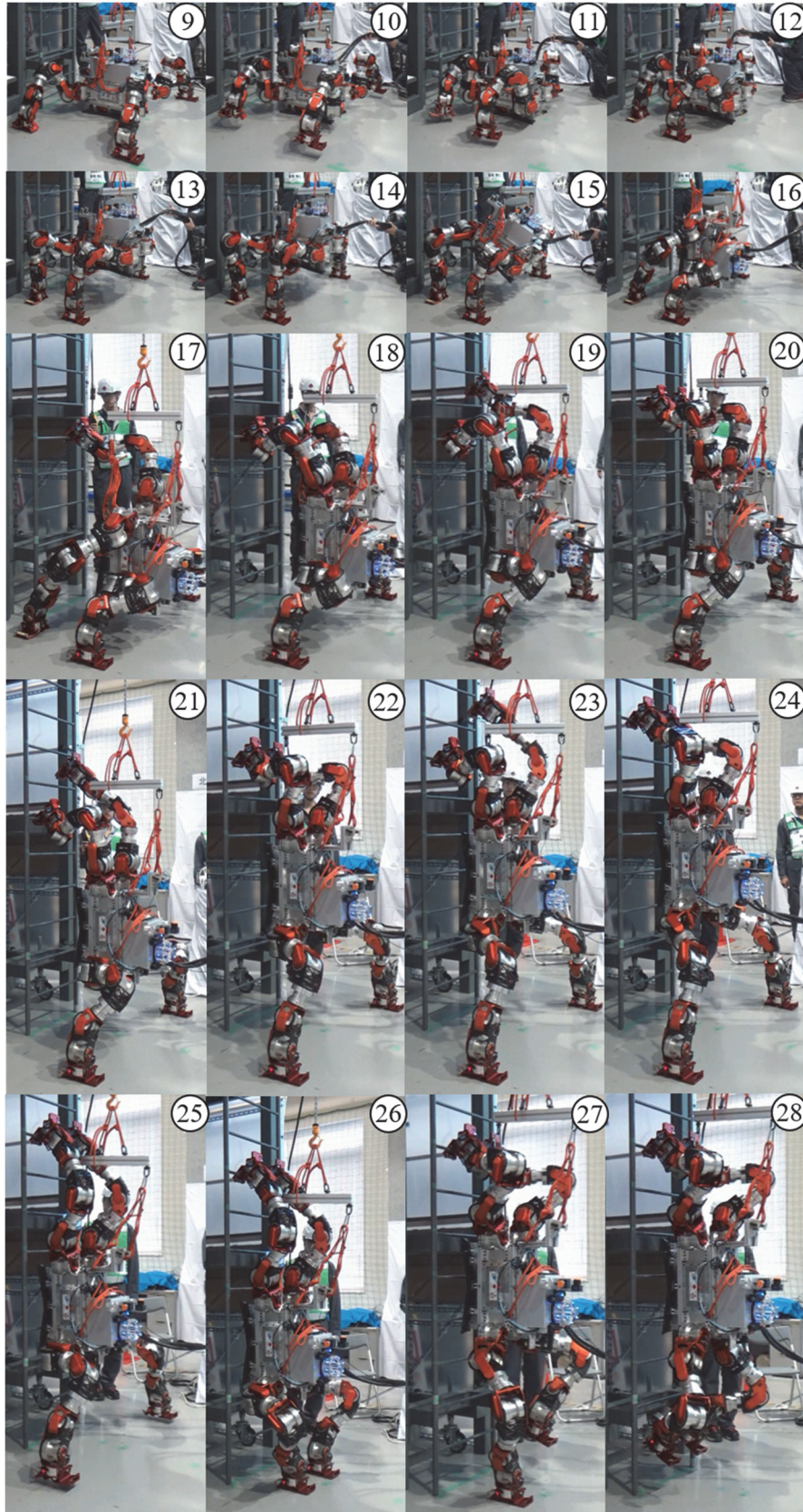


Fig. D.9 Snapshots of the sequence of “transition”.





## E. Specification of the ladder in JIS used in this thesis

Table E-1 Specifications about vertical ladders in JIS (JIS B 9713-4) [49].

Term	Value (range) mm
Rung interval	225~300
Side pole distance	400~600 (300~400 is also acceptable if conditions limited)
Distance from wall to the attached ladder	No less than 150



## Publications

### International journal

- [1] T. Matsuzawa, A. Koizumi, K. Hashimoto, **X. Sun**, S. Hamamoto, T. Teramachi, N. Sakai, S. Kimura and A. Takanishi, "Crawling and Foot Trajectory Modification Control for Legged Robot on Uneven Terrain", *International Journal of Mechatronics and Automation (IJMA)*, 2018 (accepted).

### International conference proceedings

- [1] **X. Sun**, S. Hayashi, K. Hashimoto, T. Matsuzawa, Y. Yoshida, N. Sakai, A. Imai, M. Okawara, K. Kumagai, T. Matsubara, K. Yamaguchi and A. Takanishi, "Error Compensation System with Proximity Sensors for Vertical Ladder Climbing of the Robot "WAREC-1"", *IEEE-RAS 18th International Conference on Humanoid Robots (Humanoids)*, pp.40-46, 2018.
- [2] T. Matsuzawa, A. Imai, K. Hashimoto, T. Teramachi, **X. Sun**, S. Kimura, N. Sakai, Y. Yoshida, K. Kumagai, T. Matsubara, K. Yamaguchi and A. Takanishi, "End-effector with a Hook and Two Fingers for the Locomotion and Simple Work of a Four-limbed Robot", *IEEE/RSJ International Conference on Intelligent Robots and Systems (IROS)*, pp.2727-2732, 2018.
- [3] T. Matsuzawa, T. Matsubara, K. Hashimoto, T. Teramachi, **X. Sun**, S. Kimura, N. Sakai, Y. Yoshida, A. Imai, K. Kumagai, K. Yamaguchi, K. Namura and A. Takanishi, "Body Mechanism with Linear Spikes for Slippage Reduction of Four-limbed Robot Crawling on Uneven Terrain", *ROMANSY 22-Robot Design, Dynamics and Control.*, Springer International Publishing, pp.280-287, 2018.
- [4] **X. Sun**, K. Hashimoto, S. Hamamoto, T. Teramachi, T. Matsuzawa, S. Kimura, N. Sakai, S. Hayashi, Y. Yoshida and A. Takanishi, "Planning and Control of Stable Ladder Climbing Motion for the Four-limbed Robot "WAREC-1", *IEEE/RSJ International Conference on Intelligent Robots and Systems (IROS)*, pp.6547-6554, 2017.
- [5] K. Hashimoto, S. Kimura, N. Sakai, S. Hamamoto, A. Koizumi, **X. Sun**, T. Matsuzawa, T. Teramachi, Y. Yoshida, A. Imai, K. Kumagai, T. Matsubara, K. Yamaguchi, G. Ma and A. Takanishi, "WAREC-1 - A Four-Limbed Robot Having High Locomotion Ability with Versatility in Locomotion Styles", *IEEE/RSJ International Conference on Intelligent Robots and Systems (IROS)*, pp.5398-5405, 2017.
- [6] K. Hashimoto, S. Kimura, N. Sakai, S. Hamamoto, A. Koizumi, **X. Sun**, T. Matsuzawa, T. Teramachi, Y. Yoshida, A. Imai, K. Kumagai, T. Matsubara, K. Yamaguchi, G. Ma and A. Takanishi, "WAREC-1 - A Four-Limbed Robot Having High Locomotion Ability with Versatility in Locomotion Styles", *International Symposium on Safety, Security and Rescue*

- Robotics (SSRR), pp. 172-178, 2017.
- [7] T. Matsuzawa, K. Hashimoto, **X. Sun**, T. Teramachi, S. Kimura, N. Sakai, Y. Yoshida, A. Imai, K. Kumagai, T. Matsubara, K. Yamaguchi, W. Tan and A. Takanishi, "Crawling Gait Generation Method for Four-Limbed Robot Based on Normalized Energy Stability Margin", International Symposium on Safety, Security and Rescue Robotics (SSRR), pp. 223-229, 2017.
- [8] T. Matsuzawa, A. Koizumi, K. Hashimoto, **X. Sun**, S. Hamamoto, T. Teramachi N. Sakai, S. Kimura and A. Takanishi, "Crawling Motion and Foot Trajectory Modification Control for Legged Robot on Rough Terrain", IEEE International Conference on Mechatronics and Automation (ICMA), pp. 1977-1982, 2017.
- [9] **X. Sun**, K. Hashimoto, S. Hamamoto, A. Koizumi, T. Matsuzawa, T. Teramachi and A. Takanishi, "Trajectory Generation for Ladder Climbing Motion with Separated Path and Time Planning", IEEE/RSJ International Conference on Intelligent Robots and Systems (IROS), pp.5782-5788, 2016.
- [10] **X. Sun**, K. Hashimoto, A. Koizumi, S. Hamamoto, T. Matsuzawa, T. Teramachi and A. Takanishi, "Path-Time Independent Trajectory Planning of Ladder Climbing with Shortest Path Length for a Four-limbed Robot", 6th IEEE RAS/EMBS International Conference on Biomedical Robotics and Biomechatronics (BioRob), pp.188-194, 2016.
- [11] T. Matsuzawa, A. Koizumi, K. Hashimoto, **X. Sun**, S. Hamamoto, T. Teramachi, S. Kimura, N. Sakai and A. Takanishi, "Crawling Gaits for Four-limbed Robot and Simulation on Uneven Terrain", IEEE-RAS 16th International Conference on Humanoid Robots (Humanoids), pp.1270-1275, 2016.
- [12] T. Matsuzawa, K. Hashimoto, T. Teramachi, K. Uryu, **X. Sun**, S. Hamamoto, A. Koizumi and A. Takanishi, "End-Effector for Disaster Response Robot with Commonly Structured Limbs and Experiment in Climbing Vertical Ladder", *ROMANSY 21-Robot Design, Dynamics and Control.*, Springer International Publishing, pp.311-319, 2016.
- [13] **X. Sun**, K. Hashimoto, A. Koizumi, S. Hamamoto, T. Matsuzawa, T. Teramachi and A. Takanishi, "Event-based climbing motion planning for a quadruped robot ", International Conference on Advanced Mechanics (ICAM), pp.78-79, 2015.
- [14] T. Matsuzawa, K. Hashimoto, **X. Sun**, K. Uryu, A. Koizumi, S. Hamamoto, T. Teramachi and A. Takanishi, "Development of Disaster Response Robot with Commonly Structured Limbs and Experiment in Climbing Vertical Ladder", International Conference on Advanced Mechanics (ICAM), pp.142-143, 2015.

## Japanese conference proceedings

- [1] 橋本健二, 孫瀟, 瓜生和寛, 小泉文紀, 濱元伸也, 寺町知峰, 松澤貴司, 高西淳夫, “極限環境下で作業可能な災害対応ロボットの開発 (第1報: 極限環境の分類と4肢ロボットの基本構想)”, 日本機械学会ロボティクス・メカトロニクス講演会2015, 予稿集, 1A1-T03.
- [2] 松澤貴司, 寺町知峰, 橋本健二, 孫瀟, 瓜生和寛, 小泉文紀, 濱元伸也, 高西淳夫, “極限環境下で作業可能な災害対応ロボットの開発 (第2報: 多様な移動様式が可能な4肢ロボットと垂直はしご昇降実験)”, 第33回日本ロボット学会, 学術講演会予稿集, 3K1-05.
- [3] 寺町知峰, 濱元伸也, 橋本健二, 孫瀟, 瓜生和寛, 松澤貴司, 小泉文紀, 高西淳夫, “極限環境下で作業可能な災害対応ロボットの開発 (第3報: 棧や支柱を用いた垂直はしご昇降の実現)”, 第33回日本ロボット学会, 学術講演会予稿集, 3K1-06.
- [4] 橋本健二, 小泉文紀, 松澤貴司, 孫瀟, 濱元伸也, 寺町知峰, 酒井伸明, 木村駿介, 高西淳夫, “極限環境下で作業可能な災害対応ロボットの開発 (第4報: 4肢ロボットの匍匐移動法の提案)”, 日本機械学会ロボティクス・メカトロニクス講演会2016, 予稿集, 1A2-09b7.
- [5] 松澤貴司, 小泉文紀, 橋本健二, 孫瀟, 濱元伸也, 寺町知峰, 木村駿介, 酒井伸明, 高西淳夫, “極限環境下で作業可能な災害対応ロボットの開発 (第5報: 4肢ロボットの匍匐移動における進行方向制御)”, 日本機械学会ロボティクス・メカトロニクス講演会2016, 予稿集, 1A1-09b3.
- [6] 濱元伸也, 吉田雄貴, 橋本健二, 孫瀟, 寺町知峰, 松澤貴司, 木村駿介, 酒井伸明, 高西淳夫, “極限環境下で作業可能な災害対応ロボットの開発 (第6報: 安定判別規範を用いた2点支持による垂直はしご昇降の実現)”, 第34回日本ロボット学会, 学術講演会予稿集, 2C1-01.
- [7] 孫瀟, 林翔太, 橋本健二, 小泉文紀, 濱元伸也, 松澤貴司, 寺町知峰, 高西淳夫, “極限環境下で作業可能な災害対応ロボットの開発 (第7報: 垂直はしご昇降動作における経路・時間分離かつ経路最短なエンドエフェクタ軌道計画)”, 第34回日本ロボット学会, 学術講演会予稿集, 2C1-02.
- [8] 酒井伸明, 小泉文紀, 橋本健二, 松澤貴司, 孫瀟, 濱元伸也, 木村駿介, 寺町知峰, 高西淳夫, “極限環境下で作業可能な災害対応ロボットの開発 (第8報: 匍匐移動を目的とした4肢ロボットの胴体構造)”, 第34回日本ロボット学会, 学術講演会予稿集, 2C1-06.
- [9] 松澤貴司, 小泉文紀, 橋本健二, 孫瀟, 濱元伸也, 寺町知峰, 酒井伸明, 木村駿介, 高西淳夫, “極限環境下で作業可能な災害対応ロボットの開発 (第9報: 4肢ロボットの匍匐移動時の足先軌道修正制御)”, 第34回日本ロボット学会, 学術講演会予稿集, 2C1-07.

- [10] 木村駿介, 酒井伸明, 橋本健二, 孫瀟, 小泉文紀, 濱元伸也, 寺町知峰, 松澤貴司, 高西 淳夫, “極限環境下で作業可能な災害対応ロボットの開発 (第10報: 中空構造を持つ高出力アクチュエータユニット)”, 第34回日本ロボット学会, 学術講演会予稿集, 2C2-01.
- [11] 橋本健二, 木村駿介, 酒井伸明, 小泉文紀, 濱元伸也, 孫瀟, 松澤貴司, 寺町知峰, 高西淳夫, “極限環境下で作業可能な災害対応ロボットの開発 (第11報: 4肢ロボットWAREC-1 の設計と製作)”, 第34回日本ロボット学会, 学術講演会予稿集, 2C2-02.
- [12] 松澤貴司, 橋本健二, 孫瀟, 寺町知峰, 木村駿介, 酒井伸明, 吉田雄貴, 今井朝輝, 熊谷健吾, 松原孝将, 山口航希, 陳偉信, 高西淳夫, “極限環境下で作業可能な災害対応ロボットの開発 (第15報: 安定指標に基づく4肢ロボットの腹ばい運動生成法)”, 第35回日本ロボット学会, 学術講演会予稿集, 1K1-01.
- [13] 松原孝将, 松澤貴司, 橋本健二, 孫瀟, 寺町知峰, 木村駿介, 酒井伸明, 吉田雄貴, 今井朝輝, 熊谷健吾, 山口航希, 名村圭祐, 高西淳夫, “極限環境下で作業可能な災害対応ロボットの開発 (第16報: 腹ばい移動時の滑動を低減する4肢ロボットの胴体機構)”, 第35回日本ロボット学会, 学術講演会予稿集, 1K1-02.
- [14] 山口航希, 松澤貴司, 橋本健二, 孫瀟, 寺町知峰, 木村駿介, 酒井伸明, 吉田雄貴, 今井朝輝, 熊谷健吾, 松原孝将, 高西淳夫, “極限環境下で作業可能な災害対応ロボットの開発 (第17報: 4肢ロボットの移動速度を向上する能動車輪機構)”, 第35回日本ロボット学会学術講演会予稿集, 1K1-03.
- [15] 今井朝輝, 寺町知峰, 橋本健二, 松澤貴司, 孫瀟, 木村駿介, 酒井伸明, 吉田雄貴, 熊谷健吾, 松原孝将, 山口航希, 高西淳夫, “極限環境下で作業可能な災害対応ロボットの開発 (第18報: フック形状を有し移動と単純な作業に使用可能な4肢ロボットのエンドエフェクタ)”, 第35回日本ロボット学会学術講演会予稿集, 1K2-02.
- [16] 熊谷健吾, 橋本健二, 寺町知峰, 松澤貴司, 木村駿介, 酒井伸明, 孫瀟, 吉田雄貴, 今井朝輝, 松原孝将, 山口航希, 高西淳夫, “極限環境下で作業可能な災害対応ロボットの開発 (第19報: 浸漬冷却可能なアクチュエータユニットの製作と評価)”, 第35回日本ロボット学会学術講演会予稿集, 1K2-03.
- [17] 橋本健二, 酒井伸明, 内藤博, 松澤貴司, 今井朝輝, 孫瀟, 並木明夫, 劉楊, 郭伝宇, 毛利哲也, 高西淳夫, “極限環境下で作業可能な災害対応ロボットの開発 (第20報: 高出力ハンドの統合と遠隔操作によるバルブ開閉の実現)”, 第62回システム制御情報学会研究発表講演会, 141-1.
- [18] 松澤貴司, 林翔太, 橋本健二, 孫瀟, 高西淳夫, “極限環境下で作業可能な災害対応ロボットの開発 (第21報: 4肢ロボットの腹ばい運動の全方向移動制御)”, 日本機械学会ロボティクス・メカトロニクス講演会2018, 2A2-L05.

- [19] 松澤貴司, 今井朝輝, 酒井伸明, 吉田雄貴, 山口航希, 孫瀧, 橋本健二, 高西淳夫, “極限環境下で作業可能な災害対応ロボットに関する研究 (第22報: 移動と単純な作業が可能なエンドエフェクタを用いた電動ドリルによる穿孔作業の実現) ”, 第24回 日本IFTToMM会議シンポジウム, セッション1.
- [20] 内藤博, 酒井伸明, 橋本健二, 孫瀧, 松澤貴司, 木村駿介, 林翔太, 吉田雄貴, 今井朝輝, 大河原正篤, 熊谷健吾, 松原孝将, 山口航希, 高木一輝, 高西淳夫, “極限環境下で作業可能な災害対応ロボットに関する研究 (第23報: 4肢ロボットの多様な移動様式と遠隔作業に対応可能なエンドエフェクタ) ”, 第36回日本ロボット学会学術講演会, 1D3-07.
- [21] 名村圭祐, 松澤貴司, 橋本健二, 孫瀧, 酒井伸明, 林翔太, 吉田雄貴, 今井朝輝, 大河原正篤, 熊谷健吾, 松原孝将, 山口航希, 内藤博, 高木一輝, 高西淳夫, “極限環境下で作業可能な災害対応ロボットに関する研究 (第24報: 胴体接地を活用した段差踏破が可能な4肢ロボットの開発) ”, 第36回日本ロボット学会学術講演会, 1D3-04.

We hereby admit that above thesis is worth enough to present as doctoral dissertation.

Referees:

Principle Referee

Atsuo Takanishi, Doctor of Engineering, Professor, Waseda University

Atsuo Takanishi      29/11/2018

Referee

Mitsuo Umezu, Doctor of Engineering and Doctor of Medical Science, Professor, Waseda University

Mitsuo Umezu      29/11/2018

Referee

Tomoyuki Miyashita, Doctor (Engineering), Professor, Waseda University

Tomoyuki Miyashita      29/11/2018

Referee

Hiroyasu Iwata, Doctor (Engineering), Professor, Waseda University

Hiroyasu Iwata      29/11/2018

Referee

Kenji Hashimoto, Doctor (Engineering), Associate Professor, Meiji University

Kenji Hashimoto      29/11/2018